Smart Antennas at Handsets for the 3G Wideband CDMA Systems and Adaptive Low-Power Rake Combining Schemes

Suk Won Kim

Dissertation submitted to the Faculty of the
Virginia Polytechnic Institute and State University
in partial fulfillment of the requirements for the degree of

Doctor of Philosophy
in
Computer Engineering

Dong S. Ha, Chair
James R. Armstrong
F. Gail Gray
Scott F. Midkiff
Jeffrey H. Reed

July 2, 2002
Blacksburg, Virginia

Key Words: Smart Antennas, Low-Power Design, Adaptive Rake Combiner, Hybrid Combining

Smart Antennas at Handsets for the 3G Wideband CDMA Systems and Adaptive Low-Power Rake Combining Schemes

Suk Won Kim

ABSTRACT

Smart antenna technology is a promising means to overcome signal impairments in wireless personal communications. When spatial signal processing achieved through smart antennas is combined with temporal signal processing, the space-time processing can mitigate interference and multipath to yield higher network capacity, coverage, and quality.

In this dissertation, we propose a dual smart antenna system incorporated into handsets for the third generation wireless personal communication systems in which the two antennas are separated by a quarter wavelength (3.5 cm). We examine the effectiveness of a dual smart antenna system with diversity and adaptive combining schemes and propose a new combining scheme called hybrid combining. The proposed hybrid combiner combines diversity combiner and adaptive combiner outputs using maximal ratio combining (MRC). Since these diversity combining and adaptive combining schemes exhibit somewhat opposite and complementary characteristics, the proposed hybrid combining scheme aims to exploit the advantages of the two schemes.

To model dual antenna signals, we consider three channel models: loosely correlated fading channel model (LCFCM), spatially correlated fading channel model (SCFCM), and envelope correlated fading channel model (ECFCM). Each antenna signal is assumed to have independent Rayleigh fading in the LCFCM. In the SCFCM, each antenna signal is subject to the same Rayleigh fading, but is different in the phase due to a non-zero angle of arrival (AOA). The LCFCM and the SCFCM are useful to evaluate the upper and the lower bounds of the system performance. To model the actual channel of dual antenna signals lying in between these two channel models, the ECFCM is considered. In this model, two Rayleigh fading antenna signals for each multipath are assumed to have an envelope correlation and a phase difference due to a non-zero AOA. To obtain the channel profile, we adopted not only the geometrically based

single bounce (GBSB) circular and elliptical models, but also the International Telecommunication Union (ITU) channel model.

In this dissertation, we also propose a new generalized selection combining (GSC) method called minimum selection GSC (MS-GSC) and an adaptive rake combining scheme to reduce the power consumption of mobile rake receivers. The proposed MS-GSC selects a minimum number of branches as long as the combined SNR is maintained larger than a given threshold. The proposed adaptive rake combining scheme which dynamically determines the threshold values is applicable to the three GSC methods: the absolute threshold GSC, the normalized threshold GSC, and the proposed MS-GSC. Through simulation, we estimated the effectiveness of the proposed scheme for a mobile rake receiver for a wideband CDMA system. We also suggest a new power control strategy to maximize the benefit of the proposed adaptive scheme.

Dedication

This dissertation is dedicated to my wife, Eun Hee, my daughters, Min Joo and Amy Gina, and my son, Brian Sanghyun, for all their love and support.

Acknowledgments

First above all, I would like to thank God for his grace and love. I would like to express my gratitude and appreciation to my advisor, Dr. Dong S. Ha, for his guidance and support throughout my graduate career at Virginia Tech. His suggestions and advice allowed me to overcome the difficult times during my research. I also would like to thank Dr. James R. Armstrong, Dr. F. Gail Gray, Dr. Scott F. Midkiff, and Dr. Jeffrey H. Reed for serving on the advisory committee. My special thanks go to Dr. Reed and Dr. Jeong Ho Kim for their helpful and insightful comments and encouragements.

I would like to give thanks to Samsung Electronic Co., Ltd. for awarding me a scholarship to pursue the Ph. D. degree. Special thanks are directed to people in Samsung Electronic Co., Ltd., Dr. Kwang Hyun Kim, Dr. Yun Tae Lee, and Mr. Ja Man Koo, for their encouragements and supports.

Byung-Ki Kim, Kyung Kyoon Bae, and SeongYoup Suh deserve thanks for their helpful discussions about the dissertation. I am also thankful to the group members: Han Bin Kim, Jia Fei, Carrie Aust, Meenatchi Jagasivamani, Steve Richmond, Nate August, Jos Sulistyo, Hyung-Jin Lee, Jina Kim, Chad Pelino, WooCheol Chung, Kyehun Lee, and Sookyoung Kim. I have spent a lot of good time with my friends and their family: Dong-Jin Lee, Jae Young Choi, Byeong-Mun Song, Tae-In Hyon, Jae-Hong Park, Jahng Sun Park, Jun Hyung Kim, Chang-Hyun Jang, and Hwandon Jun. I have also spent lots of valuable time with the church members and their family: Jeong-Hoi Koo, Gwi Bo Byun, Junghwa Cho, Sang Eon Chun, Seung Yo Lee, and Mun Ki Lee.

Finally, I would like to give my appreciations to my family: my wife, Eun Hee Lee, my children, Min Joo, Amy Gina, and Brian Sanghyun, my parents, Sung Ho Kim and Kyu Ja Kim, and my parents-in-law, Jang Suk Lee and Myo Soon Kim.

Table of Contents

List of Figures

List of Tables

Chapter 1 Introduction

A smart antenna is an antenna array (or multiple antennas) that can adapt to the environment in which it operates [1]. Smart antenna technology has been used to overcome signal impairments in wireless personal communications. When spatial signal processing achieved through a smart antenna is combined with temporal signal processing, the space-time processing can mitigate propagation distortion and interference to enable higher network capacity, coverage, and quality [2]-[9]. A smart antenna not only suppresses interference, but also combats multipath fading by combining multiple antenna signals.

To process multiple antenna signals, two combining schemes—diversity combining and adaptive combining—can be employed. Diversity combining exploits the spatial diversity among multiple antenna signals and achieves higher performance. There are four classical diversity combining schemes: switched diversity, selection diversity, equal gain combining, and maximal ratio combining (MRC) [10]. After weighting each antenna signal proportional to its signal to noise ratio (SNR), MRC combines each signal, thus providing maximum output SNR. Adaptive combining is based on dynamic reconfiguration in that the antenna weights are dynamically adjusted to enhance the desired signal while suppressing interference signals to maximize signal to interference plus noise ratio (SINR). It achieves the same performance as the MRC without presence of interference. The performance of adaptive combining is sometimes limited under certain circumstances, such as when the angular separation between desired signal and interference is small or the noise level is high [9].

Because of concerns with high system complexity and high power consumption, smart antenna techniques have been considered primarily for base stations so far [11]-[18]. A common belief is that closely spaced antennas are ineffective for exploiting diversity. However, recent

measurement results indicate that even closely spaced antennas (such as 0.15 wavelength) provide a low envelope correlation to yield a diversity gain [19].

Recently, smart antenna techniques have been applied to mobile terminals [20]-[23]. For example, the high data rate (HDR) system (adopted as IS-856 and also known as 1xEV DO) developed by Qualcomm employs dual antennas at a mobile station [20]. A dual antenna system for handsets was also investigated for the digital European cordless telephone (DECT) system for the indoor radio channel [21]. Also, one of the third generation wireless personal communication systems, third generation partnership project (3GPP) [24],[25], requires antenna diversity at base stations and optionally at mobile stations [26]. Antenna diversity is also applied to the IEEE 802.11 wireless local area network (WLAN) system [27]. Due to the compact size and stringent cost of handsets and the limited battery capacity, smart antennas at handsets should have low circuit complexity and low power dissipation. To justify employment of smart antennas at handsets, the performance gain should be large enough to offset the additional cost and power consumption.

In this dissertation, we propose a dual smart antenna system incorporated into handsets for the third generation (3G) wireless personal communication systems in which the two antennas are separated by a quarter wavelength (3.5 cm) [28]-[32]. We present the effectiveness of a dual smart antenna system and propose a new combining scheme called a hybrid combiner (HC) [31]. A diversity combiner (DC) combines two rake receiver outputs using a diversity combining scheme such as the MRC, while an adaptive combiner (AC) combines corresponding finger outputs from the two antennas with dynamically adjusted antenna weights. Since the two combining schemes exhibit somewhat opposite and complementary characteristics, the proposed HC aims to exploit the advantages of the both schemes.

Because the channel model influences the design of receivers and their performance, appropriate channel modeling is important for evaluation of a smart antenna system. To model dual antenna signals, we consider three channel models: loosely correlated fading channel model (LCFCM), spatially correlated fading channel model (SCFCM), and envelope correlated fading channel model (ECFCM). Each antenna signal is assumed to have independent Rayleigh fading in the LCFCM. In the SCFCM, each antenna signal is subject to the same Rayleigh fading, but is different in the phase due to a non-zero angle of arrival. These two channel models are simple and useful to evaluate the upper and the lower bounds of the system performance. To model the

actual channel of dual antenna signals lying in between these two channel models, we modify the procedure developed by Ertel and Reed [33] and propose an envelope correlated fading channel model (ECFCM). Two Rayleigh fading antenna signals for each multipath in the ECFCM are assumed to have an envelope correlation and a phase difference due to a non-zero angle of arrival.

To obtain the channel profile (such as delay, average power, and angle of arrival of each multipath signal), we adopted not only a statistical channel model such as the geometrically based single bounce (GBSB) circular and elliptical models [34]-[36] but also a measurement based channel model such as the International Telecommunication Union (ITU) channel model [37].

A rake receiver adopts multiple fingers to exploit diversity of multipath signals called diversity combining. In general, a larger number of fingers would improve the SNR at the cost of higher circuit complexity and hence higher power dissipation. In practice, the number of rake fingers is in the rage of two to five. Since a rake receiver operates at the chipping rate, it is one of the most power-consuming blocks in a baseband signal processor for a code division multiple access (CDMA) receiver. MRC combines *all* finger outputs with the weight of each finger signal proportional to its SNR. MRC provides the maximum output SNR; thus it is an optimal solution for a diversity receiver [10]. We use fingers and branches interchangeably in this dissertation.

Instead of selecting all the branches, generalized selection combining (GSC) methods choose the best m branches out of L branches depending on the SNR or the signal strength [38]-[50]. Note that the MRC is a special case of a GSC where the number of selected branches m is fixed at L. The number of selected branches m is decided *a priori* in [38]-[50], while it varies dynamically in [51]-[53]. For the latter approach, selection of branches whose SNRs are larger than a given threshold is proposed in [51] and [52], and it is called absolute threshold GSC (AT-GSC). Alternatively, selection of a branch whose relative SNR over the maximum SNR among all branches, $\frac{SNR_i}{SNR_{\max}}$, is larger than a threshold is proposed in [51] and [53]. This method is called normalized threshold GSC (NT-GSC).

GSC methods intend to save hardware and/or reduce power dissipation. If m is fixed and less than L, it reduces the complexity of the rake receiver and hence the power dissipation of the rake receiver circuit. Since m changes dynamically in the range of 1 to L for the AT-GSC and the

NT-GSC, the two schemes do not save hardware. In fact, increased hardware complexity is necessary to be able to change *m*. However, the AT-GSC and the NT-GSC can reduce power dissipation by turning off unselected branches. Two major design considerations regarding the AT-GSC and the NT-GSC are:

(i) determination of threshold values, and

(ii) effectiveness of the two methods in terms of power saving and practical implementation.

A threshold value should be set to meet the required quality of service (QoS), and a maximal number of branches should be turned off as long as the required QoS is satisfied. The bit error rate (BER) is often used as the metric for the QoS. For example, a BER of 10^{-3} may be necessary for voice communications. This suggests that if the combined SNR is over a certain threshold, then the BER is below a certain level to meet the required QoS.

In this dissertation, we also propose a new GSC method called minimum selection GSC (MS-GSC) and an adaptive rake combining scheme to determine the threshold values for GSCs. Our MS-GSC selects a minimum number of branches as long as the combined SNR is maintained larger than a given threshold. Our proposed adaptive rake combining scheme is applicable to the three GSC methods—the AT-GSC, the NT-GSC, and the proposed MS-GSC. Through simulation, we estimated the effectiveness of the proposed scheme for a mobile rake receiver for a wideband CDMA (WCDMA) system. We also suggest a new power control strategy to maximize the benefit of the proposed adaptive scheme.

In summary, the focus of the presented research is to investigate the feasibility of smart antennas at 3G handsets. The feasibility study includes:

(i) performance of smart antennas at 3G handsets, and

(ii) low-power design of a rake receiver.

The performance gain of a smart antenna system was evaluated using the Signal Processing Worksystem (SPW) tool of Cadence and Matlab. The considered 3G wireless personal communication systems are the 3GPP WCDMA system and the cdma2000 system. For the cdma2000 system, the SPW tool was used to model the system completely and to evaluate the performance. For the 3GPP WCDMA system, Matlab was used in order to evaluate the performance with various operating conditions.

The dissertation is organized as follows. A preliminary study of smart antenna techniques, 3G systems, channel models, low-power design, GSC methods, and Monte Carlo simulation is

briefly described in Chapter 2. Our proposals, including a dual smart antenna system at handsets with a hybrid combiner, channel models, and an adaptive rake combiner with a new GSC method, are presented in Chapter 3. The simulation environments and results to evaluate the proposed smart antenna systems are provided in Chapter 4. The simulation results applied to a mobile rake receiver to verify the proposed adaptive rake combining method are presented in Chapter 5. Finally, Chapter 6 concludes the dissertation.

Chapter 2 Preliminaries

We provide preliminary studies for the proposed research in this chapter. The basic concepts of smart antenna systems and previous works related to smart antennas at handsets are described. The third generation wireless systems, the channel models, and low-power VLSI designs are also reviewed. Finally, a brief description on the generalized selection combining technique and Monte Carlo simulation approach is provided.

2.1 Smart Antennas

In this section, we describe the basic concepts of smart antenna systems and review previous works related to smart antennas at handsets.

2.1.1 Introduction to Smart Antennas

Signal impairments in wireless personal communications are mainly due to intersymbol interference (ISI) and co-channel interference (CCI). The transmitted signal arrives at the receiver with different time delays through the time-varying multipath channel. The received signal symbols are smeared and overlapped with one another. This signal distortion is called ISI [54]. Frequency reuse and multiple access cause the CCI, which are inherent features of cellular systems. Temporal and/or spatial signal processing is applied to mitigate signal impairments. Temporal signal processing reduces the ISI using an equalizer or a rake receiver. The equalizer compensates the channel distortion and the rake receiver distinguishes each delayed signal and combines them constructively. Meanwhile, spatial signal processing reduces the CCI using a smart antenna. The smart antenna provides the output by properly combining each antenna

signal. Through this operation, it is possible to extract the desired signal and to suppress interference. When spatial signal processing is combined with temporal signal processing, the space-time processing can further repair the impairments to result in higher network capacity, coverage, and quality [2]-[9].

Figure 2-1 shows a block diagram of an antenna array system, in which the signals received by each antenna element are weighted and combined to generate an output signal.

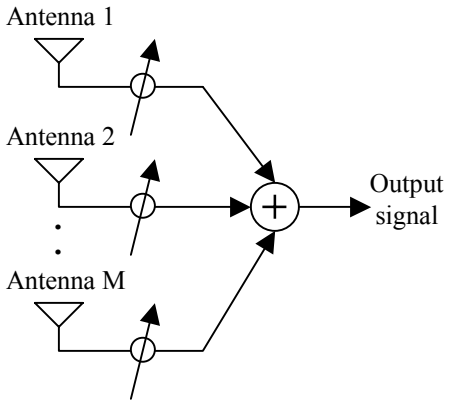

Figure 2-1. Antenna Array System

The antenna gain is defined as the reduction in the required received signal power for a given average output signal-to-noise ratio (SNR), while the diversity gain is defined as the reduction in the required average output SNR for a given bit error rate (BER). An antenna array system provides the antenna gain as well as the diversity gain. The diversity gain against multipath fading depends on the correlation of the fading among the antennas. Higher diversity gain can be obtained when the correlation among antenna signals is low [10].

Three basic configurations of antennas are used to provide the diversity gain as shown in Figure 2-2. A configuration for spatial diversity is shown in Figure 2-2 (a). The correlation of the fading is related to the separated distance between antennas. The second one shown in Figure 2-2 (b) is for polarization diversity, where horizontal and vertical polarization is used to achieve diversity. The angle diversity uses several narrow beam antennas. Figure 2-2 (c) is a sector antenna in which four narrow beam antennas (each narrow beam antenna covers a section of 30°) cover a sector of 120°.

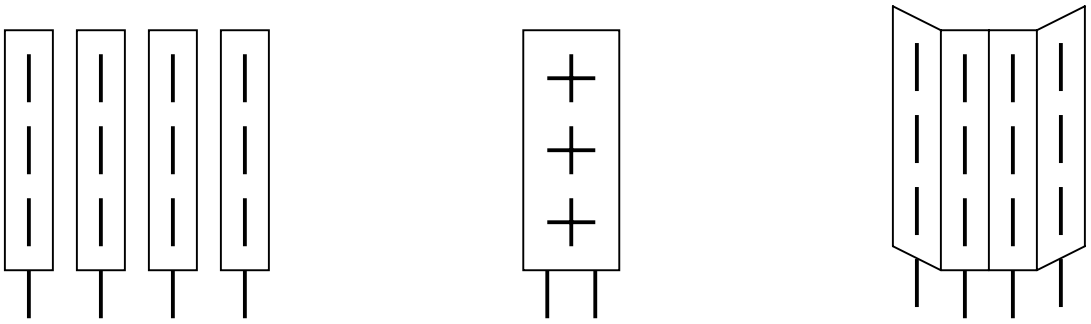

(a) Spatial diversity (b) Polarization diversity (c) Angle diversity

Figure 2-2. Antenna Diversity

A linear antenna array is a uniformly spaced antenna array with identical antenna elements. For the configuration of the spatial diversity antenna, the linear antenna array can provide the diversity gain with the low correlation if the antennas are separated far enough (the separation is a few or tens of carrier wavelengths). When antennas are placed in proximity, the correlation between the antenna signals is high. In this case, the adaptive filter theory can be applied to extract the desired signal while suppressing the interference signal [55]. To extract the desired signal and to suppress the interference signal, complex antenna weights are used to change the phase and the magnitude of the received signal. Consider the case where two antennas are separated by $\lambda/2$, where λ is a carrier wavelength, and a desired signal is incident on the antenna array with the angle of arrival θ_1 and an interference signal with the angle of arrival θ_2, as shown in Figure 2-3 (a). The only difference between the desired signal (S_1) received at antenna 1 and the desired signal (S_2) received at antenna 2 is the phase difference, which is $\pi\sin\theta_1$ in this configuration. Similarly, the phase difference between the interference signals received at each antenna is $\pi\sin\theta_2$. To extract the desired signal and to suppress the interference signal, the antenna weights should satisfy the following equations.

$$W_1^* + e^{-j\pi\sin\theta_1} W_2^* = 1, \tag{2-1a}$$

$$W_1^* + e^{-j\pi\sin\theta_2} W_2^* = 0. \tag{2-1b}$$

The above two equations are derived from the following two conditions (the unity gain to the desired signal and the zero gain to the interference signal);

$$|S_1W_1^* + S_2W_2^*| = |S_1W_1^* + S_1e^{-j\pi\sin\theta_1}W_2^*| = |S_1||W_1^* + e^{-j\pi\sin\theta_1}W_2^*| = |S_1|, \quad (2\text{-}2a)$$

$$|I_1W_1^* + I_2W_2^*| = |I_1W_1^* + I_1e^{-j\pi\sin\theta_1}W_2^*| = |I_1||W_1^* + e^{-j\pi\sin\theta_1}W_2^*| = |I_1|*0 = 0. \quad (2\text{-}2b)$$

The antenna weights, $W_1 = ½$ and $W_2 = -½j$, are found if the angles of arrival are $\theta_1 = \pi/6$ and $\theta_2 = -\pi/6$, respectively. The antenna beam pattern for this case is shown in Figure 2-3 (b), in which the antenna beam pattern provides the gain toward the direction ($\theta_1 = \pi/6$) of the desired signal and suppresses the gain towards the direction ($\theta_2 = -\pi/6$) of the interference signal.

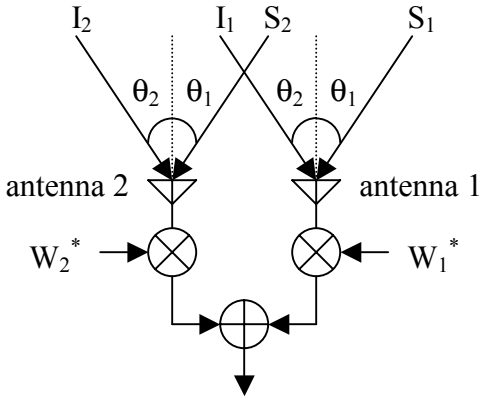

(a) Antenna array with signals

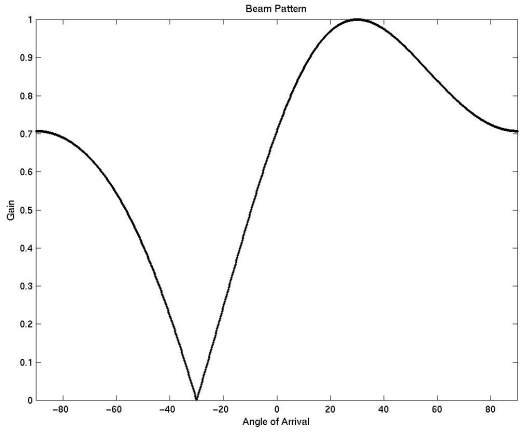

(b) Antenna beam pattern

Figure 2-3. Antenna Array and Beam Pattern

2.1.2 Smart Antenna Algorithms

There are two kinds of smart antenna schemes to compute the antenna weights and to combine the antenna signals. The first scheme is the **diversity combining**, in which the antenna signals are combined to maximize the output SNR. The second one is the **adaptive combining** (in a wide sense) or the **beamforming**, in which the antenna weights are dynamically adjusted to enhance the desired signal while suppressing interference signals to maximize signal to interference plus noise ratio (SINR). The performance of the adaptive combining is sometimes limited under certain circumstances, such as when the angular separation between desired signal and interference is small or the noise level is high [9].

There are four basic schemes in the diversity combining technique: selection diversity, switched diversity, equal gain combining, and maximal ratio combining. Selection diversity (SD) is the simplest method of all, in which a diversity branch having the highest SNR is selected and directed to the output. It is also called selection combining (SC). The switched diversity does not switch the branch until the SNR or the signal strength of the currently selected branch becomes lower than a given threshold. The maximal ratio combing (MRC) scheme weights each antenna signal by its SNR before combining. The MRC provides the maximal output SNR and is hence called MRC. The MRC achieves high performance, but it is difficult to accurately compute the SNR of each antenna signal. The equal gain combining (EGC) scheme simply adds each antenna signal with an equal weight. For example, each antenna signal is weighted by 1/M for an M-element antenna array.

The mean SNRs of three diversity combining schemes are presented in Table 2-1, where a diversity combiner with M diversity branches (antennas) is employed, in which each diversity branch has a mean SNR $\boldsymbol{\Gamma}$ [10]. For reference, the mean SNRs with two diversity branches (antennas) are also provided in the table.

Table 2-1. Mean SNR with a Diversity Combining [10]

Diversity Scheme	M Branches	Two Branches (M = 2)
MRC	$M\Gamma$	2Γ (3 dB)
EGC	$[1+(M-1)\frac{\pi}{4}]\Gamma$	1.785Γ (2.52 dB)
SD	$\sum_{k=1}^{M}\frac{1}{k}\Gamma$	1.5Γ (1.76 dB)

An adaptive antenna array continuously adjusts its antenna weights by means of a feedback control. Sometimes, it is called a smart antenna in a narrow sense. Several criteria can be used to compute antenna weights for the adaptive combining. The criteria include maximum SINR, minimum mean square error (MMSE), minimum variance, and least square (LS) [56]. All criteria intend to maximize the output SINR under various assumptions. When only noise is considered, the adaptive antenna performs the same task as the diversity antenna with the MRC. In the presence of strong interference, the adaptive antenna shows a better performance compared with the diversity antenna with the MRC even if the number of interferences is greater than the number of antennas [57]. There are two kinds of beamforming systems: multibeam antenna and adaptive combining (in a narrow sense). The multibeam antenna system selects one fixed beam among the multiple pre-defined beams, which offers the maximum output SINR. Even though multibeam antenna system adaptively selects the beam pattern, it provides non-uniform gain and limited interference suppression [4] since the beam pattern is pre-defined and the number of beam patterns is limited. Meanwhile, the adaptive combining system adaptively and freely changes its antenna beam pattern by tracking the antenna weights. The adaptive combining system with M antennas can form up to M-1 nulls to cancel up to M-1 interference signals [58]. The antenna weights must adapt fast enough to track the fading of the desired and interfering signals. However, the antenna weights must also change much more slowly than the data rate.

Two approaches are used to compute the antenna weights that maximize the output SINR for the adaptive combining (in a narrow sense). The first approach is to obtain the antenna weights by computing the direct matrix inversion. Wiener filter belongs to this approach [55]. The second one is to obtain the antenna weights by computing the weights recursively or

adaptively. The steepest-descent method and the least-mean-square algorithm belong to the second approach [55].

According to Wiener filter theory, the optimum antenna weights, $\mathbf{w}_o$, are obtained by

$$\mathbf{w}_o = \mathbf{R}^{-1}\mathbf{p}, \tag{2-3}$$

where $\mathbf{R}$ is the correlation matrix of the input vector of antenna signals and $\mathbf{p}$ is the cross-correlation vector between the input vector and the desired response. This algorithm requires computation of the matrix inversion, which results in high system complexity. The steepest-descent method is a gradient-based adaptation algorithm [55], in which the antenna weights are recursively obtained as following:

$$\mathbf{w}(n+1) = \mathbf{w}(n) + \mu[\mathbf{p} - \mathbf{R}\mathbf{w}(n)], \tag{2-4}$$

where $\mathbf{w}(n)$ is the antenna weight vector, μ is the step size, and $\mathbf{R}$ and $\mathbf{p}$ are the same as the above ones.

The most widely used adaptive algorithm is based on the least-mean-square (LMS) algorithm, in which antenna weights are recursively obtained to minimize the mean square error using the following equations:

$$\mathbf{w}(n+1) = \mathbf{w}(n) + \mu\mathbf{u}(n)\mathbf{e}^*(n), \tag{2-5a}$$

$$\mathbf{e}(n) = \mathbf{d}(n) - \mathbf{y}(n), \text{ and} \tag{2-5b}$$

$$\mathbf{y}(n) = \mathbf{w}^H(n)\mathbf{u}(n), \tag{2-5c}$$

where $\mathbf{u}(n)$ is the input vector of the antenna signals and $\mathbf{e}(n)$ is the error signal between the desired response $\mathbf{d}(n)$ and the weighted antenna output $\mathbf{y}(n)$ (* represents a complex conjugation and ^{H} represents a Hermitian operation–transposition and complex conjugation). If the step size μ is chosen such that $0 < \mu < 2/P$ (where P is the sum of powers of each antenna input signal), the algorithm guarantees the convergence of the antenna weights. The most benefit of the LMS algorithm is its simplicity compared to other adaptive algorithms.

The LMS algorithm, however, suffers from a gradient noise amplification problem if the input signal $\mathbf{u}(n)$ is large, i.e., the correction term $\mu\mathbf{u}(n)\mathbf{e}^*(n)$ is large. To circumvent the problem, the following normalized LMS (N-LMS) algorithm is usually used:

$$\mathbf{w}(n+1) = \mathbf{w}(n) + \frac{\mu}{\|\mathbf{u}(n)\|^2}\mathbf{u}(n)\mathbf{e}^*(n), \tag{2-6}$$

where μ is a step size in the range of $0 < \mu < 2$. The N-LMS algorithm exhibits a faster rate of convergence and better stability than the ordinary LMS algorithm for both uncorrelated and correlated input data [55].

When the adaptive algorithm is applied to a wireless communication system, the circuit complexity of the adaptive algorithm is an important factor to select the algorithm. It is a particularly important factor for mobile handsets, since low complexity is highly desirable for handsets. Due to the simplicity of the algorithm, the LMS algorithm and the N-LMS algorithm are widely used for the adaptive antenna array systems [59],[60].

2.1.3 Smart Antennas at Handsets

Because of concerns with high system complexity and high power consumption, smart antenna techniques have been considered primarily for base stations so far [11]-[18]. A common belief is that closely spaced antennas are ineffective for exploiting diversity. An analytical model for the relationship between the envelope correlation and the antenna spacing is as follows [61]:

$$\rho_e = J_0^2\left(\frac{2\pi d}{\lambda}\right), \tag{2-7}$$

where ρ_e is the envelope correlation of two diversity antenna signals, J_0 is the Bessel function of the first kind with zero order, d is the antenna spacing, and λ is the carrier wavelength. Figure 2-4 represents the relationship presented in (2-7). However, recent measurement results indicate that even closely spaced antennas (such as 0.15 wavelength) provide a low envelope correlation to yield a diversity gain [19]. These experimental results also indicate that the envelope correlation of dual spatial diversity antennas for the narrowband signal is in the range from 0.12 to 0.74 for various environments provided the two antennas are closely spaced ($0.1\lambda \sim 0.5\lambda$). The feasibility of implementing dual antennas at mobile handsets was investigated in [62].

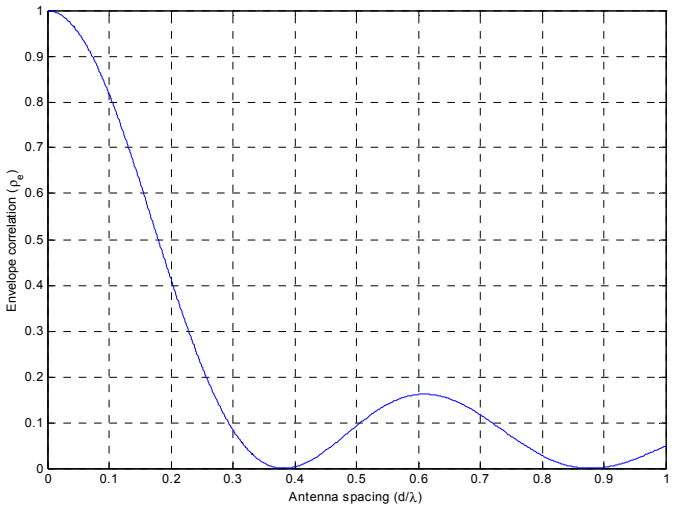

Figure 2-4. Envelope Correlation versus Antenna Spacing

The 3GPP [24] requires antenna diversity at base stations and optionally at mobile stations [25]. Antenna diversity is also applied to the IEEE 802.11 wireless local area network (WLAN) system [27]. Recently, the smart antenna technique has been applied to mobile terminals [20]-[23].

The high data rate (HDR) system (adopted as IS-856 and also known as 1xEV DO) developed by Qualcomm employs dual antennas at a mobile station [20]. Each antenna signal was applied to its own rake receiver that combines signals from different multipaths as shown in Figure 2-5. Then, maximal ratio diversity combining was used to combine the two rake receiver signals. The increase of the throughput was reported in [20]. The average throughput for outdoor stationary users was around 750 kbps with a single antenna and 1.05 Mbps with dual antennas. The average throughput for mobile users was around 500 kbps with a single antenna and 900 kbps with dual antennas [20].

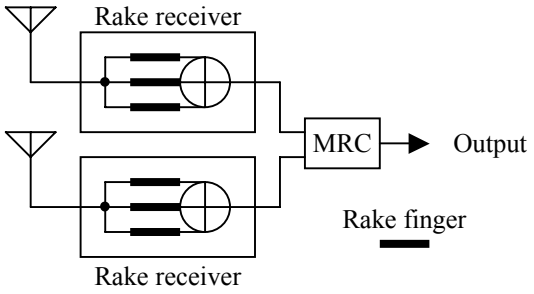

Figure 2-5. Dual Antenna System for the HDR

A dual antenna system for handsets was also applied to the digital European cordless telephone (DECT) system for the indoor radio channel [21]. Figure 2-6 shows the block diagram of the system. The dual antenna handset receiver selects one of the two signals of the receivers based on the SINR. Each receiver processes a signal that is an equal combination of the signal from one antenna and the phase-shifted signal from the other antenna. It was reported that transmit power for the dual antenna system was reduced by 9 dB at the coverage of 99% for normal walking speed (around 5 km/h) compared with the single antenna system [21].

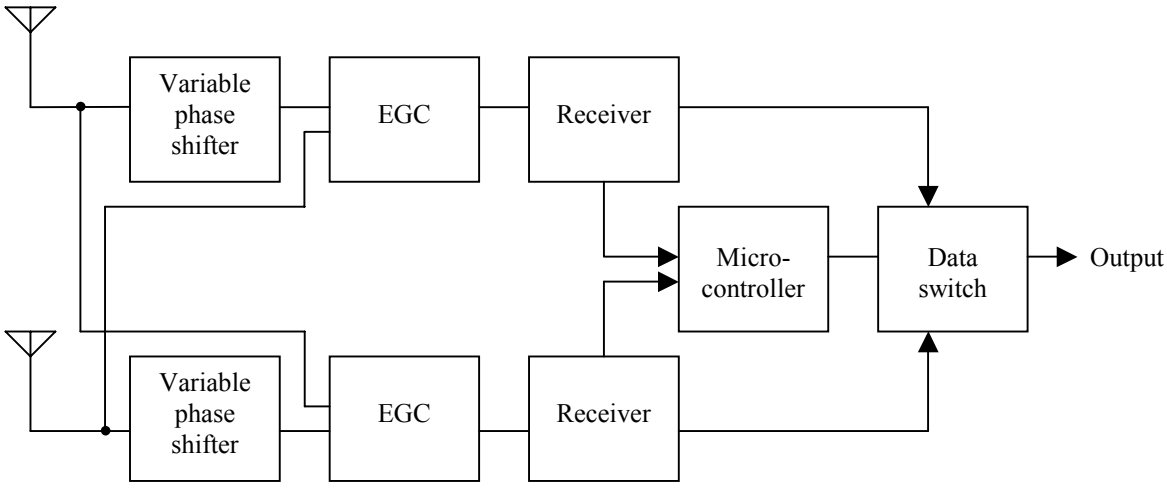

Figure 2-6. Smart Antenna Handsets for the DECT System

Wong and Cox proposed a dual antenna system which could be applied to handheld devices as well as base stations [22],[23]. Summing the signals from two antennas with proper weights in complex number cancels the dominant interference and hence increases the signal-to-interference ratio (SIR). To compute the antenna weights, a technique to optimize the SIR was proposed. Unlike the above two methods, the signal weighting and summing was implemented at the radio frequency (RF) level instead of at the baseband signal level. Thus, it reduces the complexity of the diversity combiner since it requires only one baseband processor. Computer simulation results show that the improvement of their method in the SIR was more than 3.8 dB compared with the conventional two-antenna selection diversity system [22],[23].

One of key features in a 3G cellular system is a high data rate. For a high data rate, a lower BER and a smaller spreading factor are required. Thus, higher transmitting power at a base station is necessary, which results in increased interferences to the cell. By applying smart antenna techniques to handsets, the received SINR at handsets can be improved. Thus, the base station transmits less power to a smart antenna handset than a conventional single antenna handset.

Figure 2-7 shows the conceptual BER performances of a single antenna system and a smart antenna system. As shown in the figure, the benefit of a smart antenna system over a single antenna system can be exploited in two ways: reduced SINR or improved BER. The benefit results in the increased capacity and coverage when the BER or the quality of service (QoS) is fixed. Meanwhile, the benefit is the improved QoS when the capacity is maintained. Smart antenna at handsets can be applied to any wireless personal communication systems such as frequency division multiple access (FDMA), time division multiple access (TDMA), and code division multiple access (CDMA) systems. The FDMA or the TDMA system can obtain the benefit of the increased capacity only if all handsets within a cell are equipped with smart antennas. The reason is that the capacity limiter for the TDMA or the FDMA system is the frequency reuse factor. In contrast, even partial deployment of smart antenna handsets can provide the benefit of the increased capacity for the CDMA system, since the CDMA is an interference-limited system. In this case, the gain of the increased capacity is depends on the percentage of deployment of smart antenna handsets.

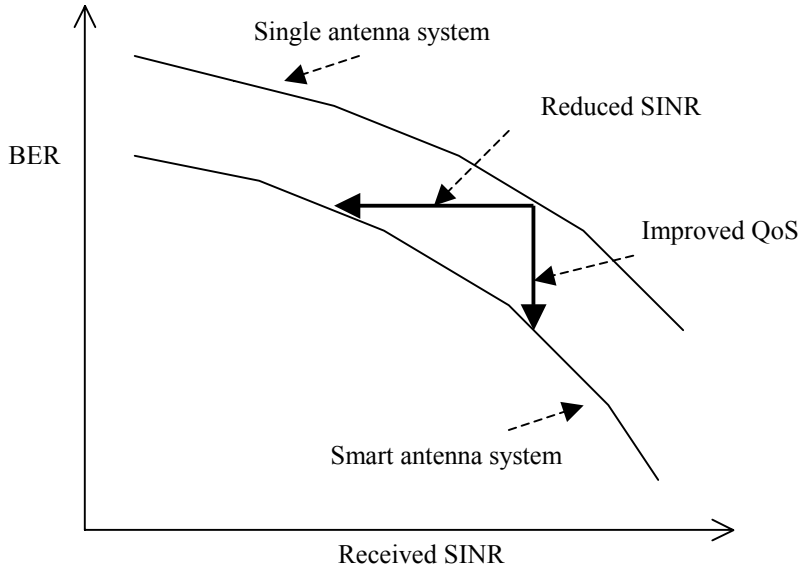

Figure 2-7. Smart Antenna System versus Single Antenna System

2.2 Third Generation Wireless Personal Communication Systems

The CDMA technology will proliferate as the next generation wireless personal communication systems [63],[64]. There are two proposed wideband CDMA systems as the third generation (3G) standards, which meet the International Telecommunication Union (ITU) International Mobile Telecommunications (IMT)-2000 requirements. The first standard is the Wideband CDMA (WCDMA) system, often called Third Generation Partnership Project (3GPP)[24], that was proposed by Europe and Japan. The 3GPP system was designed to be backward compatible with the Global System for Mobile communication (GSM) system, which is a second generation TDMA standard deployed in Europe. The second standard is the cdma2000 system [65] proposed by Telecommunications Industry Association (TIA). The cdma2000 system is evolved from IS-95, which is a second generation CDMA standard deployed in the North America and Korea. For the 3GPP system, there are two modes for the radio access technologies: a time division duplex (TDD) mode and a frequency division duplex (FDD) mode. The 3GPP system with the FDD mode is a CDMA system, but the 3GPP system

with the TDD mode is a combined system of CDMA and TDMA. We consider the 3GPP system with the FDD mode in this dissertation. Hereafter, we will refer to the 3GPP system with the FDD mode as the 3GPP system.

Both the 3GPP system and the cdma2000 system are based on CDMA. However, they are different in chipping rate, spreading code, forward error correction, and others. The most prominent difference between the 3GPP system and the cdma2000 system lies in the synchronization. For the cdma2000 system, all base stations are synchronized, i.e., the system clock of each base station is synchronized to the global positioning system (GPS) clock. So the cdma2000 system is called a synchronous system. Meanwhile, the system clocks used in the 3GPP base stations do not need to be synchronized. Thus, it is called an asynchronous system. Both the 3GPP system and the cdma2000 system continuously provide a common pilot signal in the forward link from the base station to a mobile station. The pilot signal is used to estimate the channel condition, including the signal strength and the phase. This information is used to coherently combine multipath signals.

2.2.1 The 3GPP System

A simple block diagram of a downlink transmitter for the 3GPP system is shown in Figure 2-8. Each bit of physical channels (PCH) is quadrature phase shift keying (QPSK) modulated. The modulated I (in-phase) and Q (quadrature) bits are channelized by multiplying orthogonal variable spreading factor (OVSF) codes at the chipping rate of 3.84 Mcps. All channelized signals are combined first and then scrambled by a complex long code, which is generated from the Gold code set. The scrambled signal and the unscrambled signal of the synchronization channel (SCH) are combined together. The combined signal is pulse-shaped by a root-raised cosine FIR filter with a roll-off factor of $\alpha = 0.22$. The shaped signal is transmitted through the wireless channel. A detailed description of the 3GPP WCDMA system is available in [24] and [25].

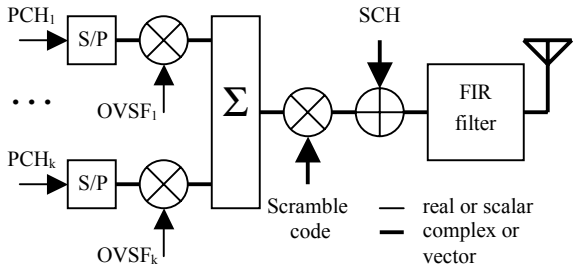

Figure 2-8. Block Diagram of a Downlink Transmitter for the 3GPP System

The transmitted signal $s(t)$ with K users can be represented in the complex form as

$$s(t) = [\alpha_0 d_0(t) C_{ch,0}(t) + \alpha_1 d_1(t) C_{ch,1}(t) + ... + \alpha_K d_K(t) C_{ch,K}(t)] S_{dl}(t), \quad (2\text{-}8)$$

where α_k, $d_k(t)$, and $C_{ch,k}(t)$ are parameters that represent signal strength, user data, and an OVSF code for each user k (k = 1, 2, …, K). $S_{dl}(t)$ is a scramble code for the signal $s(t)$. Note that the first term in (2-8) is for the common pilot channel (CPICH), where $d_0(t)$ represents the fixed pilot symbol (1+i) in QPSK format (i denotes the imaginary unit).

The received signal $r(t)$ at the mobile station receiver is represented as

$$r(t) = \sum_{m=1}^{M} \sqrt{2S_m}\, \xi_m(t) s(t-\tau_m) + I(t) + n(t), \quad (2\text{-}9)$$

where M is the number of multipaths, S_m is the average received signal power associated with the m_{th} path, $\xi_m(t)$ is the complex channel gain for the m_{th} multipath component with time delay τ_m, $I(t)$ is interferences from adjacent cells, and $n(t)$ is a background noise [57]. A rake receiver despreads received multipath signals and coherently combines them. The coherent combining of multipath signals necessitates each multipath signal to be multiplied by the channel coefficient estimated from the despread CPICH signal.

The pilot signal (k = 0) for the m_{th} multipath is despread as shown below:

$$y_{0,m}(n) = \frac{1}{T_p} \int_{nT_p+\tau_m}^{(n+1)T_p+\tau_m} r(t)[S_{dl}(t-\tau_m) C_{ch,0}(t-\tau_m)]^* dt, \quad (2\text{-}10)$$

where T_p is the pilot symbol period, n is the symbol index, and the symbol * represents the complex conjugation. The k_{th} user signal (k = 1, 2, …, K) for the m_{th} multipath is despread in the same manner as shown in (2-10) and is given in (2-11).

$$y_{k,m}(n) = \frac{1}{T_k}\int_{nT_k+\tau_m}^{(n+1)T_k+\tau_m} r(t)[S_{dl}(t-\tau_m)C_{ch,k}(t-\tau_m)]^* dt, \quad (2\text{-}11)$$

where T_k is the data symbol period of the k_{th} user.

Then, the user signal from each multipath $y_{k,m}(n)$ is coherently combined to produce an output signal as shown below:

$$z_k(n) = \sum_{m=1}^{L} y_{k,m}(n)\, y_{0,m}^*(n), \quad (2\text{-}12)$$

where L is the number of rake fingers (which is equal to or smaller than the number of multipaths M). It should be noted that if the spreading factor of the k_{th} user signal SF_k is smaller than that of the pilot signal SF_p, then the same pilot signal $y_{0,m}(n)$ is applied to obtain the $\frac{SF_p}{SF_k}\left(=\frac{T_p}{T_k}\right)$ successive user signal outputs.

2.2.2 The cdma2000 System

Figure 2-9 shows a block diagram of a typical forward link of the cdma2000 system. One frame of user data bits is randomly generated with a variable traffic data rate of 9600 bps, 4800 bps, 2700 bps, or 1500 bps. The generated data bits are appended with cyclic redundancy check (CRC) and tail bits. The data bits are convolutional coded with the rate of ¼ and the constraint length of 9 and block interleaved. Then, data bits are parallelized for QPSK data modulation, and each parallel data bit is spread by Walsh code with the spreading factor of 64 and the chipping rate of 1.2288 Mcps. The resultant data signal is added with the pilot signal, the paging signal, the sync signal, and all the other users' signals. The added signal is quadrature modulated by two short-PN sequences and up-sampled by 8, and then is applied to shaping filters. The shaped signal is transmitted through the channel.

The received signal is shaped back and down-sampled by 8. A four-finger rake receiver despreads each multipath signal and combines the despread multipath signals. The despread and combined signal is applied to the channel decoder consisting of a block deinterleaver, a Viterbi decoder, and a CRC decoder. A detailed description of the cdma2000 system is available in [65].

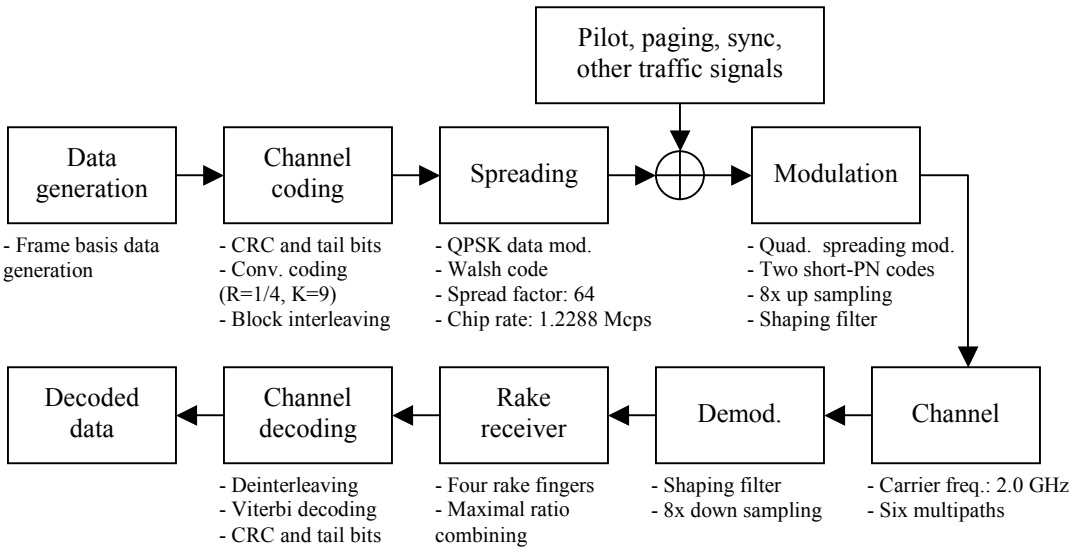

Figure 2-9. Forward Link of the cdma2000 System

2.3 Channel Model

Because the channel model influences the design of receivers and their performance, channel modeling is important for evaluation of a smart antenna system. In the uplink of the 3G systems, each user signal is transmitted asynchronously and traverses different paths from the mobile station to the base station. Thus, the main source of interference is coming from other users' signals within the same cell (intra-cell interference). However, in the downlink of the 3G systems, the signal transmitted from the base station is the superposition of all active users' signals and common control signals. The desired user signal and multiple access interference signals traverse the same paths, but they are inherently orthogonal with each other. So it does not pose a serious problem at handsets.

A multipath signal is effectively an interference signal to another multipath signal. However, a rake receiver can manage multipath signals to its advantage to improve the quality of received signal. Another source of interference in the downlink is coming from adjacent cells (inter-cell interference), which can have a substantial impact on the performance. Note that the

latter case becomes manifest when the soft handover occurs. Since the number of adjacent base stations and hence the number of interference signals from these base stations is small, a dual antenna system is a good candidate to combat such interference. It should be noted that a receiver with M antennas can suppress M-1 interfering signals [58].

For a wireless channel model, three components are considered for a typical variation in the received signal level [66]. The three components are mean path loss, lognormal fading (or slow fading), and Rayleigh fading (or fast fading), as shown in Figure 2-10. Both theoretical and measurement based models indicate that an average received signal level decreases logarithmically with distance (which is the mean path loss). The difference in path loss at different locations at the same transmitter-receiver distance is modeled as a lognormal random variable (which is the lognormal fading). Reflections due to many scatters in the vicinity of the receiver cause the received signal to be time varying, in which the envelope of a multipath signal follows a Rayleigh distribution (which is the Rayleigh fading). A channel model also needs to consider these spreads: i) delay spread due to multipath propagation, ii) Doppler spread due to mobile motion, and iii) angle spread due to scatter distribution.

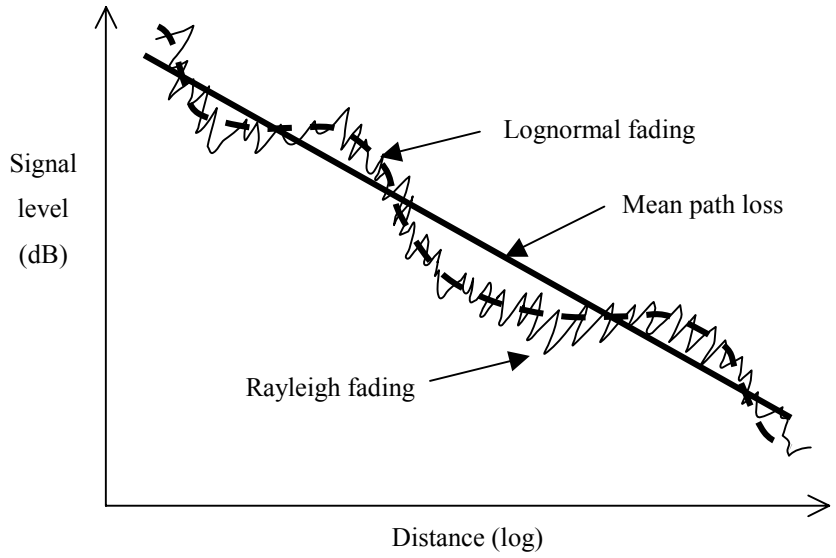

Figure 2-10. Variation of Received Signal Level

Based on the narrowband model for the signal received by an antenna array, a small time delay between two antennas can be modeled as a simple phase shift. Consider a case where a

signal r(t) arrives at the linear antenna array as shown in Figure 2-11. Then, the received signals, $x_1(t)$ and $x_2(t)$, at two adjacent antennas, have a phase difference. If the signal is incident on the antenna array with the angle of arrival (θ), then the phase difference between the two received signals is $2\pi d\sin\theta/\lambda$, where d is the antenna spacing, λ is the wavelength of the carrier, and θ is the angle of arrival.

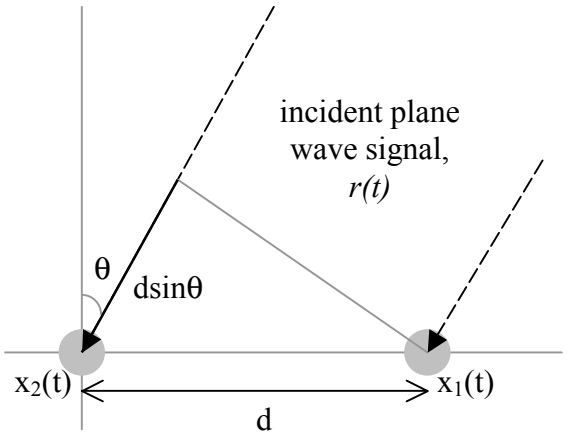

Figure 2-11. Phase Difference in the Linear Antenna Array

To obtain the channel profile (such as delay, average power, and angle of arrival of each multipath signal), not only a channel model based on statistical properties of the channel, but also a channel model based on measurement data should be considered. For a statistical channel model, the geometrically based single bounce (GBSB) circular and elliptical models [34],[36] are applied. Meanwhile, the ITU channel profiles [37] are applied for the measurement based channel model. A statistical channel model is useful in simulating a different channel environment, in which multipath parameters are changed depending on the position of the scatters. Even though multipath parameters are fixed in a measurement based channel model, it is useful to reflect the real operating channel conditions.

2.3.1 GBSB Model

There are two types of the GBSB models, circular and elliptical. The GBSB circular model is applicable for macrocell environments found in rural or suburban areas. Meanwhile, the GBSB

elliptical model is applicable for microcell environments found in urban areas. The GBSB models assume that multipath signals are created by single reflections of scatters, which are uniformly distributed in a predefined elliptical and circular geometry. Delays, average power levels, and angles of arrival (AOAs) of each multipath signal are determined from the locations of scatters.

In the GBSB circular model, scatters are assumed to locate within a circle around a mobile station as shown in Figure 2-12. The two major parameters of the model are D and τ_m, where D is the distance between a base station and a mobile station, and τ_m is the maximum time of arrival (TOA), i.e. maximum delay. The maximum TOA τ_m is used to define the radius of the circle such that the radius $R_m = \frac{c\tau_m - D}{2}$, where c is the speed of light. Related equations with detailed derivations, including the joint TOA-AOA probability density function at the mobile station, are available in [36].

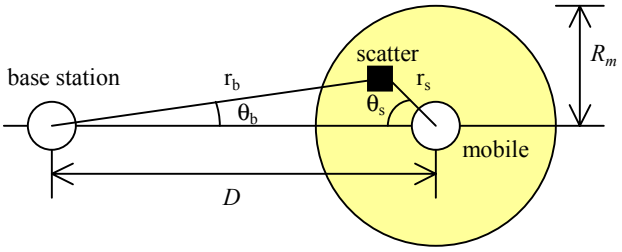

Figure 2-12. Geometry of the GBSB Circular Model

In the GBSB elliptical model, a base station and a mobile station are assumed to locate at the foci of an ellipse as shown in Figure 2-13. The two major parameters of the model are D and τ_m, where D is the distance between a base station and a mobile station, and τ_m is the maximum delay. The maximum delay τ_m is used to define the boundary (or a major axis and a minor axis) of the ellipse such that the major axis $a_m = \frac{c\tau_m}{2}$, where c is the speed of light. Due to the symmetry of the geometry with respect to the base station and the mobile station, the joint TOA-AOA probability density function of the mobile station is the same as that of the base station [36].

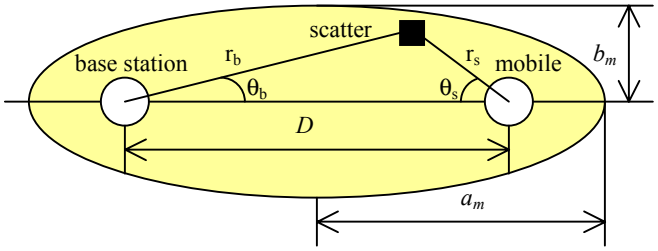

Figure 2-13. Geometry of the GBSB Elliptical Model

2.3.2 ITU Channel Model

The ITU channel model [37] is a measurement based channel model proposed for the 3GPP WCDMA system. Delay and average power of each multipath for the ITU channel models are summarized in Table 2-2. Four or six multipath signals (M) are generated in the wireless channel depending on the channel type as shown in the table, respectively. The number of rake fingers (L) used in the receiver is also presented in the table.

Table 2-2. ITU Channel Profiles

Channel Profile \ Multipath		M1	M2	M3	M4	M5	M6	No. of Fingers (L)
Pedestrian A	Delay (ns)	0	110	190	410	NA	NA	2
(M = 4)	Power (dB)	0	-9.7	-19.2	-22.8			
Pedestrian B	Delay (ns)	0	200	800	1200	2300	3700	5
(M = 6)	Power (dB)	0	-0.9	-4.9	-8.0	-7.8	-23.9	
Vehicular A	Delay (ns)	0	310	710	1090	1730	2510	4
(M = 6)	Power (dB)	0	-1.0	-9.0	-10.0	-15.0	-20.0	
Vehicular B	Delay (ns)	0	300	8900	12900	17100	20000	4
(M = 6)	Power (dB)	-2.5	0	-12.8	-10.0	-25.2	-16.0	

2.4 Low-Power VLSI Design

There have been two main drives for low-power VLSI design. One drive is the increased market demand for portable electronics powered by batteries, and the other is the advanced processing technology [68]. For portable electronics such as cellular handsets, longer operation time without replacing/recharging batteries is highly desirable. Low-power design is a key issue for such applications. As the processing technology advances, the device density increases and the feature size decreases, which in turn causes high power dissipation. High power dissipation causes a problem for the packaging and for the reliable operation. It is especially true for high performance microprocessor design.

The power dissipation of static CMOS circuits is composed of static power dissipation and dynamic power dissipation [69]. Reverse biased PN junction current and subthreshold channel are main sources of the static power dissipation. Meanwhile, capacitive current and short circuit current are main sources of the dynamic power dissipation. The dominant factor for the power dissipation in CMOS circuits is the charging/discharging of switching capacitances. Therefore, most low-power design techniques are focused to reduce power dissipation due to capacitor charging/discharging.

The capacitive power dissipation is given by the following well-known golden equation,

$$P_{cap} = \alpha C_L V^2 f \tag{2-13}$$

where α is the switching activity, C_L is the switching capacitance, V is the supply voltage, and f is the operating frequency. Thus, the low-power VLSI design is to reduce one or several of the four factors. Since the dependency of power dissipation on the supply voltage is quadratic, reduction of the supply voltage is the most dramatic for the low-power design. However, the supply voltage is often not under the designer's control. Low-power design usually requires tradeoffs between the circuit area, increased latency, and speed.

Low-power design techniques can be applied at different design abstract levels: system level, algorithm level, architecture level, circuit/logic level, and technology level. Generally, low-power design techniques applied at the higher design abstract level have more impact on reducing the total power dissipation. Although many low-power design techniques have been proposed [68],[70]-[72], some of them are specific to certain applications or systems. Thus one should consider carefully when applying a low-power design technique to his/her own system.

Figure 2-14 shows the block diagram of a generic direct sequence (DS)-CDMA receiver with L rake fingers [73]. In general, the signal processing requirements of DS-CDMA based systems can be broken down into two broad categories, namely, **chip rate** processing and **symbol rate** processing. All the blocks to the left of the dashed line in Figure 2-14 typically operate at the chip rate (which is 1.2288 MHz or 3.84 MHz for the cdma2000 system or the 3GPP WCDMA system, respectively) or a small multiple thereof, whereas all the blocks to the right of the dashed line operate at the symbol rate which is typically much lower. As noted in (2-13), the capacitive power dissipation is proportional to the operating frequency. Hence, blocks operating at a higher frequency dissipate more power, and hence low-power design of these blocks has bigger impact on the overall power dissipation. This is illustrated below. Thus, the low-power design on the blocks operated at the chip rate is a more efficient way to reduce the power dissipated by a CDMA receiver.

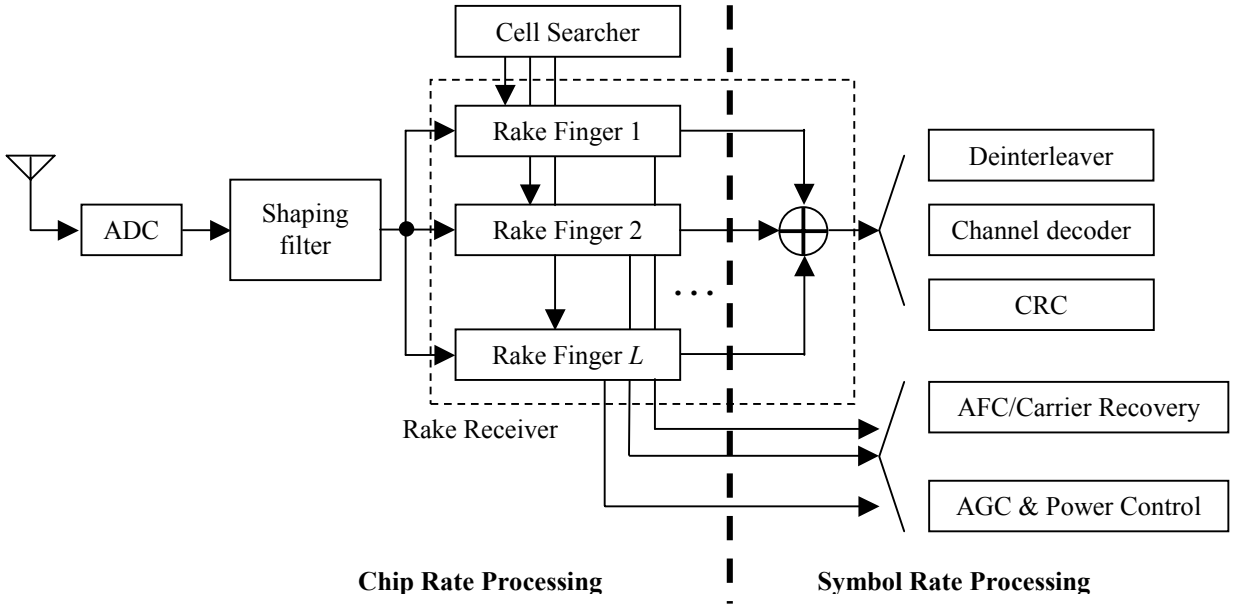

Figure 2-14. Block Diagram of a DS-CDMA Receiver

2.5 Generalized Selection Combining

In addition to classical diversity combining techniques, a generalized selection combining has been proposed, investigated, and analyzed as a new diversity combining technique [38]-[50]. Instead of selecting all the branches as for the case of MRC, the generalized selection combining (GSC) technique chooses the best m branches out of L branches depending on the SNR or the signal strength and coherently combines them. The GSC is also called hybrid SC/MRC. The number of selected branches m is decided *a priori* for the original GSC [38]-[50], while it varies dynamically in [51]-[53]. For the latter approach, selection of branches whose SNRs are larger than a given threshold is proposed in [51] and [52], and it is called **absolute threshold GSC (AT-GSC)**. Alternatively, selection of a branch whose relative SNR over the maximum SNR among all branches, $\frac{SNR_i}{SNR_{\max}}$, is larger than a threshold is proposed in [51] and [53]. This method is called **normalized threshold GSC (NT-GSC)**.

We investigate the characteristics of the three GSC methods, the original GSC, the AT-GSC, and the NT-GSC. It is assumed that the instantaneous SNR γ_i of a branch i is known and $\gamma_1 \geq \gamma_2 \geq \ldots \geq \gamma_L$ for a rake receiver with L branches.

The original GSC denoted as GSC (m, L) selects the best m branches out of L branches where m is fixed, and its combined SNR is obtained as $\sum_{i=1}^{m} \gamma_i$. The combined SNR of the original GSC is upper and lower bounded by GSC (L, L) and GSC (1, L), respectively. GSC (L, L) and GSC (1, L) are, in fact, the MRC and the SC.

The AT-GSC denoted as AT-GSC (T_a, L) selects a branch whose SNR γ_i is larger than a given threshold T_a, i.e., it finds m such that $\gamma_m \geq T_a$ and $\gamma_{m+1} < T_a$. The maximal SNR for the AT-GSC is AT-GSC (0, L), which is the MRC. The NT-GSC denoted as NT-GSC (T_n, L) selects a branch i whose normalized SNR $\frac{\gamma_i}{\gamma_1}$ is larger than a given threshold T_n. Note that γ_1 is the maximal SNR of among all the branches and $0 \leq T_n \leq 1$. The NT-GSC selects m branches such that $\frac{\gamma_m}{\gamma_1} \geq T_n$ and $\frac{\gamma_{m+1}}{\gamma_1} < T_n$. The upper and the lower bounds of the SNR for the NT-GSC are NT-GSC (0, L) and NT-GSC (1, L), respectively. Note that NT-GSC (0, L) and NT-GSC (1, L)

are the MRC and the SC, respectively. For comparison, characteristics of each GSC technique are summarized in Table 2-3.

Table 2-3. Comparison of Three Combining Techniques

Technique	Given condition	Number of selected branches	Combined SNR	Lower/upper bound
GSC	number of branches, m	fixed m	$\sum_{i=1}^{m}\gamma_i$	GSC (1, L) / GSC (L, L)
AT-GSC	threshold, T_a	variable m such that $\gamma_m \geq T_a$ and $\gamma_{m+1} < T_a$	$\sum_{i=1}^{m}\gamma_i$	AT-GSC (∞, L) / AT-GSC (0, L)
NT-GSC	threshold, T_n ($0 \leq T_n \leq 1$)	variable m such that $\frac{\gamma_m}{\gamma_1} \geq T_n$ and $\frac{\gamma_{m+1}}{\gamma_1} < T_n$	$\sum_{i=1}^{m}\gamma_i$	NT-GSC (1, L) / NT-GSC (0, L)

The combined SNRs of the GSC methods are shown in Figure 2-15. The SNRs are **average values** over a time period. Figure 2-15 (a) shows a GSC (m, L), where L = 4. A GSC (m, L) with a fixed L performs better (higher SNR and lower BER) as m increases, while a GSC (m, L) with a fixed m performs better as L increases [43]. The AT-GSC (T_a, L) and the NT-GSC (T_n, L) have the same trend in the combined SNRs, which are shown in Figure 2-15 (b). The AT-GSC and the NT-GSC performs better as the threshold value becomes smaller. Note that they can have more than four combined SNRs for a given average branch SNR.

For the AT-GSC and the NT-GSC techniques, the average number of rake fingers activated is a function of a given threshold as analyzed in [53] or is also shown in Chapter 5. The average number of rake fingers activated can be any rational number (not only an integer) for a given threshold value. Thus, the AT-GSC and the NT-GSC can be viewed as a general case of GSC (m, L), in which m can be any rational number including an integer number. As shown in Figure 2-15, the number of distinctive combined SNRs is L for the GSC, while the number of distinctive combined SNRs is equal to the number of threshold values for the AT-GSC and the NT-GSC. The number of distinctive combined SNRs is seven for the example given in Figure 2-15 (b).

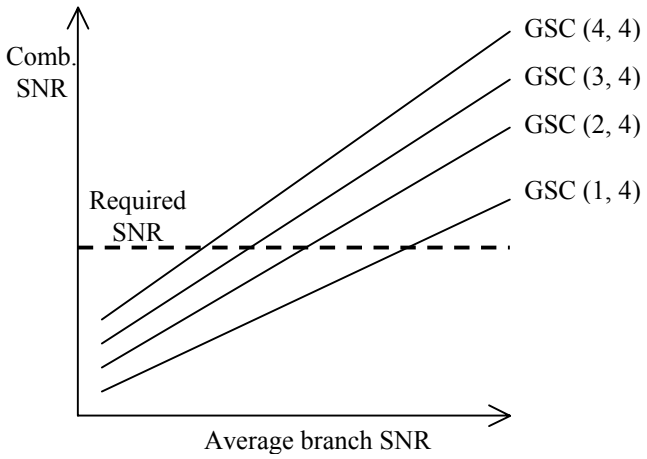

(a) Original GSC

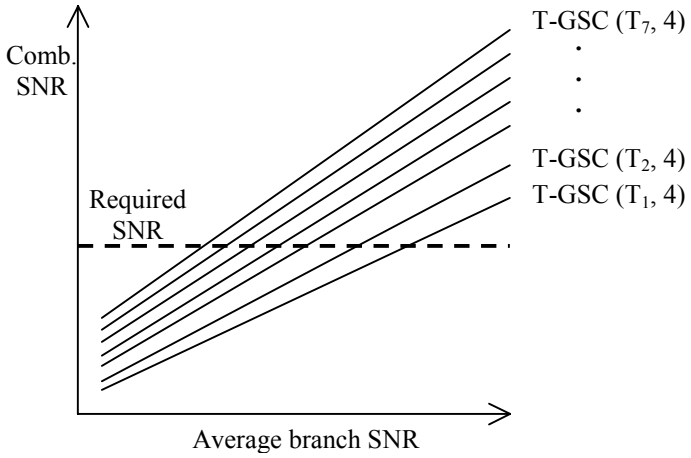

(b) AT-GSC or NT-GSC

Figure 2-15. Combined SNR for GSC, AT-GSC, and NT-GSC

It is possible for the AT-GSC that the maximal SNR is smaller than the threshold, so that none of the finger is selected. Even if all the fingers are turned off momentarily, it may be able to meet the required BER. However, such an occasion should be avoided to prevent burst errors that are difficult to correct for a channel decoder. For practical operation, we need to modify the selection rules for the AT-GSC as follows. A branch with maximal SNR is always selected, even if the maximal SNR is smaller than a given threshold. In this case, the minimal SNR AT-GSC (∞, L) becomes the SC.

2.6 Monte Carlo Simulation

Monte Carlo statistical method is used to determine the BER of a digital communication system [74]. Consider we want to measure the BER of a communication system via simulation. We should simulate the transmission of N bits and count the number of erroneous bits at the receiver. Let $N_e(N)$ be the number of errors counted in a simulation of N bits. Then, the BER is estimated as

$$\hat{P}_e(N) = \frac{N_e(N)}{N}. \tag{2-14}$$

According to the law of large numbers, the true BER can be obtained as $P_e = \lim_{N\to\infty} \hat{P}_e(N)$. However, simulating an infinite number of bits in order to determine P_e is impractical. If we want to the estimate of the BER to be within βx100 % of the true value with the probability of 1-α, then the number of bits necessary for simulation is obtained as follows [75].

$$N = \frac{1}{P_e}\left(\frac{Q^{-1}(\alpha/2)}{\beta}\right)^2, \tag{2-15}$$

where Q^{-1} is the inverse function of the Q-function. To determine the number of simulation bits, the quantity P_e should be estimated. For a large N, we can assume that $\hat{P}_e(N) \approx P_e$. Then, the number of errors is obtained using (2-14) and (2-15) and is as follows.

$$E[N_e(N)] = NP_e = \left(\frac{Q^{-1}(\alpha/2)}{\beta}\right)^2. \tag{2-16}$$

Thus, the simulation can be stopped when the number of errors given in (2-16) is reached. For example, $\left(\frac{Q^{-1}(\alpha/2)}{\beta}\right)^2 = 1536.6$ when α = 0.05 and β = 0.05. This implies that if we count about 1537 errors, then we can be assured with 95 % confidence that the estimate is within 5 % of the true value. For reference, some representative numbers for practical simulations are summarized in Table 2-4.

Table 2-4. The Number of Errors to Be Counted

α	β	$N_e(N)$
0.02 (98%)	0.02 (2%)	13530
0.02 (98%)	0.01 (1%)	54119
0.01 (99%)	0.02 (2%)	16588
0.01 (99%)	0.01 (1%)	66349

2.7 Summary

We provided preliminary studies for the proposed research in this chapter. The basic concepts of smart antenna systems and previous works related to smart antennas at handsets were described in Section 2.1. Two third generation wireless systems were briefly reviewed in Section 2.2. Some characteristics for a wireless channel as well as two models for a channel profile were shortly described in Section 2.3. The fundamental concepts for low-power VLSI design were provided in Section 2.4. A generalized selection combining method as a new diversity technique was introduced in Section 2.5. Finally, a brief description on Monte Carlo simulation approach was provided in Section 2.6.

These preliminary studies provided in this chapter will be a step stone of the proposed research described in the next chapter.

Chapter 3 Smart Antennas at Handsets and Adaptive Rake Combining Scheme

In this chapter, we propose dual smart antennas at handsets for the 3G wireless personal communication systems and a new combining scheme called hybrid combining. To model dual antenna signals, several channel models are considered. We also propose a new GSC method called minimum selection GSC and an adaptive rake combining scheme to reduce power dissipation of a mobile rake receiver.

3.1 Smart Antennas at Handsets

We propose a dual smart antenna system incorporated into handsets for the 3G wireless personal communication systems in which the two antennas are separated by a quarter wavelength (3.5 cm) [28]-[32]. To investigate the performance of the proposed dual antenna handsets, different combining schemes are exploited. To combine each multipath signal, a diversity combining [28],[30], an adaptive combining [29],[32], and a new proposed combining scheme called hybrid combining [31] are employed.

3.1.1 Diversity Combining

A diversity combiner combines the dual antenna signals using a diversity combining scheme. Three diversity combining schemes—selection diversity (SD), equal gain combining (EGC), and maximal ratio combining (MRC)—are considered. The SD scheme selects the signal with higher power. The EGC scheme simply adds two signals with an equal weight of 0.5. The

MRC scheme weights each signal by its signal level and adds them according to the formula, $a|a|+b|b|$, where a and b are the two rake receiver outputs or the two rake finger outputs.

To process the dual antenna signals, two levels of diversity combining schemes are considered. The first scheme is the rake level diversity combining in which a diversity combiner combines rake receiver outputs. The second one is the finger level diversity combining in which a diversity combiner combines finger outputs. The two schemes are shown in Figure 3-1. For simplicity, only three fingers are depicted in the figure. It should be noted that all finger signals are pre-weighted (according to the magnitude and phase information of the pilot signal) before a diversity combiner combines finger outputs.

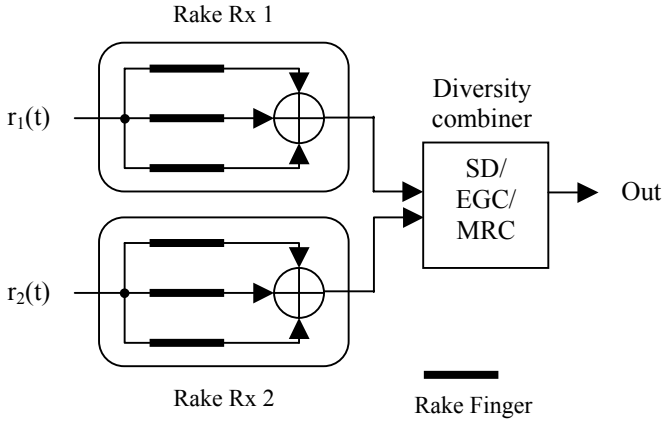

(a) Rake Level Diversity Combining

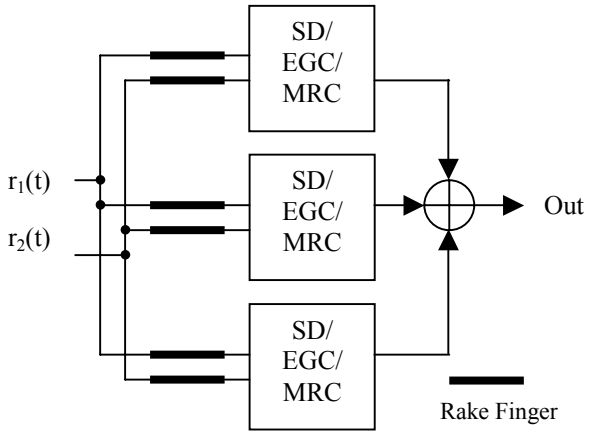

(b) Finger Level Diversity Combining

Figure 3-1. Diversity Combining

3.1.2 Adaptive Combining

To combine each multipath signal from dual antennas, an adaptive combining scheme based on the normalized least mean square (N-LMS) algorithm described in Chapter 2 is applied, in which antenna weights are recursively obtained to minimize the mean square error. The considered dual antenna system with the adaptive combiner (AC) is shown in Figure 3-2.

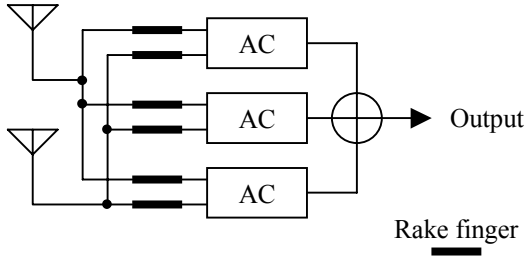

Figure 3-2. Adaptive Combining

The procedure to obtain the antenna weights is explained below. A new antenna weight $\omega^{(j)}_m(n+1)$ for the m_{th} multipath on the j_{th} antenna is computed as follows [55].

$$\omega^{(j)}_m(n+1) = \omega^{(j)}_m(n) + \mu\,(y^{(j)}_{0,m}(n) / \sum_{j=1}^{2} |\, y^{(j)}_{0,m}(n)|^2)\, e^*_{0,m}(n), \tag{3-1}$$

where $\omega^{(j)}_m(n)$ is the current antenna weight, $y^{(j)}_{0,m}(n)$ is the despread pilot signal for the m_{th} multipath on the j_{th} antenna, μ is the step size in the range of $0 < \mu < 2$, and $e_{0,m}(n)$ is the error signal. The error signal $e_{0,m}(n)$ is expressed as $\check{z}_{0,m}(n) - z_{0,m}(n)$, where $\check{z}_{0,m}(n)$ is the desired reference pilot signal for the m_{th} multipath signal and $z_{0,m}(n)$ is the combined pilot signal. We assume that the pilot signals from each antenna are ideally phase shifted and combined to obtain the desired reference pilot signal. Hence, the desired reference pilot signal $\check{z}_{0,m}(n)$ is obtained by averaging the despread pilot signal such that

$$\check{z}_{0,m}(n) = \frac{(1+\mathrm{i})}{\sqrt{2}} \frac{\sum_{l=0}^{Q-1} (|\, y^{(1)}_{0,m}(n-l)\,| + |\, y^{(2)}_{0,m}(n-l)\,|)}{Q}, \tag{3-2}$$

where Q is the number of pilot symbols to be averaged and (1+i) is the known transmitted pilot symbol. The combined pilot signal $z_{0,m}(n)$ for the m_{th} multipath is obtained using the pilot signals $y^{(j)}{}_{0,m}(n)$ from each antenna and the current antenna weights $\omega^{(j)}{}_{m}(n)$ such that

$$z_{0,m}(n) = \sum_{j=1}^{2} y^{(j)}{}_{0,m}(n)\,\omega^{(j)}{}_{m}{}^{*}(n). \tag{3-3}$$

After the antenna weights are obtained, the despread k_{th} user signal for the m_{th} multipath from each antenna is weighted and combined as

$$z_{k,m}(n) = \sum_{j=1}^{2} y^{(j)}{}_{k,m}(n)\,\omega^{(j)}{}_{m}{}^{*}(n), \tag{3-4}$$

where $y^{(j)}{}_{k,m}(n)$ is the despread k_{th} user signal for the m_{th} multipath on the j_{th} antenna and $\omega^{(j)}{}_{m}(n)$ is the obtained antenna weight. Then, the combined user signal from each multipath $z_{k,m}(n)$ is coherently combined to produce an output as shown below:

$$z_{k}(n) = \sum_{m=1}^{L} z_{k,m}(n)\, z_{0,m}{}^{*}(n), \tag{3-5}$$

where L is the number of rake fingers. If the spreading factor of the k_{th} user signal SF_k is smaller than that of the pilot signal SF_p, then the same antenna weight $\omega^{(j)}{}_{m}(n)$ is applied to obtain the $\frac{SF_p}{SF_k}$ successive user data symbols.

Finally, the antenna weight should adapt fast enough to track the fading of the desired and interfering signals, but it should be much slower than the data rate.

3.1.3 Hybrid Combining

Diversity combiner (DC) exploits the spatial diversity among multiple antenna signals and achieves higher performance when multiple antenna signals are less correlated. An adaptive combiner (AC) combines corresponding finger outputs of the two antennas with appropriate antenna weights, which are recursively obtained based on the N-LMS algorithm. Since these two combining schemes exhibit somewhat opposite and complementary characteristics, a new combining scheme is proposed to exploit the advantages of the both schemes. As observed in Chapter 4, the DC and the AC exhibit somewhat opposite trends in SINR and mobile velocity. One may be tempted to select a better performing scheme (among DC and AC) based on current

operating environment. However, the approach is impractical, as we cannot accurately estimate the performance or the BER of each scheme due to imprecise estimation of the SINR, and the difficulty of measuring the mobile velocity. To circumvent these problems, we propose a simple, yet effective, scheme called a hybrid combiner (HC). The proposed HC combines DC and AC outputs using MRC. The block diagram of the proposed HC is presented in Figure 3-3. Since it is difficult to compute the SNR, the instantaneous signal plus noise (S+N) value is used to weight each combiner output instead of its SNR.

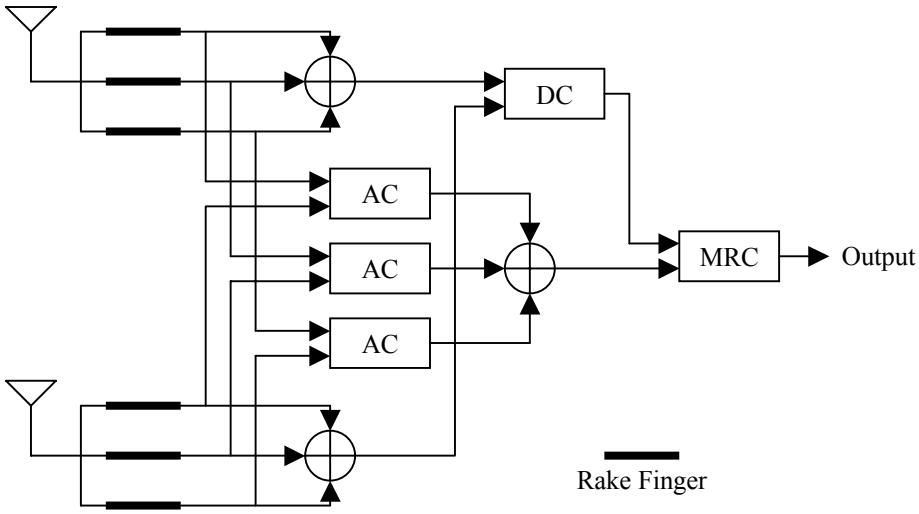

Figure 3-3. Hybrid Combiner for a Dual Antenna System

3.2 Channel Model

We assume that the dual antennas at a handset are identical, omnidirectional, and separated with a quarter wavelength of the carrier. Among the three components to be considered for a typical variation in the received signal level, the lognormal fading is not included in our channel model for the 3GPP WCDMA system; this model is implemented with Matlab tool. Later, we will include the lognormal fading in the channel model for the cdma2000 system, a model implemented with the SPW tool.

3.2.1 Loosely and Spatially Correlated Fading Channel Models

First, we consider two types of the channel model specific to the dual antenna signals: i) loosely correlated fading channel model (LCFCM) and ii) spatially correlated fading channel model (SCFCM). Each antenna signal is assumed to have independent Rayleigh fading in the LCFCM. In the SCFCM, each antenna signal is subject to the same Rayleigh fading, but is different in the phase due to a non-zero angle of arrival (AOA). Each multipath signal has a different AOA. It is assumed that a multipath signal has the same arrival time for the two antennas in the channel model. The two types of the channel model are illustrated in Figure 3-4. The signal s(t) represents the transmitted signal from the base station in the figure, and signals $r_1(t)$ and $r_2(t)$ represent the two received antenna signals at the mobile station. A channel model with less correlated dual antenna signals, which is the LCFCM in our model, is expected to yield higher diversity gain [10]. We believe that the actual channel of dual antenna signals (for both the diversity combining and the adaptive combining) lies in between these two channel models.

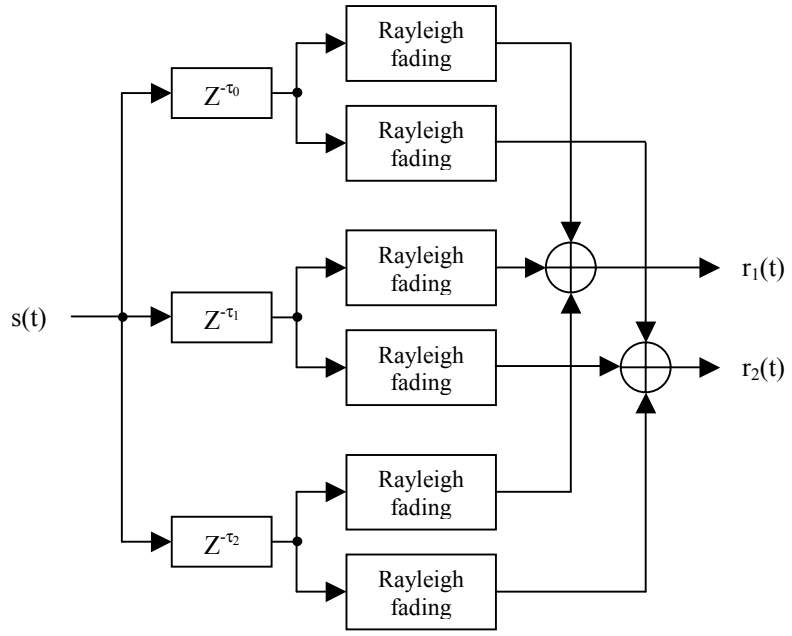

(a) Loosely Correlated Fading Channel Model

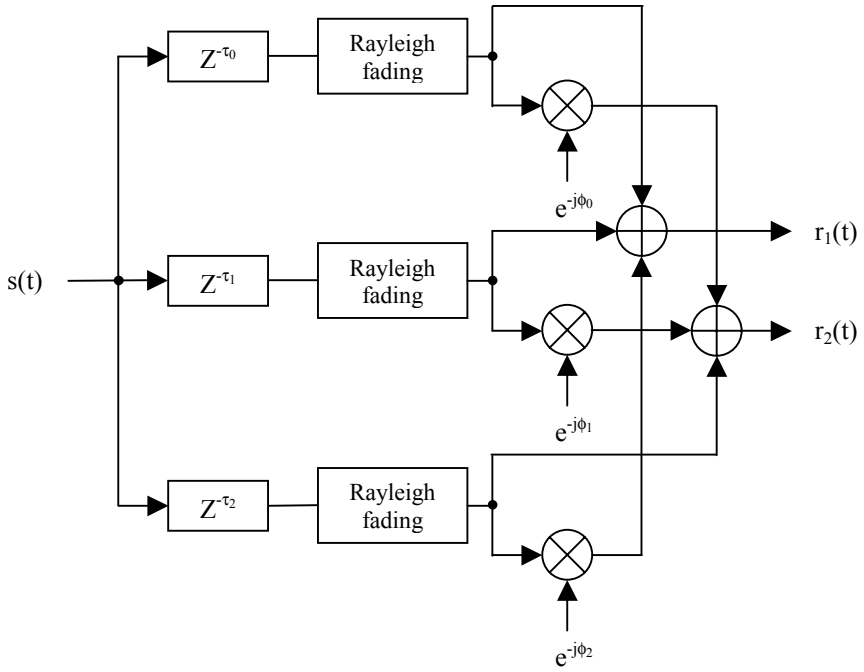

(b) Spatially Correlated Fading Channel Model

Figure 3-4. Two Types of the Channel Model

3.2.2 Envelope Correlated Fading Channel Model

Two channel models considered in the previous subsection, the LCFCM and the SCFCM, are useful to evaluate the upper and the lower bounds of the system performance. To model the actual channel of dual antenna signals lying in between these two channel models, we modify the procedure developed by Ertel and Reed [33] and propose an envelope correlated fading channel model (ECFCM).

Two Rayleigh fading antenna signals for each multipath in the ECFCM are assumed to have an envelope correlation and a phase difference due to a non-zero AOA. It is assumed that a multipath signal has a different AOA, but the same arrival time for the two antennas in the channel model. The channel model with three multipath signals is illustrated in Figure 3-5.

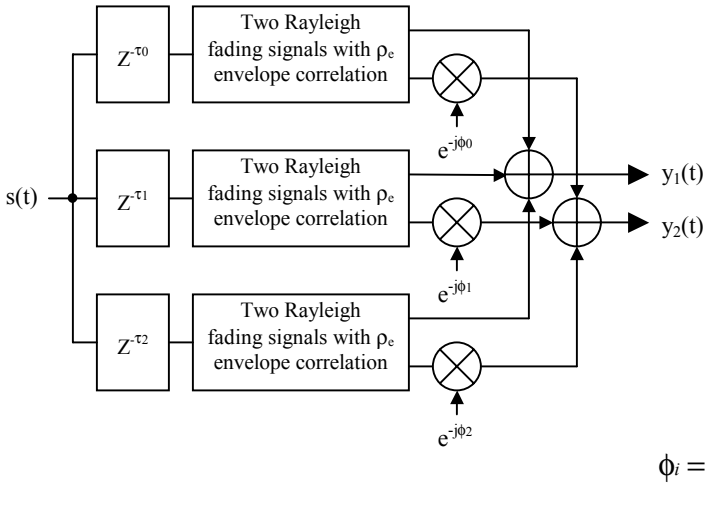

Figure 3-5. Envelope Correlated Fading Channel Model

The following procedure is used to obtain two antenna signals for each multipath. For a given envelope correlation ρ_e, two envelope correlated Rayleigh fading signals $x = [x_1\ x_2]^T$ are obtained from two uncorrelated (independent) Rayleigh fading signals $w = [w_1\ w_2]^T$ and a coloring matrix **L** such as $x = \mathbf{L}w$ [33]. The coloring matrix **L** is given as

$$\mathbf{L} = \begin{bmatrix} 1 & 0 \\ \frac{1}{\sqrt{2}}\kappa(1+j) & \sqrt{1-\kappa^2} \end{bmatrix}, \tag{3-6}$$

where κ is a parameter related to the envelope correlation ρ_e, and it is approximated by $\sqrt{\rho_e}$. (A more accurate method to obtain κ from a given ρ_e is described in [33].) As one may notice by inspection, the phase difference between two obtained signals x_1 and x_2 is independent of an AOA.

To make the phase difference a function of an AOA as a narrowband signal, new signals $y = [y_1\ y_2]^T$ can be obtained from x such that

$$y = \begin{bmatrix} y_1 \\ y_2 \end{bmatrix} = \begin{bmatrix} x_1 \\ abs(x_2)exp(j[angle(x_1) - \frac{2\pi d sin\theta}{\lambda}]) \end{bmatrix}, \tag{3-7}$$

where d, θ, and λ are the antenna distance, the AOA, and the carrier wavelength, respectively. The newly obtained signals y are the desired Rayleigh fading signals for each multipath with an envelope correlation ρ_e and a phase difference.

Experimental results indicate that the envelope correlation ρ_e of dual spatial diversity antennas for the narrowband signal is in the range from 0.12 to 0.74 for various environments provided the two antennas are closely spaced ($0.1\lambda \sim 0.5\lambda$) [19]. Figure 3-6 shows examples of envelopes and phases of two Rayleigh fading signals in the ECFCM, which are generated using the above procedure for $\rho_e = 0.5$ and 120 Hz of Doppler frequency.

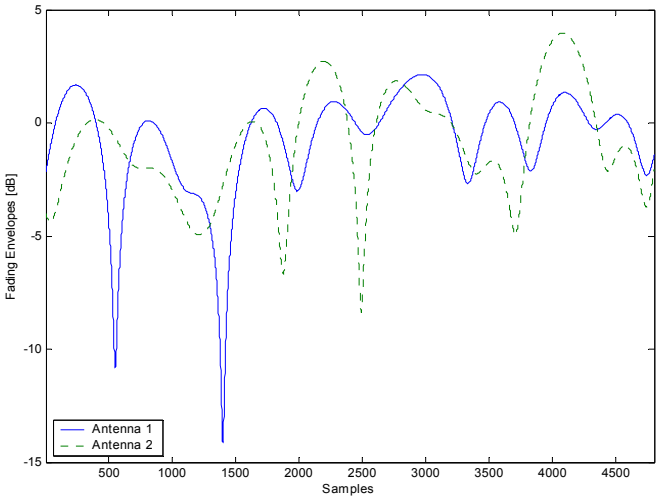

(a) Envelope

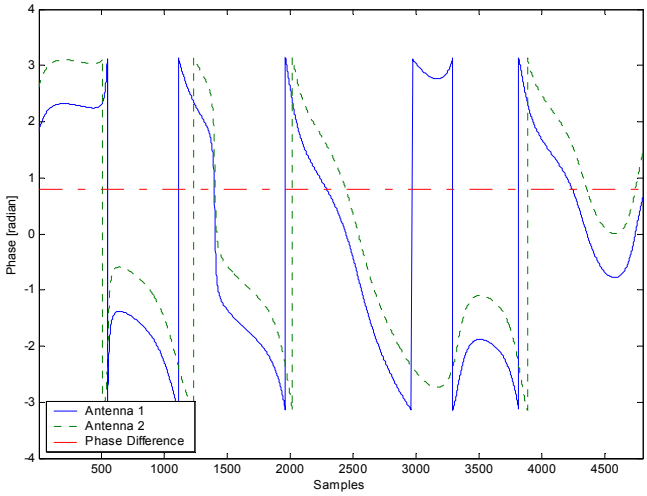

(b) Phase

Figure 3-6. Two Rayleigh Fading Signals in the ECFCM

3.2.3 Procedure to Obtain Channel Profile using the GBSB Models

The following procedure is used to obtain a channel profile using the GBSB model. A scatter is placed randomly within a predefined ellipse or circle. The distance r_b between the base station and the scatter and the distance r_s between the scatter and the mobile station are obtained from the location of the scatter. The propagation delay τ is calculated as $(r_b + r_s)/c$, where c is the

speed of light. Then a new scatter is placed randomly, and the propagation delay is calculated in the same manner. If the difference between the new propagation delay and any existing propagation delay is greater than one chip delay (which is about 260 ns for the 3GPP WCDMA system), then the scatter is selected. Otherwise, the scatter is deleted, as the multipath signal cannot be resolved by a rake finger. The process repeats until a predefined number of multipaths (or scatters) is achieved. The unit average power P_0 is assigned to the multipath signal with the smallest propagation delay τ_0. The average power of a multipath signal P_i, $i \neq 0$ is calculated using the mean path loss model [66] such that $P_i = P_0 * (\tau_i/\tau_0)^{-n}$, where τ_i is the propagation delay of the multipath and n is the path loss exponent. We set n to 3.5 in our simulation. The AOA of each multipath signal is obtained from the location of the scatter and the mobile station.

Figure 3-7 illustrates examples of the channel profiles of four multipath signals obtained through the procedure described above. The first channel profile in Figure 3-7 (a) is for the GBSB circular model, where the distance D was set to 2000 m to simulate a rural or a suburban environment and the maximum delay τ_m to 35 chips (equivalently 9.1 μs) in the process. The second channel profile in Figure 3-7 (b) is for the GBSB elliptical model, where the distance D was set to 800 m in consideration of an urban environment and the maximum delay τ_m to 20 chips (equivalently 5.2 μs) in the process. The maximum delays for the two GBSB models were chosen, so that the time difference between the maximum delay τ_m and the delay for the line-of-sight signal (= D/c) is roughly equal (which is about 9.5 chips for the 3GPP WCDMA system) for the two models. As can be observed from the two figures, all the multipath signals of the two models lie in the time window of around 10 chips due to the choice of maximum delays.

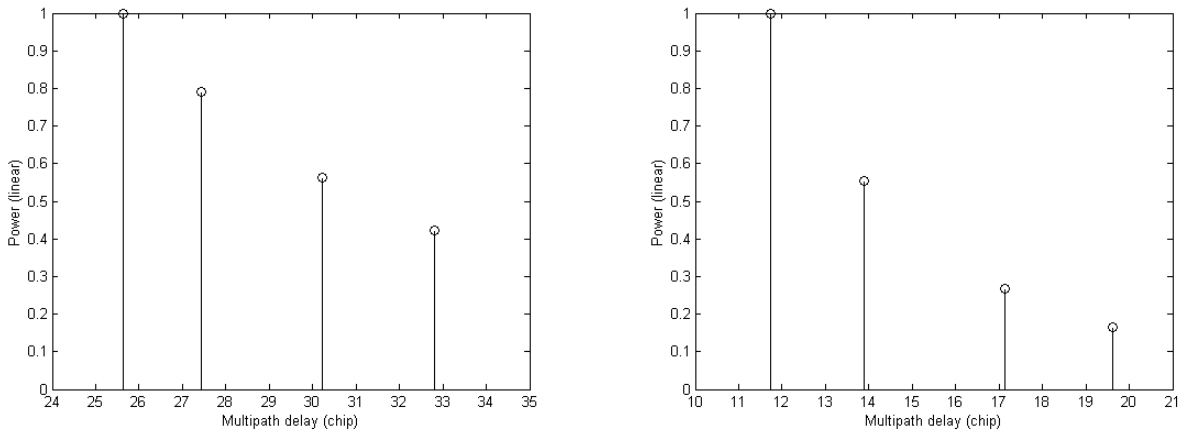

(a) GBSB Circular Model (b) GBSB Elliptical Model

Figure 3-7. Channel Profiles for the GBSB Circular and Elliptical Models

An important phenomenon for the GBSB models is that the relative distance of a multipath signal to the first multipath signal is smaller for the circular model than the elliptical model. Hence, this results in relatively smaller path loss, i.e., relatively larger signal power. The phenomenon is manifest as shown in the two figures. The phenomenom leads to an important fact. Since a multipath signal acts as interference to other multipath signals, strong multipath signals of the circular model incur strong interference. If the noise level is low for the circular model, the SINR is dominant by the interference. Therefore, the SINR of the circular model is smaller than that of the elliptical model for a low noise level. It is opposite for strong noise. The SINR of the circular model is larger than that of the elliptical model for a high noise level. The phenomenon also explains the impact of the maximum delay in the GBSB models.

3.2.4 Channel Model Including the Lognormal Fading

In addition to the LCFCM and the SCFCM, an uncorrelated fading channel model (UCFCM) is also considered for the cdma2000 system, in which the system model is implemented with the SPW tool. Each antenna signal is assumed to have the same lognormal fading in the LCFCM and the SCFCM. In the UCFCM, each antenna signal is assumed to have not only independent Rayleigh fading but also independent lognormal fading. The UCFCM is

illustrated in Figure 3-8. Since the two antenna signals are highly uncorrelated in the UCFCM, the highest diversity gain is expected.

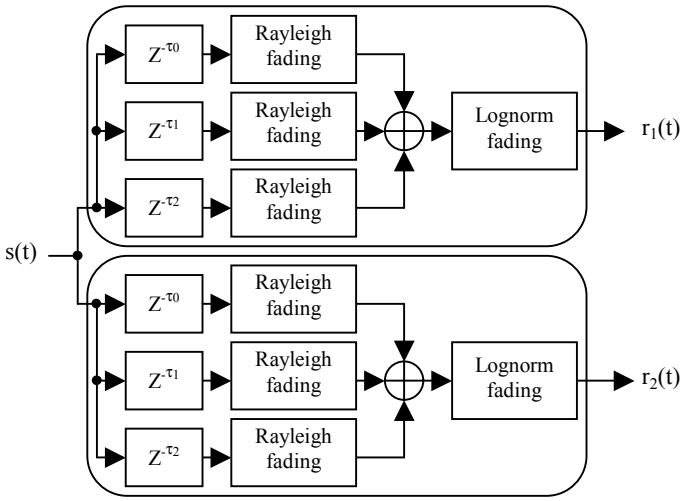

Figure 3-8. Uncorrelated Fading Channel Model

3.3 Low-Power Rake Receiver Design

In this section, we propose a new GSC method and an adaptive rake combining scheme to reduce the power consumption of mobile rake receivers. We also suggest a new power control strategy for base stations to maximize the benefit of the proposed adaptive scheme. We apply the proposed methods to a single antenna system, but these methods can be applied to a dual antenna system, too.

3.3.1 Minimum Selection GSC

We propose a new GSC method called minimum selection GSC (MS-GSC). Our MS-GSC method selects a minimum number of branches as long as the combined SNR is maintained larger than a given threshold. The proposed MS-GSC denoted as MS-GSC (T_m, L) selects a minimum number of branches whose combined SNR is larger than a given threshold T_m, i.e., find a minimum m such that $\sum_{i=1}^{m} \gamma_i \geq T_m$. In contrast to the AT-GSC and the NT-GSC, the MS-

GSC performs better as the threshold value becomes larger. The combined SNRs for the proposed MS-GSC are shown in Figure 3-9 (a), and the number of distinctive combined SNRs is equal to the number of the threshold values. The SNR of the MS-GSC for a given threshold is ideally independent of the average branch SNRs.

For a practical implementation, the signal level or strength is used instead of a branch SNR, which is difficult to measure. Since the received signal contains the desired signal as well as noise, the signal strength represents signal plus noise (S+N) value. Even if the signal strength is used for the original GSC, the AT-GSC, and the NT-GSC, the trend remains the same. However, the trend for the MS-GSC changes as shown in Figure 3-9 (b). When the SNR of each branch is low/high, the amount of the noise is relatively large/small. Thus, the combined (S+N) shows a low/high SNR.

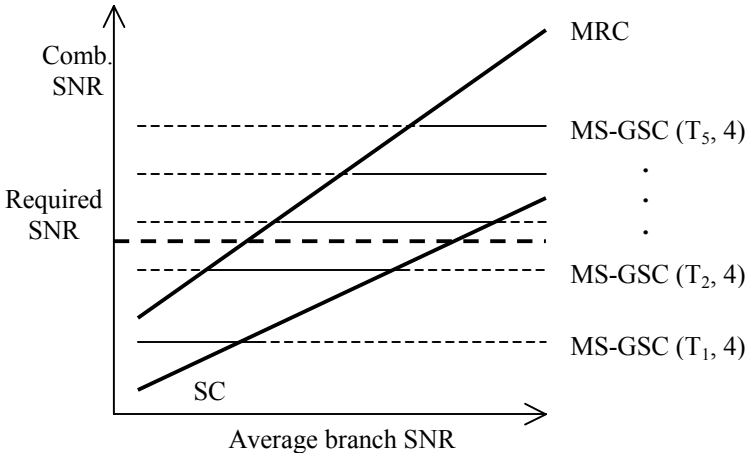

(a) Ideal MS-GSC

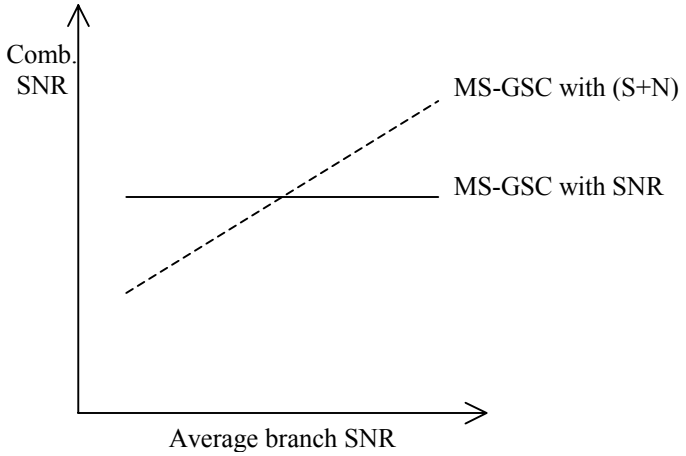

(b) Practical MS-GSC with (S+N)

Figure 3-9. Combined SNR for MS-GSC

The operation of the MS-GSC is as follows. The MS-GSC starts with a given threshold T and an initial condition GSC (k, L). The combined signal strength is periodically measured. If the combined signal strength is less than the threshold, then one more rake finger is activated in the next period. Since the signal with the smaller delay is stronger in general, the finger with the smallest delay is selected. Note that the delay information is provided by a cell searcher. If the combined signal strength is marginally greater than the threshold, then a rake finger with the

lowest signal strength is turned off in the next period. Otherwise, the current rake combining with k fingers is maintained.

Comparing with the AT-GSC and the NT-GSC, the proposed MS-GSC has two benefits. Since the combined signal strength in the MS-GSC is maintained constantly, the statistics of erroneous bits have a low standard deviation, which is presented in Chapter 5. This may result in less burst errors, which leads to a better error correction for a channel decoder. The second benefit is that the MS-GSC enables power reduction by turning off unselected fingers. The MS-GSC can meet the given threshold condition by turning on another finger with the smallest delay or turning off a finger with the lowest signal strength. In contrast, the AT-GSC and the NT-GSC necessitate activation of each finger momentarily to measure the signal strength, so that it can determine if the signal strength is above the threshold value or not.

We also need to modify the selection rules for the MS-GSC for practical operation. The MS-GSC selects all branches even if all combined SNR or (S+N) is smaller than a given threshold. We apply the modified rule for our simulation in Chapter 5.

3.3.2 Adaptive Rake Combining Scheme

We determine a set of N threshold values $\{T(1), T(2), \ldots, T(N)\}$ for each GSC using a system simulation, where each GSC performs better as the index of the threshold value increases. This implies that $T(1) > T(2) > \ldots > T(N)$ for the AT-GSC and the NT-GSC and $T(1) < T(2) < \ldots < T(N)$ for the MS-GSC. A larger N leads to, on average, a larger number of branches turned off, but it results in more complex hardware and more frequent changes of threshold values. Therefore, a larger N does not guarantee more power reduction. The **SNR range** of a threshold value T(i) is the range in which the required BER is met for T(i), but not with T(i-1). The SNR range of a threshold value T(i) is illustrated in Figure 3-10. As shown in the figure, the SNR range for the threshold value T(i) is good enough to meet the required BER.

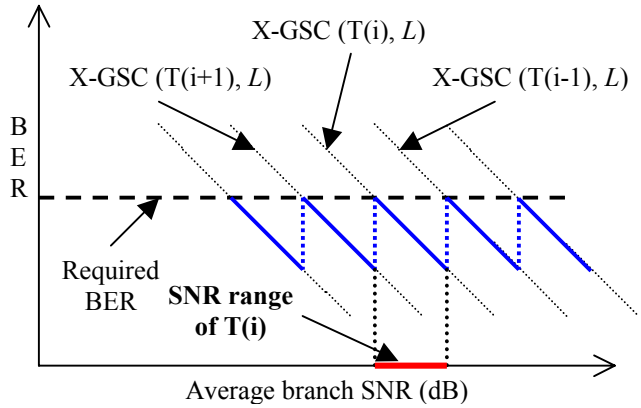

Figure 3-10. SNR Range of the Threshold Value

We propose an adaptive scheme to determine threshold values for the three GSC methods, the AT-GSC, the NT-GSC, and the proposed MS-GSC. Threshold values of a GSC method should be adjusted dynamically to turn off a maximal number of branches, while maintaining the required BER. Since we use BERs as the metric for the QoS, a mechanism is necessary to estimate the current BER. When a Viterbi decoder is employed for the system, the error metric of the survived path at the end of the forward processing is the current BER. For the case of turbo decoders, the number of iterations or the rate of convergence can be used as the metric. The block diagram of the proposed system is presented in Figure 3-11, in which the control logic adjusts the threshold value dynamically based on the inputs from the channel decoder.

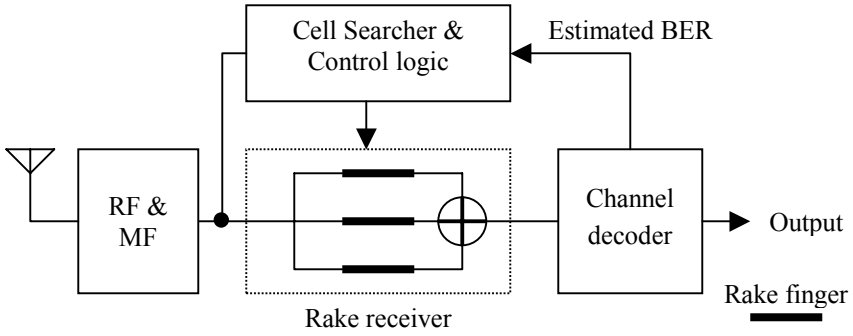

Figure 3-11. Block Diagram of the Proposed Adaptive Scheme

The proposed adaptive scheme consists of two loops, an outer loop and an inner loop. The outer loop adaptively adjusts the threshold value as described next. The inner loop dynamically

changes the finger selection to meet the required condition with the threshold value provided from the outer loop.

Figure 3-12 shows the operation of the outer loop. Suppose that the current threshold of a GSC method is T(*i*). Current BER is periodically estimated at the end of each frame. If the estimated BER is higher than the required BER, then the threshold index is increased to T(*i*+1) in order to lower the BER in the next frame. If the BER reaches the right end of the SNR range of the current threshold T(*i*), then the threshold index is decreased to T(*i*-1). Otherwise, the current threshold *T*(*i*) is maintained.

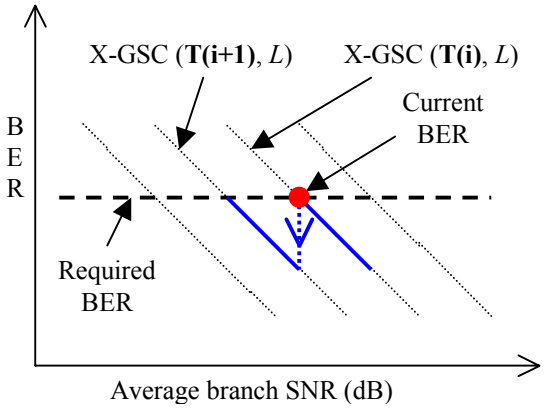

(a) Increasing a Threshold Index

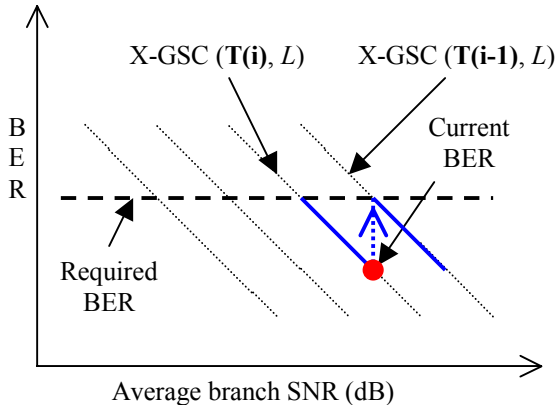

(b) Decreasing a Threshold Index

Figure 3-12. Operation of GSCs

The power saving of the proposed adaptive scheme is highly dependent on the operating condition and the employed threshold set. The average number of rake fingers activated $\overline{m}$ is obtained as $\overline{m} = \sum_{i=1}^{N} A_i P_i$, where N is the number of threshold values $\{T(i)\}$, A_i is the average number of rake fingers activated for a threshold value T(i), and P_i is the probability of the proposed adaptive scheme operating in the SNR range of the threshold value T(i). Then, the power saving with the proposed adaptive scheme over the MRC rake combiner is obtained as $\frac{L-\overline{m}}{L}$. Thus, if we know each probability P_i, then the power saving with the proposed adaptive scheme could be estimated. The probability P_i depends on the channel condition and the power control strategy.

In the following, we analyze the power saving of the proposed adaptive scheme under *equal probability*, i.e., P_i is equal for i = 1, 2, … N. *Suppose that a threshold set is chosen such that the difference between the average numbers of rake fingers activated for two consecutive threshold values is* δ. In other words, the average number of the rake fingers activated is 1, 1+δ, 1+2δ, …, L-δ, L for a threshold value T(1), T(2), …, T(N), respectively. Let us consider the case of δ = 1, equivalently, $N = L$. Then, the probability P_i of the proposed adaptive scheme operating in the SNR range of each threshold is $\frac{1}{L}$. Since the number of rake fingers activated for the threshold value T(i) is i, where i = 1, 2, …, L, the average number of rake fingers activated $\overline{m}$ is $\sum_{i=1}^{L} \frac{i}{L}$ or $\frac{L+1}{2}$. Thus, the power saving with the proposed adaptive scheme over the MRC rake combiner is obtained as $\frac{L-1}{2L}$.

Next, we consider the case of δ < 1 and kδ = 1 for some integer k. Each SNR range for the case of δ = 1 is subdivided into k pieces except for the range of SNR_1 in which one finger is always turned on. Figure 3-13 shows the case of δ = 0.5 and k = 2, where the average number of rake fingers activated with each threshold value is 1, 1.5, 2, 2.5, 3, …, L-0.5, L. *Suppose that the probability of the proposed adaptive scheme operating in each subrange with an* SNR_n *range is equal* and is $\frac{1}{k}$. Then, the average number of rake fingers activated in each group except SNR_1 is

obtained as $\frac{2n-1+\delta}{2}$, where n = 2, 3, …, L. Therefore, the overall average number of rake fingers activated $\overline{m}$ is approximated to $\frac{L+\delta}{2}$. The derivation of the above two equations is presented at the end this subsection. Thus, the power saving with the proposed adaptive scheme over the MRC rake combiner is obtained as $\frac{L-\delta}{2L}$. The power saving for our scheme increases as L increases with the maximum value of 0.5 for L = ∞. As an illustration, the power saving of the proposed scheme is 44.5 %, 45.9 %, and 46.7 % when L is 3, 4, and 5, respectively, with δ = 0.33.

The proposed adaptive scheme can also work with the original GSC. There are only L different SNR ranges for the original GSC. The outer loop increases or decreases the number of rake fingers activated to maintain the required BER. Selecting additional finger or turning off one of the currently activated fingers may follow the same operation as the MS-GSC does. The adaptive scheme for the original GSC can be considered as a special case of other GSCs, in which δ = 1. The power saving of the original GSC over the MRC rake combiner is $\frac{L-1}{2L}$.

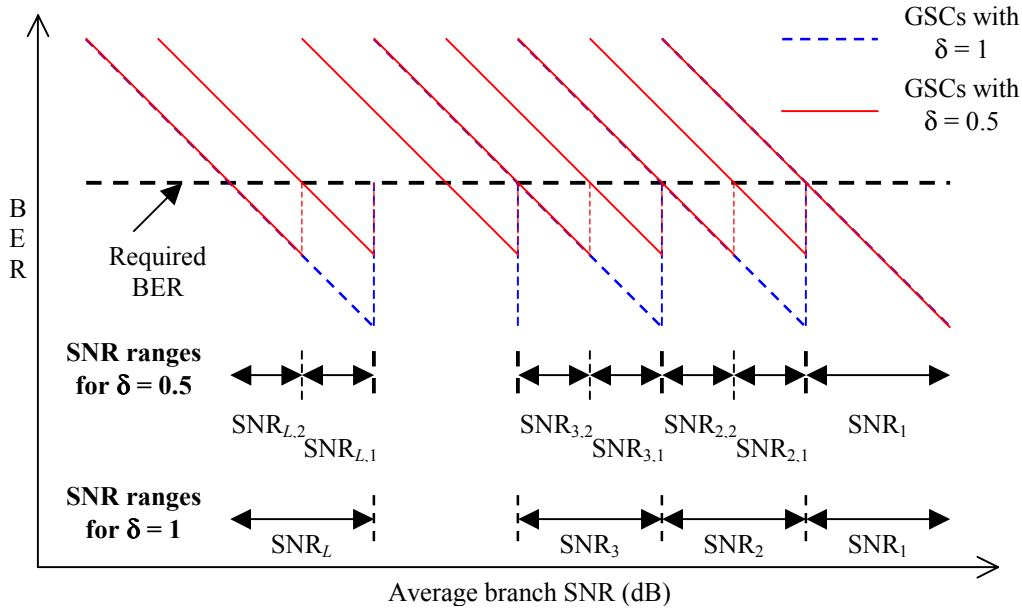

Figure 3-13. SNR Ranges with Different Threshold Sets

The average number of rake fingers activated in each group except the first group is obtained as follows. The average number of rake fingers activated for each subrange of an SNR_n range is $(n\text{-}1)+\delta$, $(n\text{-}1)+2\delta$, …, $(n\text{-}1)+k\delta$, where $n = 2, 3, \ldots, L$. Since the probability of operating in each subrange within an SNR_n range is $\frac{1}{k}$, the average number of rake fingers activated in each group is computed as follows.

$$\frac{1}{k}\{(n-1+\delta)+(n-1+2\delta)+\ldots+(n-1+k\delta)\} \tag{3-8a}$$

$$=\frac{1}{k}\{k(n-1)+(\delta+2\delta+\ldots+k\delta)\} \tag{3-8b}$$

$$=\left\{(n-1)+\frac{(k+1)\delta}{2}\right\} \tag{3-8c}$$

$$=\frac{2n-1+\delta}{2} \text{ (since } k\delta = 1). \tag{3-8d}$$

The overall average number of rake fingers activated, $\overline{m}$, is approximated as follows. The average number of rake fingers activated in each group is 1 (when n = 1) and $\frac{2n-1+\delta}{2}$ (when n = 2, 3, …, L). Since the probability of operating in each SNR range is assumed as $\frac{1}{L}$, $\overline{m}$ is computed as follows.

$$\overline{m}=\frac{1}{L}\left\{1+(\frac{3+\delta}{2})+(\frac{5+\delta}{2})+\ldots+(\frac{2n-1+\delta}{2})+\ldots+(\frac{2L-1+\delta}{2})\right\} \tag{3-9a}$$

$$\geq\frac{1}{L}\left\{(\frac{1+\delta}{2})+(\frac{3+\delta}{2})+(\frac{5+\delta}{2})+\ldots+(\frac{2n-1+\delta}{2})+\ldots+(\frac{2L-1+\delta}{2})\right\} \text{ (since } 0<\delta\leq 1) \tag{3-9b}$$

$$=\frac{1}{L}\left\{(\frac{1}{2}+\frac{3}{2}+\ldots+\frac{2L-1}{2})+(\frac{L\delta}{2})\right\} \tag{3-9c}$$

$$=\frac{1}{L}\left\{\frac{L^2}{2}+\frac{L\delta}{2}\right\} \tag{3-9d}$$

$$=\frac{L+\delta}{2}. \tag{3-9e}$$

3.3.3 Power Control Strategy

The objective of the proposed adaptive rake combining scheme is to turn off as many fingers as possible to reduce the power dissipation, while maintaining the required QoS. The strategy of the conventional power control aims to maintain the received signal power level at a mobile station, so that the signal level combined with the MRC would meet the required QoS. Hence, the rake receiver of the mobile station dissipates the maximum power. To maximize the benefits of the proposed rake combining method, we suggest the base station should transmit the maximum allowable power so that the smallest number of fingers is turned on at the mobile station. The maximum allowable power should be determined subject to the acceptable interference to other active users in its own cell and neighboring cells.

3.4 Summary

We proposed dual smart antennas at handsets for the 3G wireless personal communication systems in this chapter. Smart antennas at handsets with a new combining scheme called hybrid combining were proposed in Section 3.1. To model dual antenna signals at handsets, three channel models—LCFCM, SCFCM, and ECFCM—were considered in Section 3.2. Finally, a new GSC method and an adaptive rake combining scheme to reduce the power consumption of mobile rake receivers were proposed in Section 3.3. A new power control strategy for base stations to maximize the benefit of the proposed adaptive scheme was suggested in Section 3.3, too.

The proposed system and schemes described in this chapter will be evaluated and verified in the following two chapters.

Chapter 4 Performance of Smart Antennas at Handsets

In this chapter, we present the simulation results to evaluate the performance of the proposed dual smart antenna system at handsets for the 3G wireless personal communication systems. Simulation results with three different combining schemes for the 3GPP WCDMA system are presented first. Then, the simulation results of the dual smart antenna handsets for the cdma2000 system are presented.

4.1 Performance of Diversity Combining for the 3GPP System

Simulation results to evaluate the performance of the dual smart antenna handsets with the diversity combining scheme for the 3GPP system are presented in this section.

4.1.1 Simulation Environment

A signal from a base station propagates through the channel. The two types of the channel model, SCFCM and LCFCM, described in Chapter 3 are employed for the simulation. The GBSB elliptical and circular models are adopted to generate the channel profile of multipath signals. The signals received at the dual antennas of a handset are applied to their own rake receivers after pulse shaped by an FIR filter, as shown Figure 4-1. A diversity combiner combines the two rake receiver outputs using a diversity combining scheme (Only the rake level diversity combining is considered). Three diversity combining schemes, SD, EGC, and MRC, were considered in our simulation. For the MRC, we obtain the output according to the formula, $a|a|+b|b|$, where a and b are the two rake receiver outputs. We call it as square law combining (SLC).

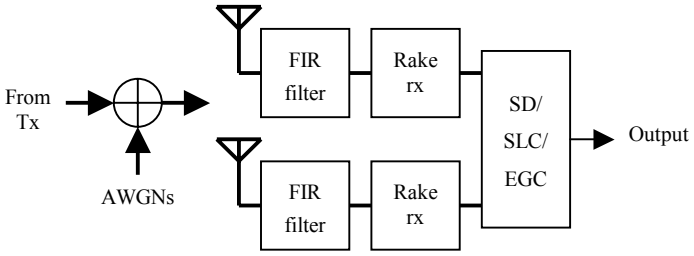

Figure 4-1. Dual Smart Antenna Receiver with Diversity Combiner

In our simulation, the output of a diversity combiner is hard decided to either 1 or 0, and compared with the original data bits to evaluate the system performance in terms of BER. For simplicity, we modeled the interference from adjacent cells as additive white Gaussian noise (AWGN).

The environment considered in our simulation is as follows. The following model parameters, called *baseline parameters* in this section, were assumed. The distance between the two antennas at handsets is $\lambda/4$ (3.5 cm). The distance from the desired base station to the mobile station is 2000 m in the GBSB circular model, and the maximum multipath delay is 35 chips. The distance from the desired base station to the mobile station is 800 m in the GBSB elliptical model, and the maximum multipath delay is 20 chips. The mobile velocity is 60 km/hr, which results in 119 Hz of maximum Doppler frequency for a 2.14 GHz carrier frequency. Eight users' signals of a spreading factor 32 and the common pilot (CPICH) signal are channelized, combined, scrambled, pulse-shaped, and transmitted through the channel. Twenty percent of the total transmitted power is allocated to the CPICH, and the remaining 80% of the power is divided equally and allocated to each user signal. Four multipath signals with the channel profile obtained from the GBSB models arrive at handset antennas. A rake receiver with three rake fingers is considered at handsets.

4.1.2 Simulation Results under the GBSB Circular Model

The GBSB circular model is employed to generate channel profiles for the simulation. The simulation results with three diversity combining schemes and two types of the channel model

are presented in Figure 4-2. Figure 4-2 (a) and (b) are the performance of the single and of the dual antenna systems under the SCFCM and the LCFCM, respectively. The y-axis of a plot is the BER, and the x-axis is the ratio of the symbol energy of the first multipath signal to the AWGN. The top graph in each plot is the BER of a single antenna (SA) system. The second, the third, and the bottom graphs are the BERs of the dual antenna system with SD, SLC, and EGC diversity combining schemes, respectively. As can be seen from the two figures, the dual smart antenna system always performs better than a single antenna system for both channel models. For the dual smart antennas, the EGC performs the best among the three diversity combining schemes. For the purpose of comparison, the performance of the dual smart antenna system with the EGC diversity combining scheme alone under the two channel models and that of a single antenna system is shown in Figure 4-2 (c). The performance gain of the EGC diversity combining over a single antenna system is 3.6 dB for the SCFCM at BER = 10^{-1} and 4.6 dB for the LCFCM. The performance gain increases further with a lower BER. For example, the gain is 6.4 dB for the SCFCM at BER = $4x10^{-2}$ and 7.5 dB for the LCFCM. As expected, the higher performance gain is achieved under the LCFCM than the SCFCM.

It is worth noting that the BER is saturated beyond a certain level of Eb/No for both single and dual antenna systems, i.e., the increase of the transmitter power beyond a certain level fails to further decrease the BER. This is explained as the increased transmitter power increases the signal level of all multipath signals, i.e., the power level of the interference signals.

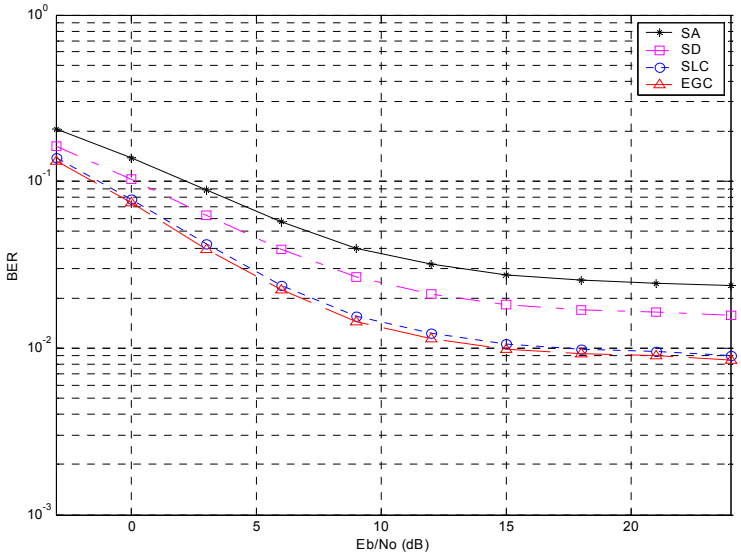

(a) BERs under the SCFCM

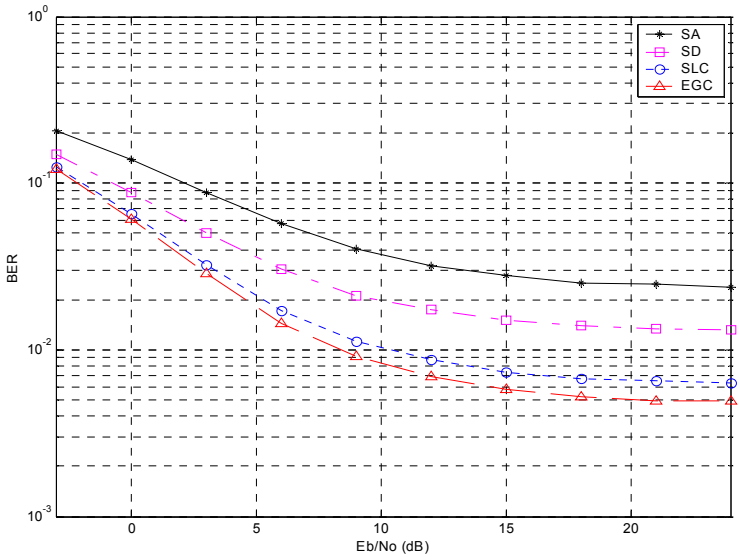

(b) BERs under the LCFCM

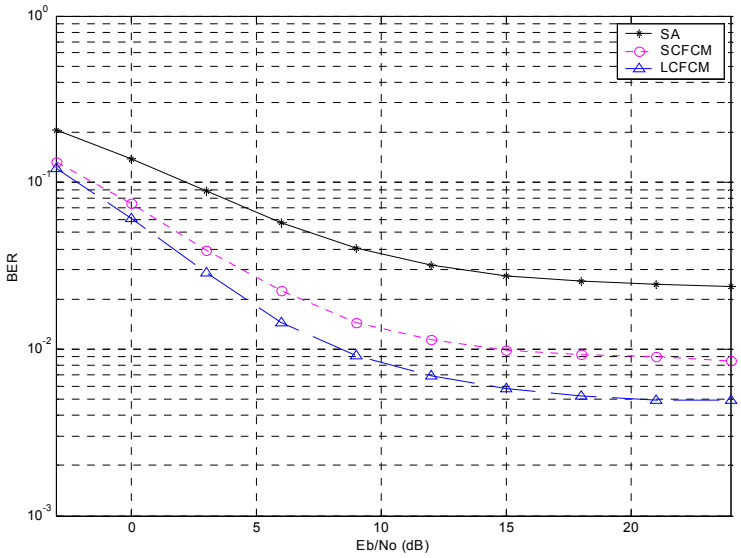

(c) BER Bound with the EGC

Figure 4-2. BERs with Three Diversity Combining Schemes and Two Channel Models

To investigate the impact of individual parameters, we also simulated variations of several individual parameters and present the results below. *Hereafter, we consider only the EGC diversity combining scheme for the dual smart antenna system*. Firstly, we investigated the impact of the distance of two antennas at handsets under the SCFCM. The simulation results with the antenna distances of λ/8, λ/4, and λ/2 under the SCFCM are presented in Figure 4-3. Note that all the other parameters are the same as the baseline parameters in the simulation, and the antenna distance is λ/4 for the baseline. The top graph represents the BER of a single antenna system. The bottom cluster of the three graphs represents the BERs of the dual antenna system where the antenna distance is λ/8, λ/4, and λ/2 from top to bottom. As the distance of two antennas increases, the correlation between two antenna signals becomes low and the dual antenna system achieves higher performance gain. Since the difference in performance between the antenna distances of λ/2 and λ/4 is small, the dual antenna system with the antenna distance of λ/4 (3.5 cm) is a good candidate for the practical implementation.

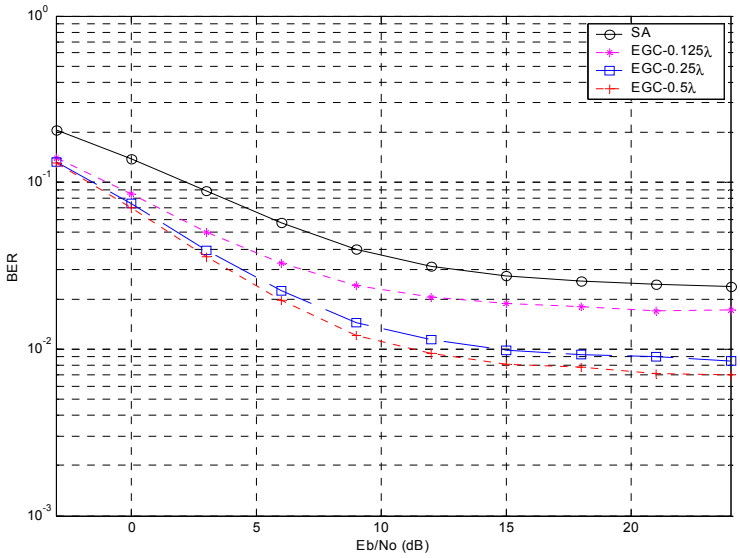

Figure 4-3. BERs with Various Antenna Distances

Secondly, we investigated the impact of the maximum delay, which is one of the two main model parameters, for the GBSB circular model. The maximum delay reflects the physical environment in which the scatters are located. The simulation results with the maximum delay of 35, 41, and 47 chips under the LCFCM are presented in Figure 4-4. Note that all the other parameters are the same as the baseline parameters, and the maximum delay is 35 chips for the baseline. The top cluster of the three graphs represents the BERs of a single antenna system, where the maximum delays are 35, 41, and 47 chips. The bottom cluster of the three graphs represents the BERs of the dual antenna system. As can be seen from the figure, the dual smart antenna system performs better than a single antenna system for all the three cases. A larger maximum delay performs better for a large Eb/No, i.e., a low noise level. However, the trend is opposite for a high noise level. The phenomenon is explained readily as discussed in the GBSB models in Chapter 3. As the maximum delay increases, the relative signal strength of a multipath to the first multipath decreases to result in a large SINR for weak noise. This leads to higher performance for larger Eb/No.

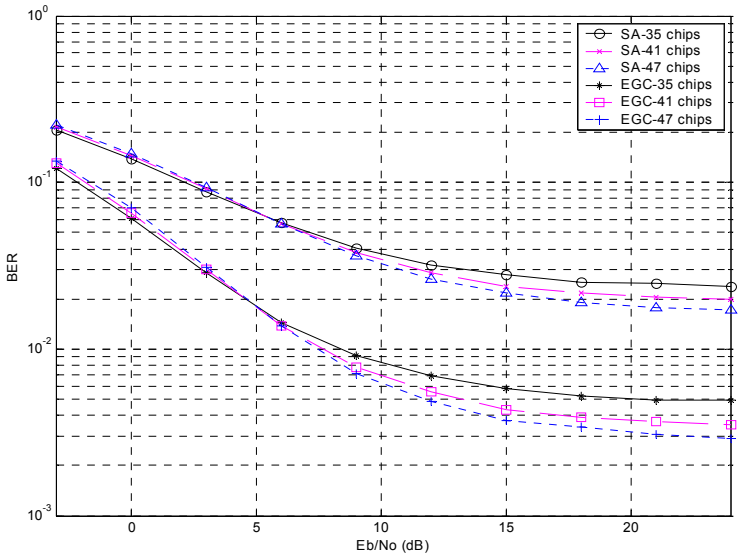

Figure 4-4. BERs with Various Maximum Delays

Thirdly, we investigated the impact of the number of users. The simulation results with the number of users of 8, 12, and 16 under the LCFCM are presented in Figure 4-5. Note that all the other parameters are the same as the baseline parameters, and the number of users is 8 for the baseline. The top cluster of the three graphs represents the BERs of a single antenna system where the number of users is 16, 12, and 8 from top to bottom. The bottom cluster of the three graphs represents the BERs of the dual antenna system where the number of users is 16, 12, and 8 from top to bottom. As the number of users increases, the relative signal power allocated to the desired user decreases, which results in increase of the power level of the interference. Hence, the performance in BER decreases. Note that the deterioration of the performance is substantial for large Eb/No. For example, the BER of the dual antenna system for 8 users is 0.49 % at Eb/No = 21 dB, while the BER becomes 2.72 % for 16 users.

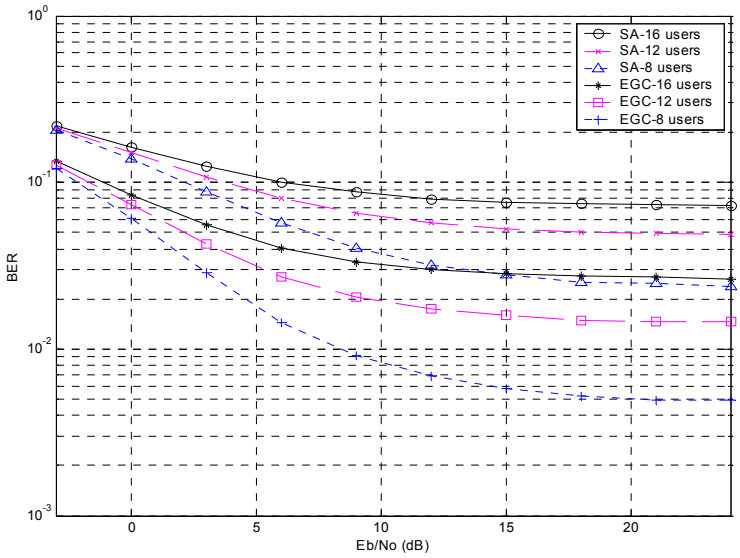

Figure 4-5. BERs with Various Numbers of Users

Finally, we investigated the impact of the number of multipaths. We considered 4, 5, and 6 multipaths under the LCFCM, and the simulation results are presented in Figure 4-6. It is noted that the number of multipaths is 4 in the baseline, and the number of rake fingers is fixed to three for all the cases. The top cluster of the three graphs represents the BERs of a single antenna system for the three different numbers of multipaths, and the bottom cluster represents the BERs of the dual antenna system. As can be seen from the figure, the dual smart antenna system performs better than a single antenna system for all the three cases. If Eb/No is small, the figure indicates that the number of multipaths has little impact on the performance. This is due to the fact that AWGN is dominant for small Eb/No. Therefore, the interference due to the other multipaths is relatively insignificant. Obviously, the interference becomes dominant for large Eb/No as the number of multipaths increases as shown in the figure.

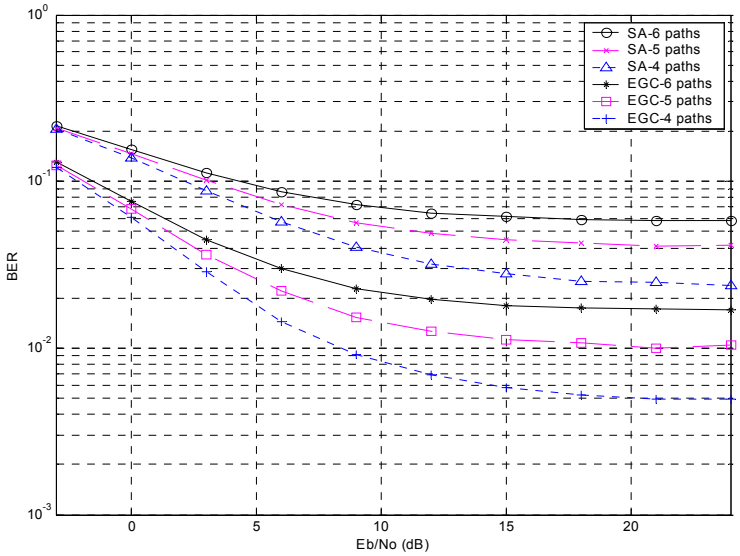

Figure 4-6. BERs with Various Numbers of Multipaths

4.1.3 Simulation Results under the GBSB Elliptical Model

To generate channel profiles for the simulation, the GBSB elliptical model is employed. The simulation results with three diversity combining schemes and two types of the channel model are presented in Figure 4-7. Figure 4-7 (a) and (b) are the performance of the single and of the dual antenna systems under the SCFCM and the LCFCM, respectively. As can be seen from the two figures, the dual smart antenna system always performs better than a single antenna system for both channel models. For the dual smart antennas, the EGC performs the best among the three diversity combining schemes. The performance of the dual smart antenna system with the EGC diversity combining scheme under the two channel models and that of a single antenna system is shown in Figure 4-7 (c). The performance gain of the dual antenna system with the EGC diversity combining over a single antenna system is 3.1 dB for the SCFCM at BER=10^{-1} and 4.1 dB for the LCFCM. The performance gain increases further with a lower BER. For example, the gain is 4.4 dB for the SCFCM at BER=$3\text{x}10^{-2}$ and 6.4 dB for the LCFCM. As expected, the higher performance gain is achieved under the LCFCM than the SCFCM.

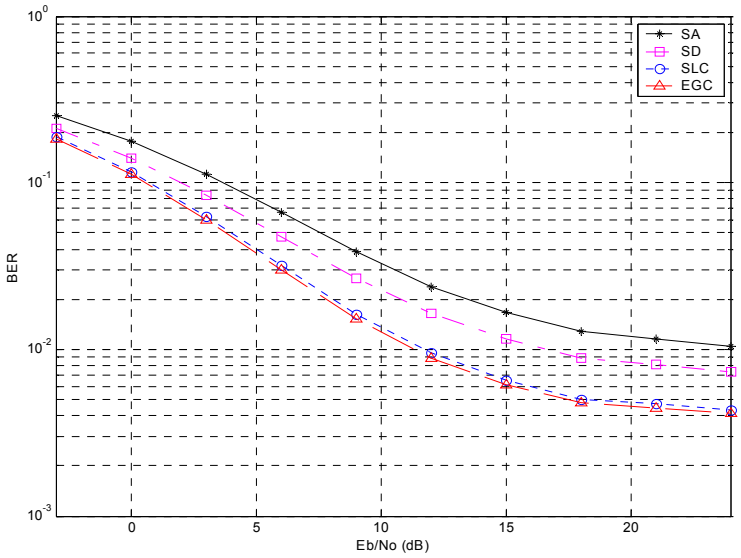

(a) BERs under the SCFCM

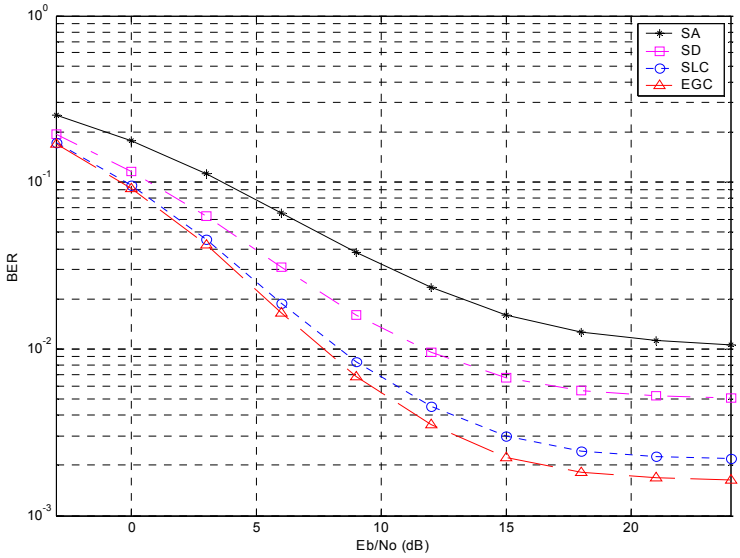

(b) BERs under the LCFCM

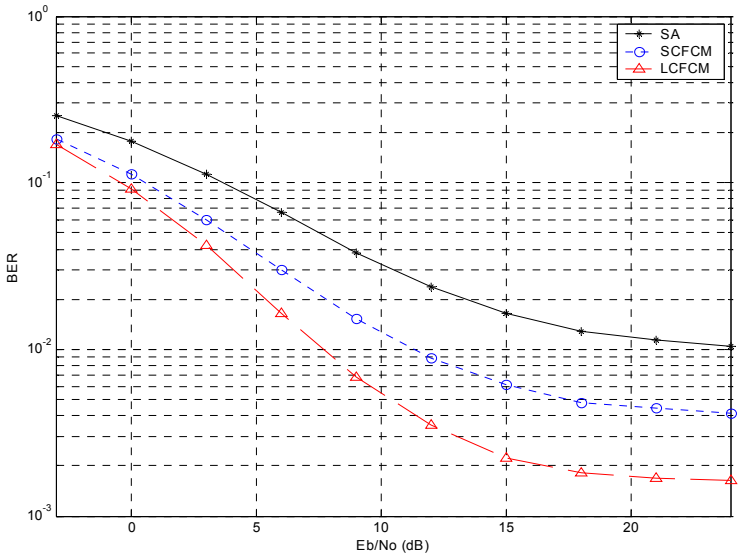

(c) BER Bound with the EGC

Figure 4-7. BERs with Three Diversity Combining Schemes and Two Channel Models

To investigate the impact of individual parameters under the GBSB elliptical model, we also simulated variations of several individual parameters and present the results below. *Hereafter, we consider only the EGC diversity combining scheme for the dual smart antenna system*. Firstly, we investigated the impact of the number of users. The simulation results with the number of users of 8, 12, and 16 under the LCFCM are presented in Figure 4-8. Note that all the other parameters are the same as the baseline parameters in the simulation. The top cluster of the three graphs represents the BERs of a single antenna system, where the number of users is 16, 12, and 8 from top to bottom. The bottom cluster of the three graphs represents the BERs of the dual antenna system, where the number of users is 16, 12, and 8 from top to bottom. As the number of users increases, the relative signal power of the desired user decreases, which results in increase of the power level of the interference. Hence, the performance in BER decreases. Note that the deterioration of the performance is substantial for large Eb/No. For example, the BER of the dual antenna system for 8 users is 0.17 % at Eb/No = 21 dB, while the BER becomes 1.27 % for 16 users.

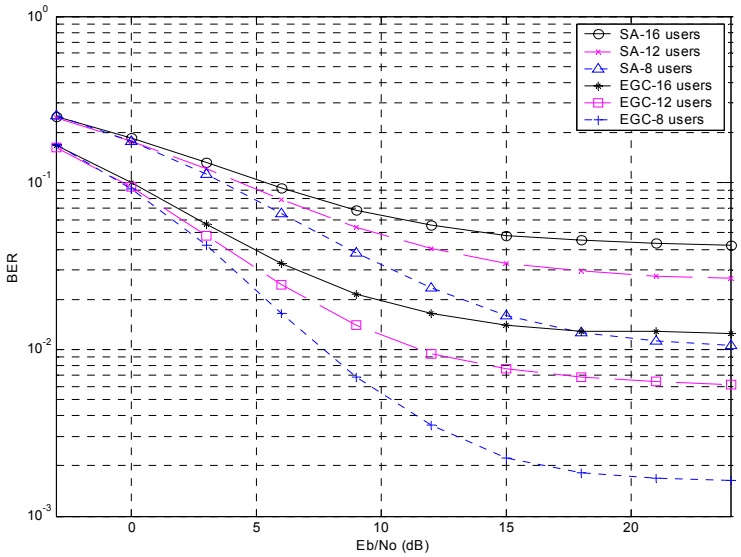

Figure 4-8. BERs with Various Numbers of Users

Secondly, we investigated the impact of the mobile velocity. We varied the mobile velocity to 30, 60, and 90 km/hr, which results in 59, 119, and 178 Hz of maximum Doppler frequency, respectively, under the LCFCM, while all the other parameters are the same as the baseline parameters. The simulation results are given in Figure 4-9. The top cluster of the three graphs represents the BERs of a single antenna system with the three mobile velocities. The bottom cluster of the three graphs represents the BERs of the dual antenna system. The simulation results reveal that the dual smart antenna system performs better than a single antenna system for all the three mobile velocities. It is notable that the impact of the mobile velocity is negligible for both single and dual antenna systems.

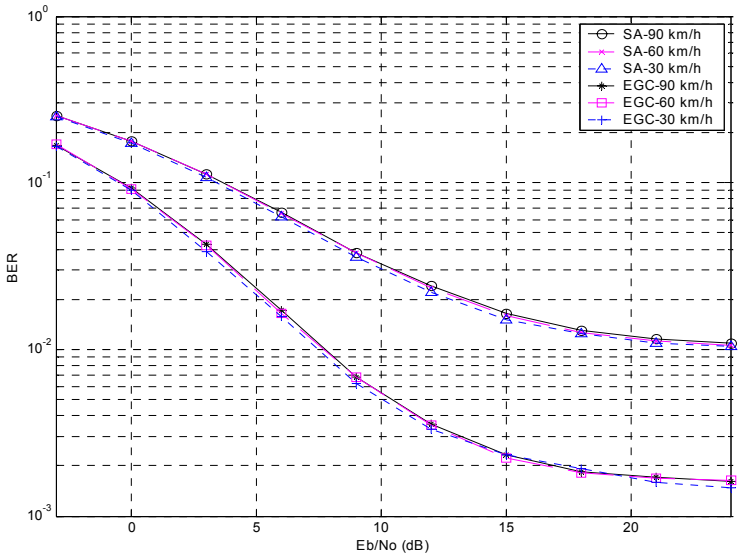

Figure 4-9. BERs with Various Mobile Velocities

Finally, we investigated the impact of the number of multipaths. We considered 4, 5, and 6 multipaths under the LCFCM, and the simulation results are presented in Figure 4-10. The top cluster of the three graphs represents the BERs of a single antenna system for the three different numbers of multipaths, and the bottom cluster represents the BERs of the dual antenna system. It should be noted that the number of rake fingers is fixed to three for all cases. As can be seen from the figure, the dual smart antenna system performs better than a single antenna system for all the three cases. If Eb/No is small, the figure indicates that the number of multipaths has little impact on the performance. This is due to the fact that AWGN is dominant for small Eb/No. Therefore, the interference due to the other multipaths is relatively insignificant. Obviously, the trend is reversed for large Eb/No as shown in the figure.

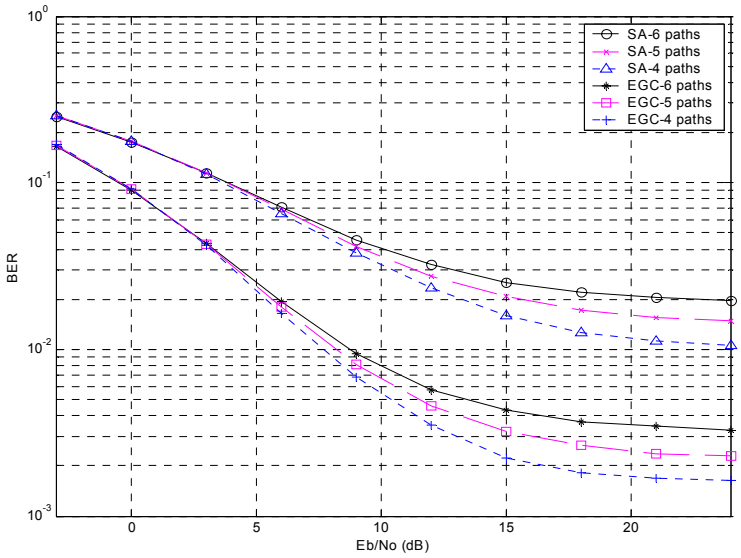

Figure 4-10. BERs with Various Numbers of Multipaths

Our simulation results show that the GBSB circular model and the GBSB elliptical model basically have the same trend. A major difference as elaborated in Chapter 3 is that the circular model performs better for larger Eb/No or weaker noise, while the elliptical model is superior for smaller Eb/No or stronger noise. The phenomenon is represented in Figure 4-11. The top cluster of the two graphs represents the BERs of a single antenna system for the GBSB elliptical and circular models, and the bottom cluster represents the BERs of the dual antenna system.

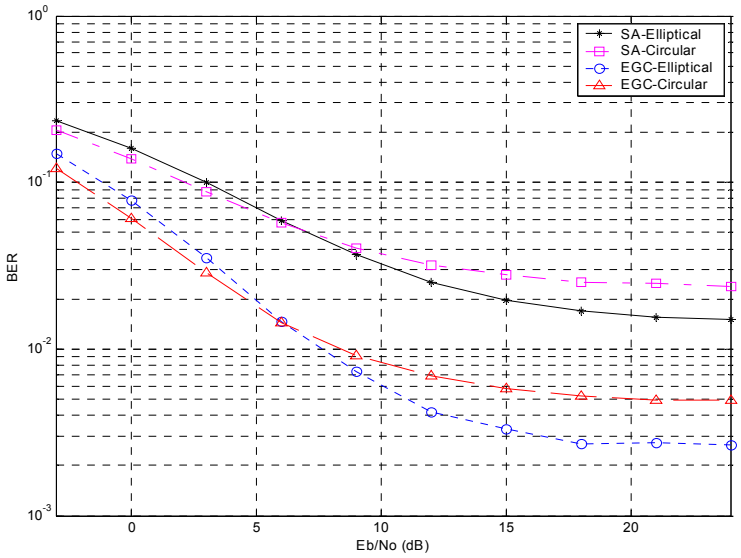

Figure 4-11. BER Comparison for the GBSB Circular and Elliptical Models

In conclusion, the simulation results of the diversity combining for the 3GPP system indicate that

i) the EGC scheme performs the best among the three diversity combining schemes. This is beneficial as the EGC scheme is simple in implementation.

ii) As expected, the higher performance gain is achieved under the LCFCM than the SCFCM. It is believed that the actual performance of a dual smart antenna lies in between the performances obtained for the LCFCM and the SCFCM models.

Based on the theory of diversity, we expect that the MRC would perform better than the EGC. However, the simulation results show that the EGC performs better than the MRC. We analyzed the reason as follows. In our channel model, the average power of the combined signal from each antenna is same. In the SCFCM, two multipath signals from each antenna are different only in the phase, thus they have the same signal power. In the LCFCM, two multipath signals from each antenna have independent Rayleigh fading. Thus, they have a different instantaneous signal power, but the averaged signal power is still same. These imply that the average SNRs of each antenna signal are same. Therefore, the EGC effectively works as the MRC since each antenna has the same average SNR. For the MRC (or the SLC), we use the signal plus noise value (S+N) instead of the SNR as a weight factor. Since the channel estimation is inaccurate

due to the noise, the diversity combining with a (S+N) weight factor might not meet the theoretical expectation. Thus, the performance of the MRC is inferior to that of the EGC. As shown in [19], there is an imbalance between the average signal powers of dual antennas under the real environment. In the real environment, the MRC would perform better than the EGC. The following simple results indicate that the MRC with a SNR weight factor performs better than the EGC if the average SNR ratio of two antenna signals is two to one, as shown in Table 4-1.

Table 4-1. Performance Comparison of the EGC and the MRC

SNR of Antenna 1	Antenna 1	Antenna 2	EGC	MRC with (S+N)	MRC with SNR
-15 dB	18.6 %	26.4 %	14.9 %	15.9 %	13.5 %
-13 dB	11.3 %	18.1 %	7.2 %	8.0 %	6.4 %
-11 dB	4.5 %	8.0 %	1.6 %	2.1 %	1.5 %

4.2 Performance of Adaptive Combining for the 3GPP System

Simulation results to evaluate the performance of the dual smart antenna handsets with the adaptive combining scheme for the 3GPP system are presented in this section. An adaptive combiner combines corresponding finger outputs of the two antennas with appropriate antenna weights, which are recursively obtained based on the N-LMS algorithm.

4.2.1 Simulation Environment

Each antenna receives not only the transmitted signal from the desired base station but also the transmitted signals from adjacent base stations. The received signal added with background noise is shaped back with the same FIR filter. Each rake finger despreads a multipath signal from each antenna. There are two rake finger outputs for each multipath signal – despread pilot signal and despread data signal. In a single antenna system, each despread data signal is coherently combined using the despread pilot signal. In a dual antenna system with the adaptive combining scheme, each despread data signal from each antenna is weighted with the antenna weight and

combined. The antenna weights are adaptively obtained using the N-LMS algorithm described in Chapter 3. Then the output of each adaptive combiner (AC) is coherently combined using the adaptively combined pilot signal. In our simulation, the coherently combined output of an antenna system (both single and dual antenna systems) is hard decided to either 1 or 0, and compared with the original data bits to evaluate the system performance in terms of BER.

The environment considered in our simulation is almost the same as the baseline parameters described in Section 4.1. The only difference is as follows. Two multipath signals from an adjacent base station (which is also assumed to transmit the combined signal of eight users' signals and the common pilot signal) and background noise (which results in 25 dB of E_b/N_0) are added at handset antennas.

The two factors that affect the performance of the N-LMS algorithm are the step size and the number of pilot symbols to be averaged. The step size, $\mu = 0.3$, and the number of pilot symbols, $Q = 3$, were chosen through trial and error. The three pilot symbol durations correspond to 0.2 ms in the real operation.

4.2.2 Simulation Results for the AC

The simulation results for the adaptive combining with the GBSB elliptical and circular models are presented in Figure 4-12. Figure 4-12 (a) and (b) represent the performances of the dual antenna system with the channel profiles obtained from the GBSB elliptical and circular models, respectively. In the figure, the y-axis is the BER and the x-axis is the ratio of the average power of the first multipath signal of the desired base station to the average power of the first multipath signal of the adjacent base station. The solid line represents the BER of a single antenna system. The dotted line represents the BER of a dual antenna system with the adaptive combining. As can be seen from the figure, the dual antenna system with the adaptive combining performs better than a single antenna system for the GBSB elliptical and circular models. The performance gain of the dual antenna system with the adaptive combining over a single antenna system is 3.3 dB for the GBSB elliptical model at BER = 5×10^{-2} and 5.5 dB for the GBSB circular model.

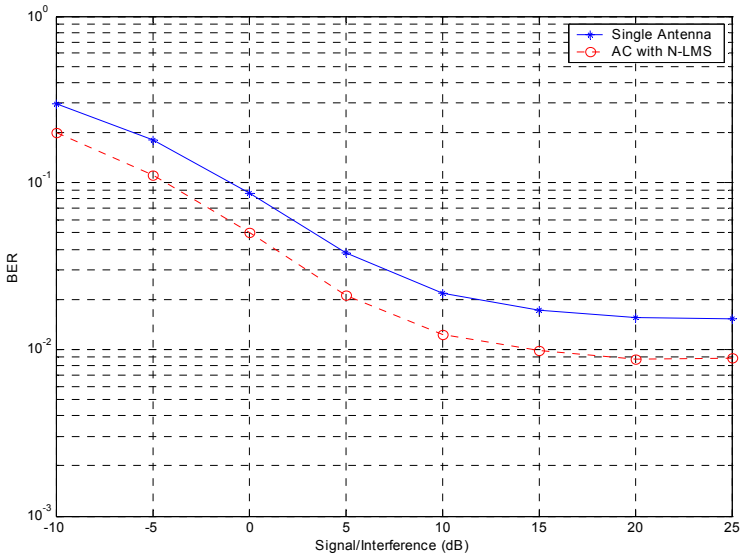

(a) BER with the GBSB Elliptical Model

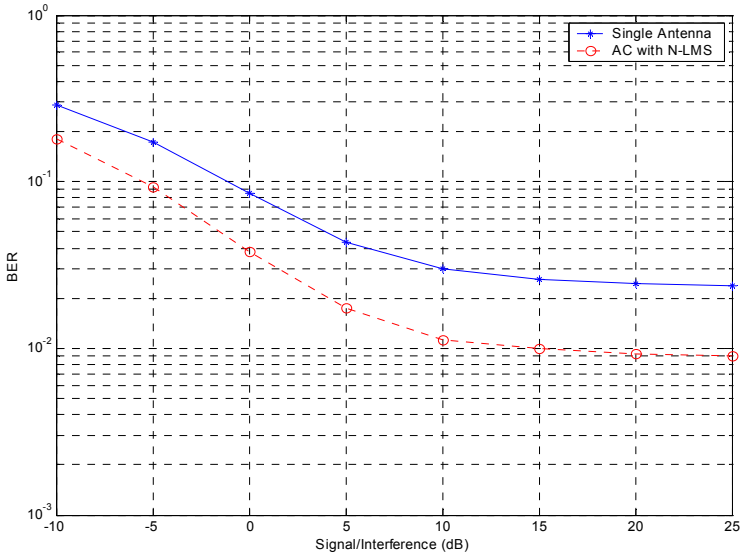

(b) BER with the GBSB Circular Model

Figure 4-12. BERs with the GBSB Elliptical and Circular Models

We investigated the impact of the mobile velocity on the performance of the dual antenna system with the adaptive combining. We varied the mobile velocity to 2, 10, 30, 60, 90, and 120 km/hr, which results in 4, 20, 59, 119, 178, and 238 Hz of maximum Doppler frequency, respectively, with the GBSB circular model. Note that all the other parameters remain the same as the baseline parameters. The simulation results are given in Figure 4-13. The top cluster of the

six graphs represents the BERs of a single antenna system with the six mobile velocities. The bottom cluster of the six graphs represents the BERs of the dual antenna system. The simulation results reveal that the dual antenna system performs better than a single antenna system for all the six mobile velocities. It is notable that the impact of the mobile velocity is insignificant for a single antenna system. However, as the mobile velocity decreases, the BER of the dual smart antenna system with the adaptive combining also decreases. As expected, the adaptive combining based on the N-LMS algorithm adapts the antenna weights well as the mobile velocity decreases.

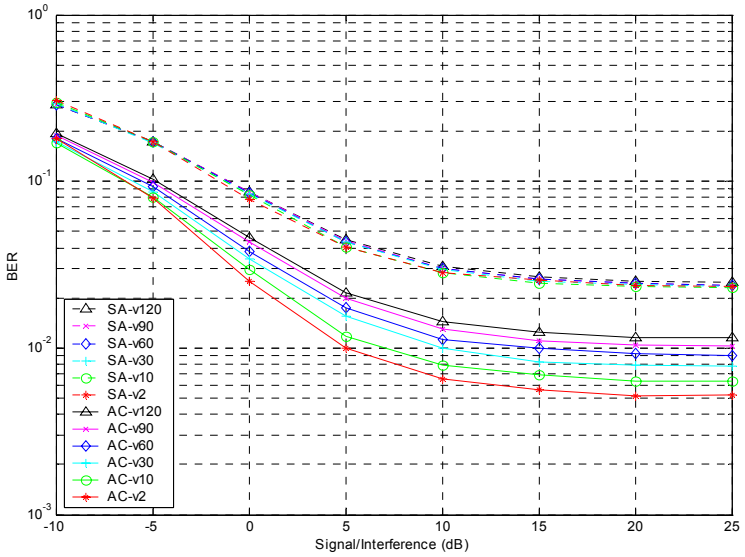

Figure 4-13. BERs with Various Mobile Velocities

The simulation results of the adaptive combining for the 3GPP system indicate that

i) the dual smart antenna system with the adaptive combining performs better than a single antenna system; its performance gain is 3.3 dB for the GBSB elliptical model at BER = $5x10^{-2}$ and 5.5 dB for the GBSB circular model.

ii) As expected, the higher performance gain is achieved as the mobile velocity decreases.

4.3 Performance of Hybrid Combining for the 3GPP System

Simulation results to evaluate the performance of the dual smart antenna handsets with the proposed hybrid combining scheme for the 3GPP system are presented in this section. The hybrid combiner (HC) combines the diversity combiner (DC) and the adaptive combiner (AC) outputs using the MRC. The instantaneous signal plus noise (S+N) value is used to weight each combiner output instead of its SNR. The ECFCM described in Chapter 3 is applied for the channel model.

4.3.1 Simulation Environment for the GBSB Models

The environment considered in our simulation is almost the same as the baseline parameters described in Section 4.1. Some differences and additional parameters are as follows. The distance and the maximum multipath delay are 4000 m and 61 chips in the GBSB circular model. The envelope correlation of two Rayleigh fading signals for each multipath in the ECFCM is chosen to be 0.5. The two handset antennas also receive interference and background noise signals. Two multipath signals from an adjacent base station, which transmits the combined signal of eight users' signals and the common pilot signal, are considered. It is noted that the average SINR is 7.4 dB (due to multipath interference) when there is no interference from an adjacent base station or noise. The background noise results in 7.0 dB average SINR without interference. This is due to the multipath interferences. A rake receiver with four rake fingers is considered at handsets. The same step size, $\mu = 0.3$, and the same number of pilot symbols to be averaged to obtain the reference signal, $Q = 3$, are employed for the N-LMS algorithm as chosen in Section 4.2.

To show the performance of each combining scheme, the plot of BER versus SINR is presented. Note that BERs of a plot are uncoded ones. To vary the SINR, the average received power of interference signals from the adjacent base station is changed. To get the average BER for a given SINR, a number of simulation runs (a simulation run covers the duration of 4 frames) are repeated until the estimated BER lies within ±2% of the true value with 99% confidence. Based on the theory of Monte Carlo simulation, the necessary number of error counts is obtained as 16588 [75]. If not explicitly specified, the channel profile obtained from the GBSB elliptical model is used in the simulation.

4.3.2 Performances of the DC and the AC for the GBSB Models

First, we present the simulation results of the DC and the AC to compare the performances of these two combining schemes under different operating conditions. The simulation results with various antenna distances (λ/8, λ/4, 3λ/8, and λ/2) are shown in Figure 4-14. Note that all the other parameters are the same as the baseline parameters in the simulation. In the figures, the first line represents the BER of a single antenna (SA) system, and the remaining lines represent the BERs of the dual antenna system where the antenna distance is λ/8, λ/4, 3λ/8, and λ/2 from top to bottom. As the distance of two antennas increases, the dual antenna system achieves higher performance gain. Since the difference in performance between the antenna distances of λ/2 and λ/4 is small, the dual antenna system with the antenna distance of λ/4 (3.5 cm) is a good candidate for the practical implementation of both DC and AC. As can be seen from the figure, the AC performs better than the DC at the low SINR (i.e., interference-limited) environment. Meanwhile, the DC performs better than the AC at the high SINR (i.e., noise-limited) environment. For example, the BER of the DC with the antenna distance of λ/4 is $0.13/0.7\text{x}10^{-2}$ for a low/high SINR = 0.45/6.6 dB, while the BER of AC is $0.11/0.93\text{x}10^{-2}$ for the same SINR. The opposite trend of two combining schemes is one of the reasons to propose the HC.

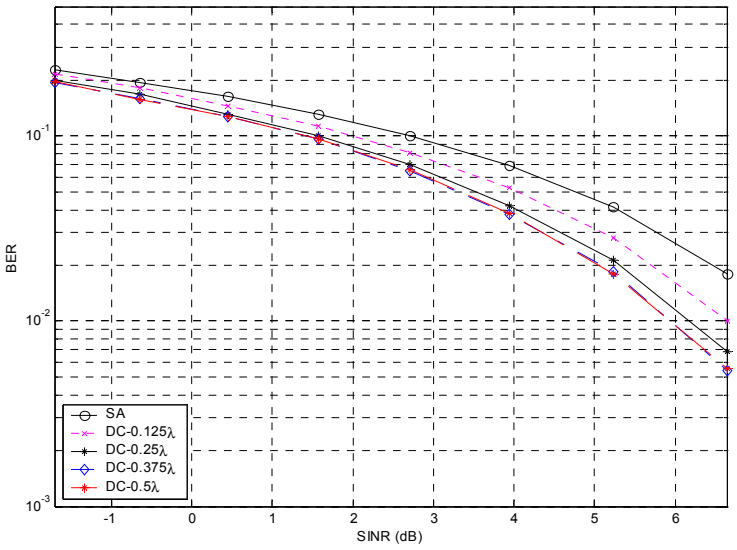

(a) Performance of the DC

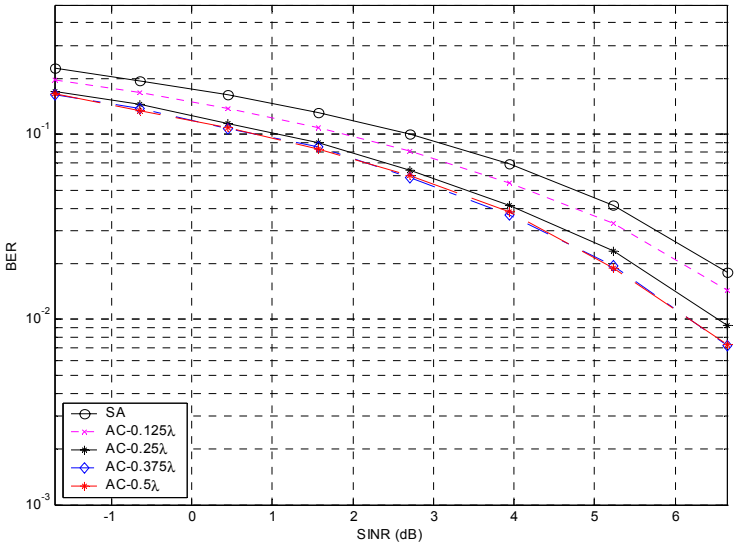

(b) Performance of the AC

Figure 4-14. Performance of the DC and the AC with Various Antenna Distances

To investigate the impact of the mobile velocity, we simulated with various mobile velocities. The simulation results with various mobile velocities are shown in Figure 4-15. We varied the mobile velocity to 2, 30, 60, 90, 120, and 150 km/hr, which results in 4, 59, 119, 178, 238, and 297 Hz of maximum Doppler frequency, respectively. In the figures, the upper cluster of graphs represents the BERs of a single antenna system with various mobile velocities, and the lower cluster of graphs represents the BERs of the dual antenna system, where the mobile velocity decreases from top to bottom for each cluster. As can be seen from the figure, the performances of a single antenna system and the dual antenna system with the DC are little affected by varying mobile velocities. However, this does not hold for the AC as apparent in Figure 4-15 (b), i.e., the performance of the AC degrades as the mobile velocity goes high. Apparently, the AC is tracking well for a low Doppler frequency, i.e., relatively slow fading of the desired and interfering signals, but is unable to adapt fast enough for a high mobile velocity. At a high SINR environment, the AC performs better than the DC for a low mobile velocity (2 or 30 km/h), but it is reversed for a high mobile velocity (faster than 60 km/h). This is another reason to consider the HC.

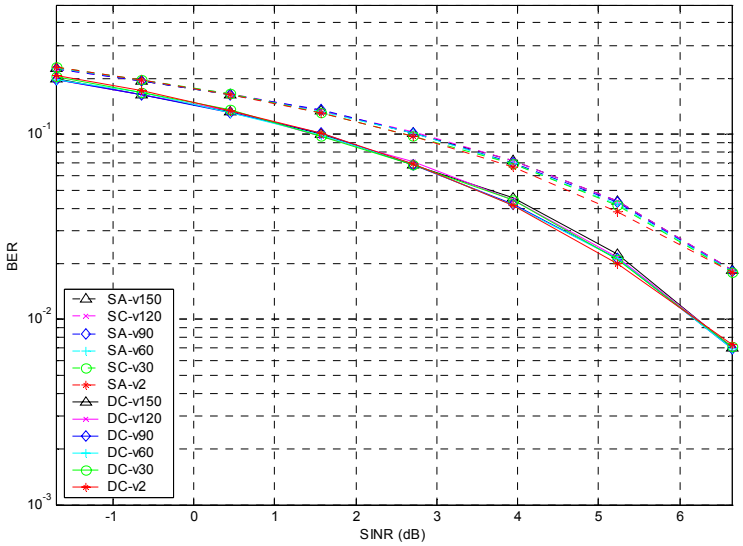

(a) Performance of the DC

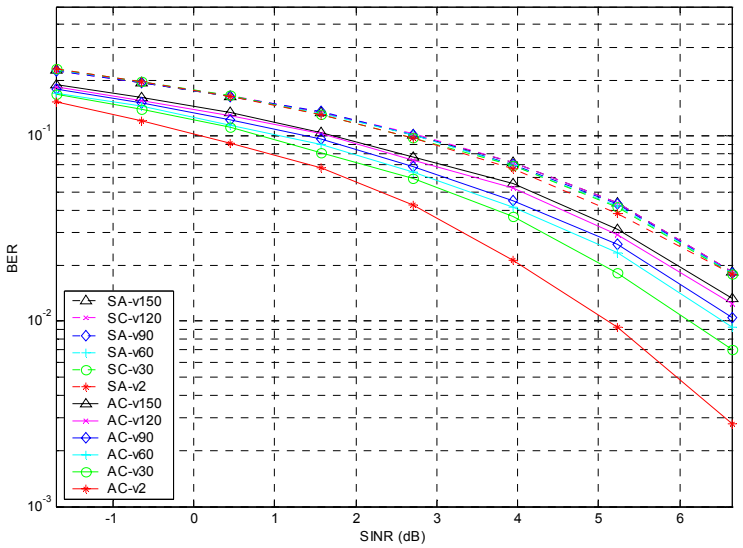

(b) Performance of the AC

Figure 4-15. Performance of the DC and the AC with Various Mobile Velocities

To investigate the performance variation due to the envelope correlation, we simulated with various envelope correlations; the simulation results are shown in Figure 4-16, where the mobile velocity is fixed to 60 km/h. The envelope correlation was varied in 0.3 increments from 0.05 to 0.95. In the figures, the top graph represents the BER of a single antenna system, and the

remaining ones for the BERs of the dual antenna system with the envelope correlations, 0.05, 0.35, 0.65, and 0.95, respectively. As expected, the DC performs better as the envelope correlation is lower. However, it is interesting to note that the AC performs better for a higher envelope correlation. The phenomenon is especially apparent for a high SINR. The opposite behavior is another motivation to investigate the proposed hybrid combining scheme.

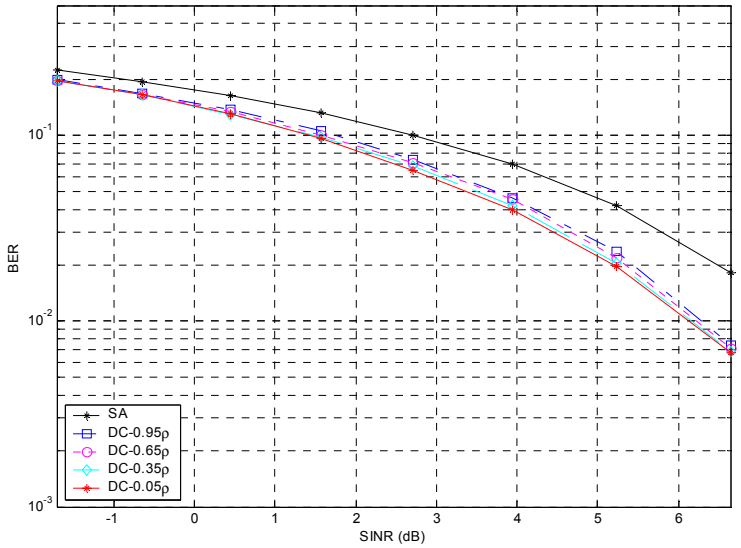

(a) Performance of the DC

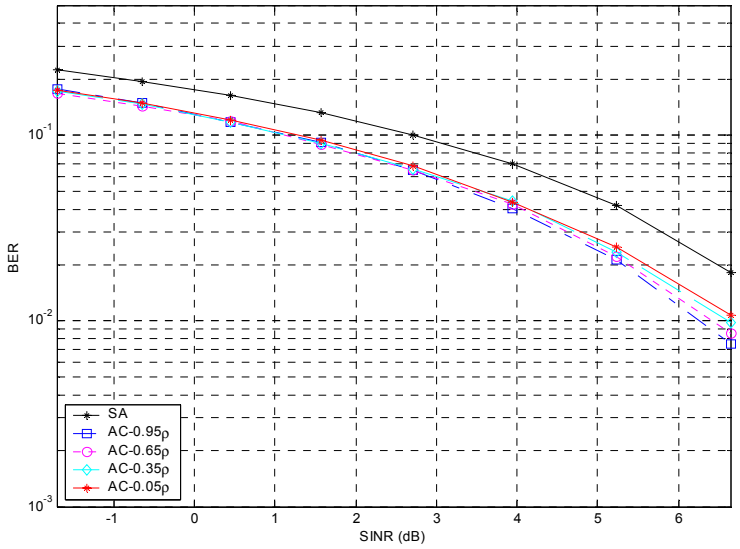

(b) Performance of the AC

Figure 4-16. Performance of the DC and the AC with Various Envelope Correlations

The performance trend between the DC and the AC for various envelope correlations is essentially the same as shown in Figure 4-17 (b), in which the envelope correlation is 0.5. The only difference is that the cross point (at which they show the same BERs) between the DC and the AC shifts to the right/left as the envelope correlation increases/decreases.

As noted earlier, two interfering signals from an adjacent base station were considered in the simulation so far. To investigate the impact of the number of interfering signals from an adjacent base station, we varied the number of interfering signals from two to four and six in our simulation. We maintained the total amount of interference power the same in the experiment, which results in the same SINR for the rake outputs. We observed the same tendency in performance (which is similar to the one shown in Figure 4-17 (b)). However, a slight decrease in performance of each combining scheme with an increase of the number of interfering signals was observed.

Finally, we experimented with the channel profiles obtained from the GBSB circular model. The simulation results with the GBSB circular model show the same trend as those with the GBSB elliptical model. The only difference is that the SINR of the rake output (which is given on the x-axis of a figure) with the GBSB circular model is lower, especially when the same

small amount of interferences from an adjacent cell is added. This is due to the effect of multipaths. The relative distance of a multipath signal to the first multipath signal is smaller for the GBSB circular model than the GBSB elliptical model. Hence, this results in relatively smaller path loss, i.e., relatively larger signal power for the multipath signal compared to the GBSB elliptical model. Since a multipath signal acts as interference to other multipath signals, strong multipath signal of the circular model results in a strong interference to other multipath signals. If the interference from an adjacent cell is weak for the circular model, the SINR is dominant by the multipath interference. Therefore, the SINR of the circular model is smaller than that of the elliptical model for weak interference from an adjacent cell.

4.3.3 Performance of the HC for the GBSB Models

As observed in Subsection 4.3.2, the DC and the AC exhibit opposite trends in SINR, mobile velocity, and envelope correlation. Thus, the proposed HC aims to exploit the advantages of the two combining schemes.

We experimented the performance of the HC for various mobile velocities. As noted earlier, the AC performs well for a low mobile velocity, while the DC is good for a high velocity. The simulation results for the mobile velocity of 2 km/hr are shown in Figure 4-17 (a). As can be seen from the figure, the AC performs the best, while the performance of the HC is equal or close to that of the AC. When the mobile velocity is increased, the HC performs better than both the AC and the DC. As a representative case, the simulation results with the mobile velocity of 60 km/hr are shown in Figure 4-17 (b). For instance, the SINR gain of the HC is 0.4 dB higher than the AC for BER = 0.1 and 0.8 dB higher than the DC. Finally, the DC performs well for a high mobile velocity. Simulation results for the mobile velocity of 120 km/hr are shown in Figure 4-17 (c). The figure shows that the performance of the HC is equal to or slightly lower than that of the DC for the high SINR environment. We observed the same trend for the velocity of 150 km/hr. In summary, the performance of the HC is better than or equal to the better performing scheme, either the DC or the AC, for *any* mobile velocity.

We experimented the HC with various envelope correlations, number of interference signals, and the GBSB elliptical and circular models. All our observations from the experiments can be summarized as the performance of the HC is the best or close to the best among the three schemes.

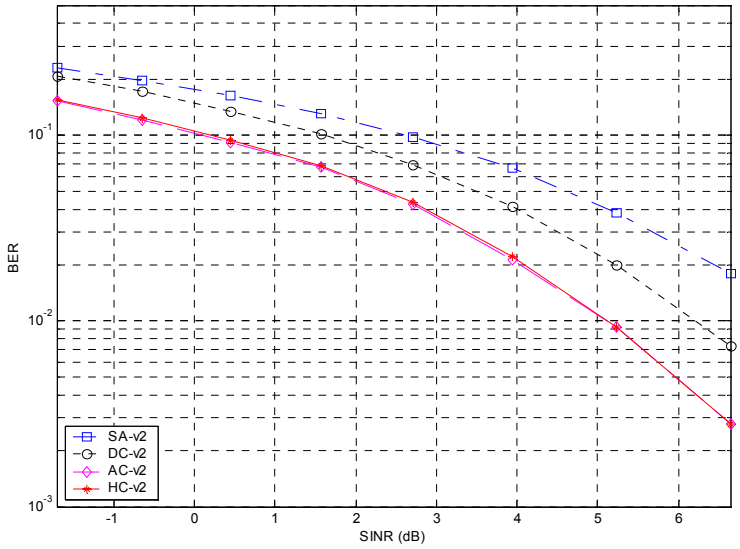

(a) Performance with the Mobile Velocity of 2 km/hr

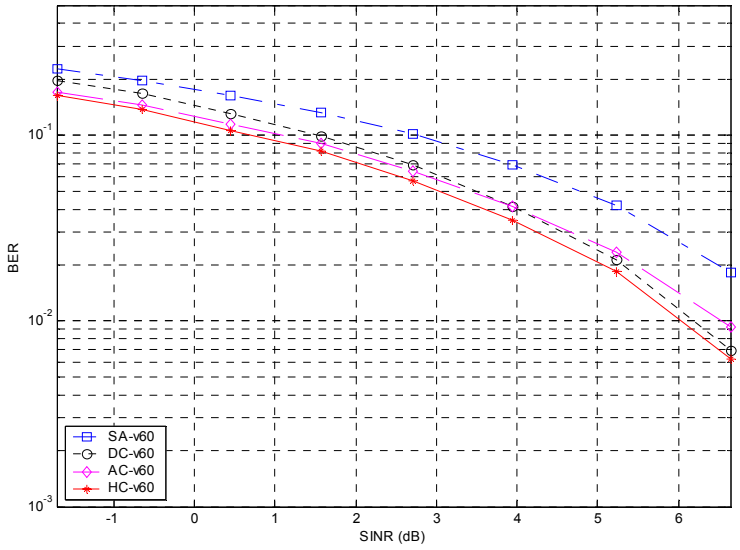

(b) Performance with the Mobile Velocity of 60 km/hr

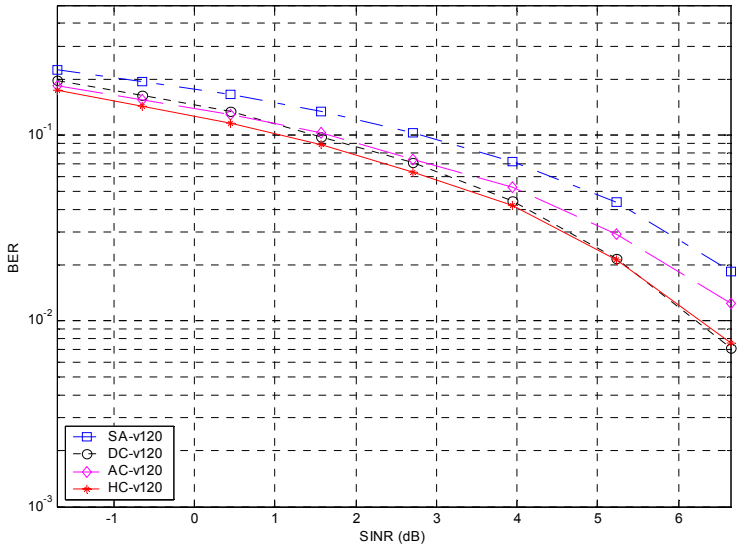

(c) Performance with the Mobile Velocity of 120 km/hr

Figure 4-17. Performance of the HC with Various Mobile Velocities

4.3.4 Simulation Environment for the ITU Channel Model

System models and parameters considered in our simulation are typical for the 3GPP WCDMA system [24] except only one transmit antenna is used at a base station. The environment considered in our simulation is almost the same as the baseline parameters described in Section 4.1. Some differences and additional parameters are as follows. To obtain the channel profile for each simulation run, we employed the ITU channel model [37]. Delay and average power of each multipath for the ITU channel profiles are summarized in Table 2.2. Four or six multipath signals (M) are generated in the wireless channel depending on the channel type as shown in Table 2.2. The envelope correlation of two Rayleigh fading signals for each multipath in the ECFCM is chosen to be 0.5. The two handset antennas also receive interference and background noise signals. Two multipath signals from an adjacent base station, which transmits the combined signal of eight users' signals and the common pilot signal, are considered as interfering signals. For the Vehicular A and B channel, the mobile velocity is assumed to be 50 km/hr, which results in 99.1 Hz of maximum Doppler frequency for a 2.14 GHz carrier frequency. The mobile velocity for the Pedestrian A and B channel is assumed to be 3 km/hr, which results in 5.9 Hz of maximum Doppler frequency. The number of rake fingers (L)

considered at the receiver for each channel type is also shown in Table 2.2. The same step size, $\mu = 0.3$ and the same number of pilot symbols to be averaged to obtain the reference signal, $Q = 3$, are employed for the N-LMS algorithm as chosen in Section 4.2.

4.3.5 The Performance of the DC, the AC, and the HC for the ITU Channel Model

First, we present the simulation results of the DC, the AC, and the HC to compare the performance of each combining scheme for each channel profile. The simulation results with each channel profile are shown in Figure 4-18. The simulation results with the ITU Pedestrian A channel profile are presented in Figure 4-18 (a). In the figures, the square, circle, diamond, and asterisk lines represent the BERs of a single antenna (SA) system, the DC, the AC, and the HC, respectively. As can be seen from the figure, the HC performs the best. The AC performs better than the DC at the low SINR (i.e., interference-limited) environment, while the DC performs better than the AC at the high SINR (i.e., noise-limited) environment. The SINR gain of the HC over a single antenna system is 4.28 dB at BER = 10^{-2} and the SINR gains of the DC and the AC over a single antenna system are 3.83 dB and 3.58 dB at the same BER, respectively. Figure 4-18 (b) shows the simulation results with the ITU Pedestrian B channel profile. As can be seen from the figure, the HC performs the best and the DC performs the worst. The performance of the AC is equal or close to that of the HC.

The simulation results with the Vehicular A channel profile are shown in Figure 4-18 (c). The HC always performs the best. The AC performs better than the DC at the low SINR environment, while the DC performs better than the AC at the high SINR environment. The simulation results with the Vehicular B channel profile show the same trend as that of the Vehicular A channel profile. The only difference is observed in the combined SINR and the BER performance, since each channel profile has a different power profile.

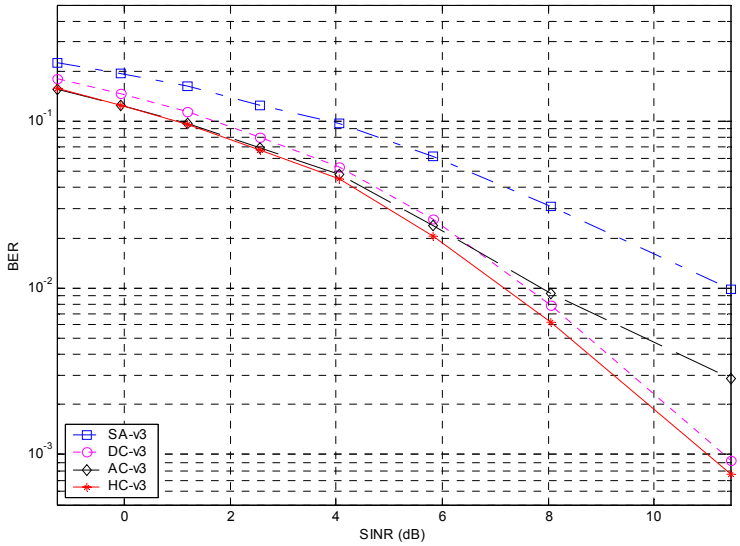

(a) Performance with the Pedestrian A with the Mobile Velocity of 3 km/hr

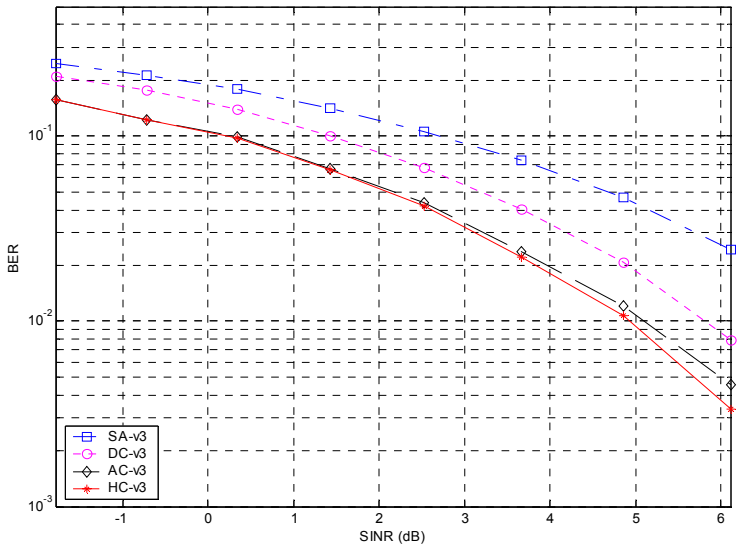

(b) Performance with the Pedestrian B with the Mobile Velocity of 3 km/hr

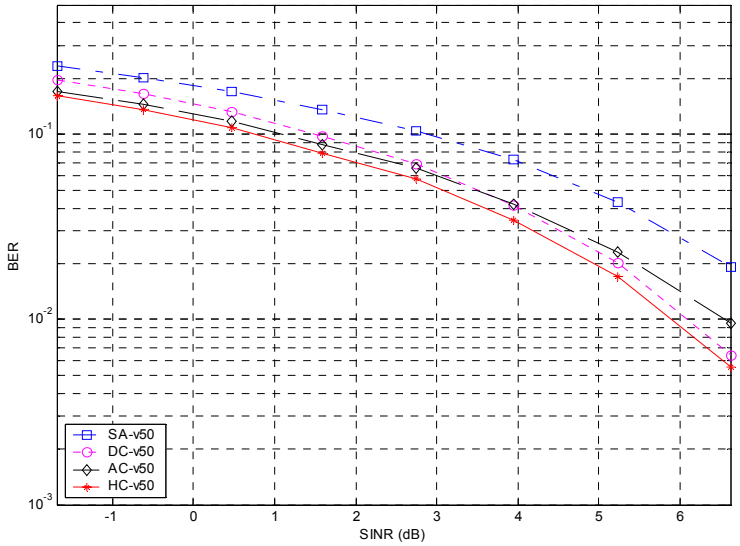

(c) Performance with the Vehicular A with the Mobile Velocity of 50 km/hr

Figure 4-18. Performance of the DC, the AC, and the HC

To investigate the impact of the antenna distance, we simulated with different antenna distances for the Pedestrian B and the Vehicular A channel profiles. Note that all the other parameters are the same as the baseline parameters in the simulation. The simulation results of the HC with various antenna distances (λ/8, λ/4, 3λ/8, and λ/2) for the Pedestrian B channel profile are shown in Figure 4-19. In the figures, the first line represents the BER of the SA, and the remaining lines represent the BERs of the dual antenna system where the antenna distance is λ/8, λ/4, 3λ/8, and λ/2, respectively. The dual antenna system with the antenna distance of 3λ/8 shows the best performance. Since the difference in performance between the antenna distances of 3λ/8 and λ/4 is small, the dual antenna system with the antenna distance of λ/4 (3.5 cm) is a good candidate for the practical implementation of the HC. The performance trends of the DC and the AC are the same as that of the HC. The same trends also hold for the Vehicular A channel profile.

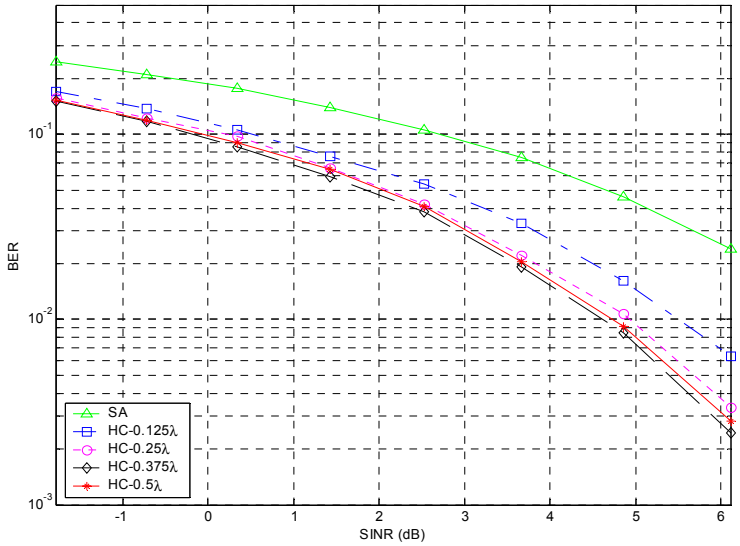

Figure 4-19. Performance of the HC with Various Antenna Distances

To investigate the impact of the mobile velocity, we simulated with various mobile velocities. The simulation results with various mobile velocities for the Vehicular A channel profile are shown in Figure 4-20. We varied the mobile velocity to 50, 85, and 120 km/hr, which results in 99.1, 168.4, and 237.8 Hz of maximum Doppler frequency, respectively. As can be seen from Figure 4-20 (a), the performances of the dual antenna system with the DC are affected little by varying mobile velocities. However, this does not hold for the AC as apparent in Figure 4-20 (b), i.e., the performance of the AC degrades as the mobile velocity goes high. Apparently, the AC is tracking well for a low Doppler frequency, i.e., relatively slow fading of the desired and interfering signals, but is unable to adapt fast enough for a high mobile velocity. Since the HC combines the DC and the AC outputs, the performance trend for the HC is the same as that for the AC.

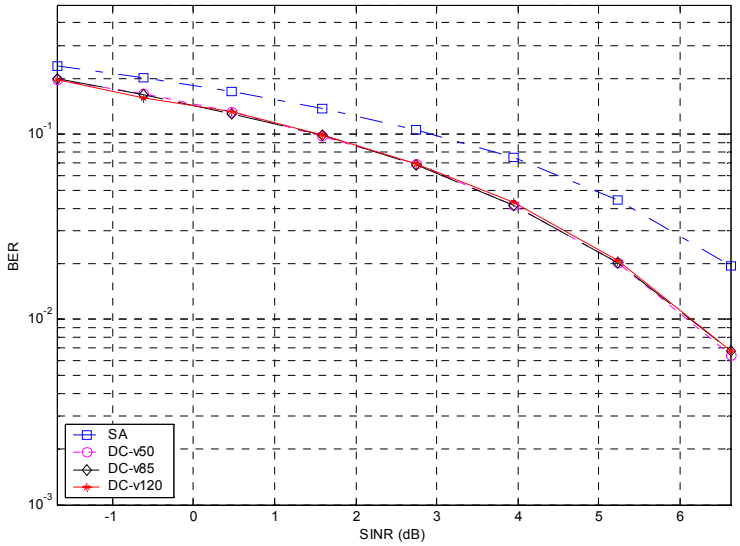

(a) Performance of the DC

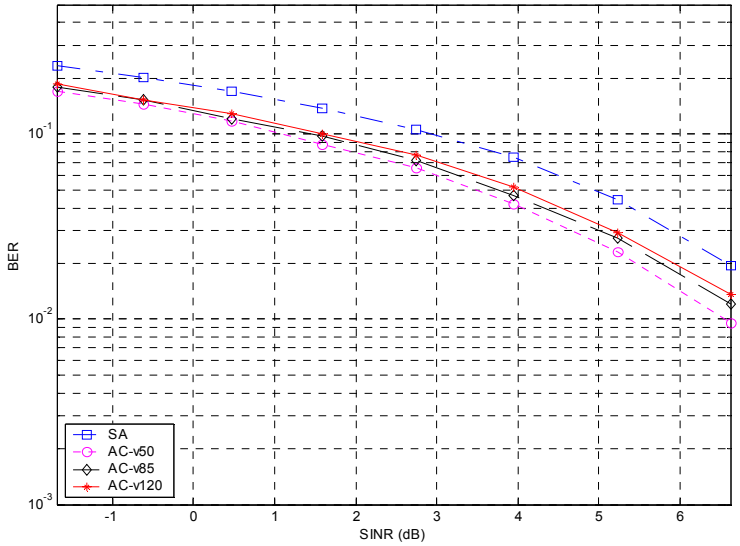

(b) Performance of the AC

Figure 4-20. Performance of the DC and the AC with Various Mobile Velocities

In conclusion, the performance of the proposed hybrid combining scheme is always better than or equal to those of the adaptive and the diversity combining schemes for all simulation environments considered.

4.4 Performance of Diversity Combining for the cdma2000 System

Simulation results to evaluate the performance of the dual smart antenna handsets with the diversity combining scheme for the cdma2000 system are presented in this section.

4.4.1 Simulation Environment

The three types of the channel model, LCFCM, SCFCM, and UCFCM, described in Chapter 3 are employed for the simulation. The signal received at a handset antenna is applied to its own demodulator and then to a four-finger rake receiver. To process the dual antenna signals, two levels of diversity combining schemes are considered. The first one is the rake level diversity combining in which a diversity combiner combines rake receiver outputs. The second one is the finger level diversity combining in which a diversity combiner combines finger outputs. Three diversity combining schemes—SD, EGC, and SLC—are considered for each level (the rake level and the finger level) of diversity combining scheme.

We assumed that the distance from the base station to the mobile station is 1000 m. We also assumed that the mobile velocity is 100 km/hr, which results in 185 Hz of maximum Doppler frequency for a 2.0 GHz carrier frequency. In simulating the system with the SPW of Cadence, we used the link budget shown in Table 4-2. From Table 4-2, only 2.5% (or 0.74 W) of the total transmitted power of 30 W is allocated to the desired user traffic channel. For the channel profile, the ITU Vehicular A channel model is applied. A proper level of AWGNs is added to the channel to achieve 9.75 dB of the signal-to-noise ratio (Eb/N_0) on the desired user traffic channel for the six multipath signals.

Table 4-2. Link Budget

Channel	Power (W)
Pilot	5.99
Paging	1.89
Sync	0.75
User traffic	0.74
Power control	0.13
Other users	20.50
Total	30.00

The simulation was performed for 3999 frames in which the period of each frame is 20 ms. Hence, it covers 80 seconds of the real operation. To evaluate the system performance, three system performance metrics were calculated as described next. After receiving a frame of data, the transmitted data rate is determined based on the CRC bits and the error metric from the Viterbi decoder. If the determined data rate is incorrect, a data rate decision error (DRDE) occurred for the frame. In such a case, a large number of bits are usually erroneous. We assume that 40% of bits of a frame are in error if a DRDE occurred in the frame. The data rate decision error rate (DER) is the ratio of the number of DRDE frames to the total number of transmitted frames (which is 3999). A frame is erroneous if a DRDE occurred and/or at least one bit in the frame is erroneous. The frame error rate (FER) is the number of erroneous frames to the total number of frames. A bit error occurs if the received bit does not match the transmitted data bit. The bit error rate (BER) is the ratio of the number of bit errors to the total number of transmitted data bits.

4.4.2 Simulation Results

We performed simulation on a Sun UltraSPARC10 workstation with 1 GB of main memory. The CPU time was not measured, but the elapsed time for the simulation is about six days for each simulation run. We performed the simulation three times for each type of the channel model. Then the three simulation results are averaged. In Table 4-3, the simulation results with three types of the channel model, two levels of diversity combining, and three

diversity combining schemes are summarized. The first two rows represent the performance of a single antenna, while the remaining five rows represent the performance of the dual antennas with different diversity combining schemes and different level of diversity combining. Two elements of each entry are the average number of frames out of 3999 frames simulated and its percentile, respectively. Since each EGC scheme for the rake level and the finger level has the same operation except for its order, their results are the same. Thus, the only one result is presented in the table.

When a single antenna is employed, the DERs and the FERs are about the same, with both measuring around 8%. Since a DRDE always causes a frame error, it can be concluded that most frame errors are due to DRDEs. When dual antennas are employed, the FERs are reduced to below 1% for all diversity combining schemes under the UCFCM. However, as the correlation of dual antenna signals increases from the UCFCM to the SCFCM, the FERs increase up to 6%. The results also indicate that i) diversity combining scheme at the finger level performs slightly better than the rake level diversity combining scheme, and ii) EGC scheme performs the best among the three diversity combining schemes. When EGC scheme is employed for the diversity combining, the average reduction ratio of the FER for the dual antenna system over the single antenna system is 13.0 dB (8.65% to 0.43%) for the UCFCM, 2.49 dB (7.98% to 4.50%) for the LCFCM, and 1.87 dB (8.51% to 5.53%) for the SCFCM. In conclusion, a smart antenna at handsets significantly improves the performance for the UCFCM, but the improvement is moderate for the other two channel models.

Table 4-3. Performance of Dual Smart Antennas

Scheme	Level	UCFCM			LCFCM			SCFCM		
		DER	FER	BER	DER	FER	BER	DER	FER	BER
Antenna 1		354.3 8.86%	355.3 8.89%	3.55%	315.7 7.89%	316.0 7.90%	3.16%	343.0 8.58%	344.3 8.61%	3.44%
Antenna 2		335.3 8.39%	336.3 8.41%	3.36%	321.0 8.03%	322.0 8.05%	3.22%	336.0 8.40%	336.7 8.42%	3.36%
SD	Rake	21.7 0.54%	22.0 0.55%	0.22%	200.0 5.00%	200.3 5.01%	2.00%	240.0 6.00%	240.3 6.01%	2.40%
	Finger	18.3 0.46%	18.7 0.47%	0.19%	193.3 4.83%	193.7 4.84%	1.93%	233.7 5.85%	235.7 5.89%	2.35%
SLC	Rake	17.3 0.43%	17.3 0.43%	0.17%	186.0 4.65%	187.3 4.68%	1.88%	226.0 5.65%	226.7 5.67%	2.27%
	Finger	16.3 0.41%	16.3 0.41%	0.16%	183.3 4.58%	184.0 4.60%	1.84%	224.0 5.60%	225.7 5.64%	2.26%
EGC	Rake	17.0 0.43%	17.0 0.43%	0.17%	179.7 4.49%	180.0 4.50%	1.80%	220.0 5.50%	221.0 5.53%	2.21%
	Finger									

4.5 Performance of Adaptive Combining for the cdma2000 System

To validate the performance gain of the dual smart antennas at handsets under the employment of the N-LMS algorithm, the cdma2000 system with the smart antenna is modeled and simulated with the SPW tool.

4.5.1 Simulation Environment

The signal received at a handset antenna is applied to its own demodulator and then to each rake finger. In a single antenna system, each rake finger output is coherently combined. In a dual antenna system with the adaptive combining scheme, each rake finger signal from each antenna is combined with the adaptively computed antenna weights. Then the output of each adaptive combiner is coherently combined. The rake finger is a basic building block for a rake receiver,

and the adaptation logic for the antenna weights is a basic building block for a smart antenna system. Logic diagrams for each building block are presented in Figure 4-21. The rake finger also includes the fine timing acquisition logic, but it is omitted in the figure for brevity.

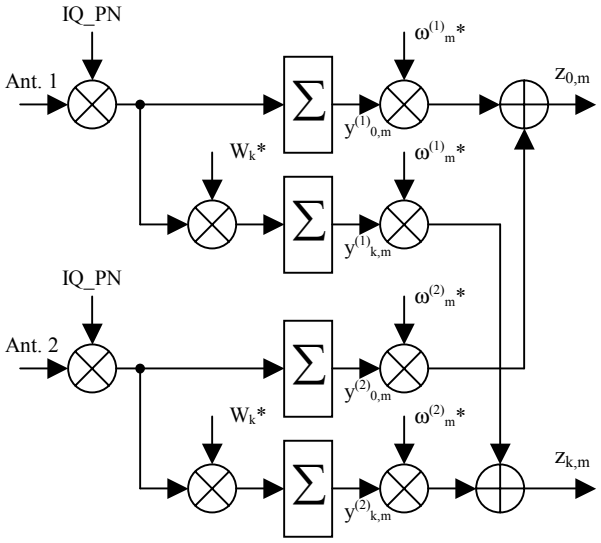

(a) Rake Finger for the *m*-th Multipath

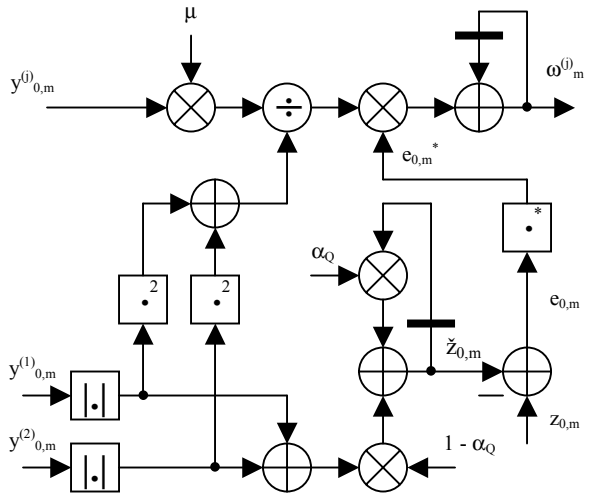

(b) Adaptation Logic for Antenna Weights

Figure 4-21. Building Blocks of an Adaptive Rake Receiver for Smart Antennas

We considered the following environment: the distance from the base station to the mobile station is 1000 m, and the standard deviation of the path loss in the lognormal fading is 10 dB, which is a typical value for outdoor channel. In simulating the system with the SPW of Cadence, we used the same link budget shown in Table 4-2. To shorten the simulation time, a simplified simulation model was used in our simulation. The number of multipath signals was limited to two in the channel model. Consequently, a rake receiver with two rake fingers for each antenna was used to despread and combine the multipath signals. For simplicity, two multipath signals were assumed to have, on average, the same level of the received signal power. One multipath signal is effectively an interference signal to the other multipath signal. AWGN is also added to the channel, and it results in 9.79 dB of SINR. To obtain the reference signal $\check{z}_{0,m}(n)$ in the N-LMS algorithm, the following infinite impulse response (IIR) method is used for the cdma2000 system instead of the finite impulse response (FIR) method for the 3GPP WCDMA system.

$$\check{z}_{0,m}(n) = \alpha_Q \check{z}_{0,m}(n-1) + (1-\alpha_Q)(|y^{(1)}_{0,m}(n)| + |y^{(2)}_{0,m}(n)|), \quad (4\text{-}1)$$

where α_Q is the forgetting factor. The forgetting factor is used to define the relative portion of the previous pilot symbols to obtain the reference signal. The two factors that affect the performance of the N-LMS algorithm are the step size and the forgetting factor. The step size, $\mu = 0.125$, and the two forgetting factors, $\alpha_Q = 0.975$ and 0.9875, were chosen through trial and error.

4.5.2 Simulation Results

We performed the simulation three times for each mobile velocity and each angle of arrival, in which one simulation run covers 3999 frames. Then the three simulation results are averaged. The simulation results with different mobile velocity and different angle of arrival are summarized in Table 4-4. Three different mobile velocities—100 km/h, 50 km/h, and 25 km/h—were considered, and the maximum Doppler frequencies for the three mobile velocities are 185 Hz, 93 Hz, and 46 Hz for a 2.0 GHz carrier frequency. Two sets of the angle of arrival were arbitrarily chosen: set 1 (AOA_1) with 20° for multipath 1 and 45° for multipath 2, and set 2 (AOA_2) with -45° for multipath 1 and 35° for multipath 2. The first two rows in the table represent the performance of a single antenna. The remaining two rows represent the performance of the dual antennas with the two different forgetting factors. The top element of

each entry is the number of erroneous frames out of 3999 frames simulated, and the bottom element is the percentile.

Table 4-4. Frame Error Rate of Dual Smart Antennas

		100 km/hr	50 km/hr		25 km/hr
		AOA_1	AOA_1	AOA_2	AOA_1
Antenna 1		588.7 14.7%	605.3 15.1%	590.0 14.8%	600.0 15.0%
Antenna 2		585.7 14.7%	598.0 15.0%	573.0 14.3%	601.0 15.0%
AC	α_Q = 0.975	488.0 12.2%	399.3 10.0%	428.0 10.7%	360.0 9.0%
	α_Q = 0.9875	520.7 13.0%	435.3 10.9%	473.3 11.8%	381.0 9.5%

When a single antenna is employed, the FERs are around 15% for all the three mobile velocities. When dual antennas are employed, the FERs are reduced in the range of 1.7% (which is from 14.7% to 13.0% for 100 km/h of the mobile velocity) to 6.0% (which is from 15.0% to 9.0% for 25 km/h of the mobile velocity). The forgetting factor α_Q = 0.975 performs better than α_Q = 0.9875 for the dual antenna system for all the three velocities. The reduction ratio of the FER for the dual antenna system under α_Q = 0.975 over the better performing single antenna system is 0.8 dB (equivalently reduction from 14.7% to 12.2%) for 100 km/h of the mobile velocity. The reduction ratio increases to 1.8 dB (equivalently from 15.0% to 10.0%) for 50 km/h of the mobile velocity under the AOA_1 and 1.3 dB (equivalently from 14.3% to 10.7%) under the AOA_2. The reduction ratio further increases to 2.2 dB (equivalently from 15.0% to 9.0%) for 25 km/h of the mobile velocity. In summary, i) as the mobile velocity decreases, the frame error rate of the dual antennas with adaptive combining also decreases, and ii) the adaptive algorithm with the forgetting factor α_Q = 0.975 performs better than that for the forgetting factor α_Q = 0.9875. In conclusion, a dual smart antenna system with adaptive combining scheme at handsets is beneficial for the cdma2000 system.

4.6 Summary

In this chapter, we presented the simulation results to evaluate the performance of the proposed dual smart antenna system at handsets for the 3G wireless personal communication systems. Simulation results for the 3GPP WCDMA system with diversity combining, adaptive combining, and hybrid combining schemes were presented in Section 4.1, Section 4.2, and Section 4.3, respectively. Then, simulation results for the cdma2000 system with diversity combining and adaptive combining were presented in Section 4.4 and Section 4.5, respectively.

All simulation results indicate that a dual smart antenna system at handsets is effective in spite of the proximity of the two antennas and the proposed system is beneficial for the 3G wideband CDMA systems.

Chapter 5 Performance of MS-GSC and Adaptive Rake Combining Scheme

In this chapter, we present the simulation results to verify the proposed minimum selection GSC method and an adaptive rake combining scheme to reduce power dissipation by a mobile rake receiver. To verify the validity of the proposed adaptive scheme, four rake combining schemes are applied to a mobile rake receiver for the WCDMA system.

5.1 Simulation Environment

System models and parameters considered in the simulation which results are presented in this chapter are typical for the 3GPP WCDMA system [24] except only one transmit antenna is used at a base station. Eight users' signals with a spreading factor 32 and the common pilot channel (CPICH) signal with a spreading factor 256 are modulated, channelized, combined, scrambled, pulse-shaped, and transmitted through the channel. Twenty percent of the total transmitted power is allocated to the CPICH, and the remaining 80% of the power is allocated equally to each user signal. For the channel profile (such as delay and average power), the ITU channel profiles described in [37] are applied.

Delay and average power of each multipath for the ITU channel profiles are summarized in Table 2.2. Four or six multipath signals (M) are generated in the wireless channel depending on the channel type as shown in Table 2.2. Each multipath signal is experienced an independent Rayleigh fading. For the Vehicular A and B channel profiles, the mobile velocity is assumed to be 50 km/hr, which results in 99.1 Hz of maximum Doppler frequency for a 2.14 GHz carrier

frequency. The mobile velocity for the Pedestrian A and B channel profiles is assumed to be 3 km/hr, which results in 5.9 Hz of maximum Doppler frequency. The despread CPICH signal of each multipath signal is utilized to estimate the channel condition, i.e., the amplitude and the phase, and thus is used as a weighting factor of each rake finger to combine the selected rake finger outputs. To reduce the simulation time, channel encoding and decoding is not included. Thus, a hard decision is made at the output of rake combiner and the output is compared with the original data bits to evaluate the BER performance. This BER is fed back to the control logic for the proposed adaptive rake combiners.

5.2 Performance of GSCs: GSC, MS-GSC, AT-GSC, and NT-GSC

First, we present the BER performances of the original GSC, the MS-GSC, the AT-GSC, and the NT-GSC. Figure 5-1 (a) shows the BER performance of the GSC with five rake fingers under the ITU Pedestrian B channel profile. GSC (m, 5) performs better as m increases. Figure 5-1 (b) shows the BER performance of the proposed MS-GSC with a threshold set of $\delta = 0.5$. As shown in the figure, the MS-GSC (T_m, 5) performs better as the threshold T_m becomes larger. The performance of the MS-GSC is lower and upper bounded by the SC and the MRC, respectively. The AT-GSC and the NT-GSC show almost the same BER performance as that of the MS-GSC with a threshold set of $\delta = 0.5$.

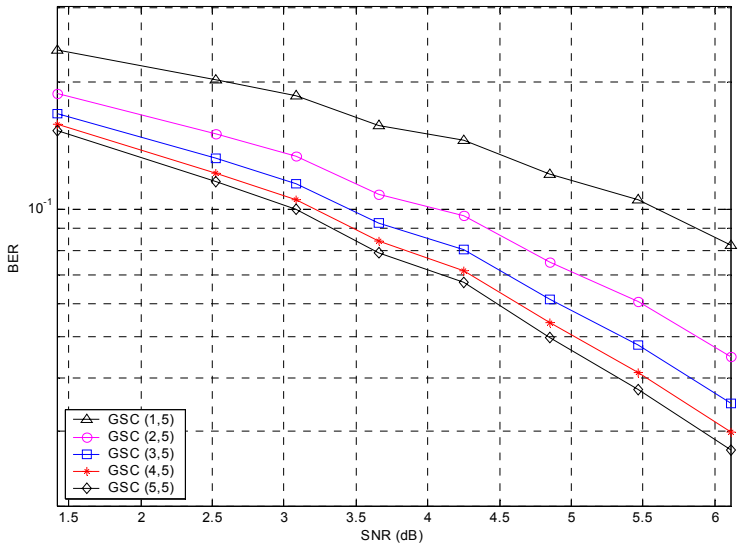

(a) Original GSC

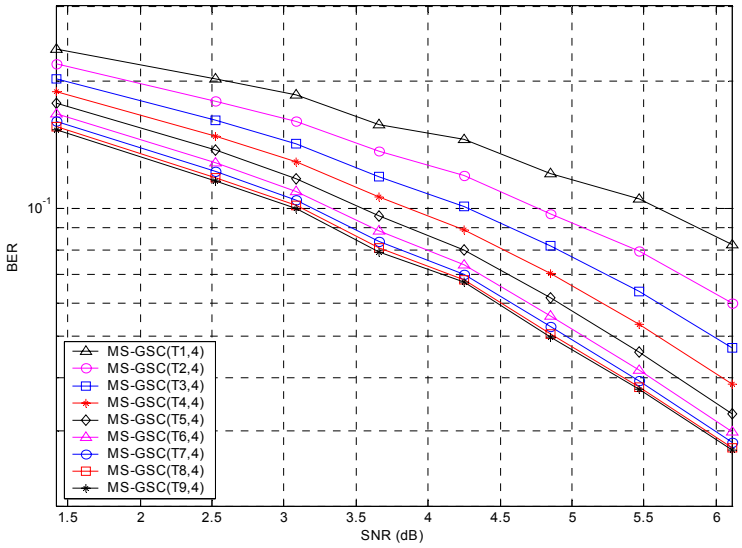

(b) MS-GSC

Figure 5-1. BER Performance with Pedestrian B Channel

Next, we present the BER performance under the ITU Vehicular A channel profile. The BER performance of the GSC with four rake fingers is presented in Figure 5-2 (a). As shown in the figure, GSC (*m*, 4) performs better as *m* goes high. However, the performance gain becomes smaller since the average power of the last multipath signals becomes smaller. The performance

gain of GSC (3, 4) over GSC (4, 4) is noticeably small. The BER performance of the AT-GSC with a threshold set of δ = 0.5 is presented in Figure 5-2 (b). As shown in the figure, the AT-GSC (T_a, 4) performs better as the threshold T_a becomes smaller. The performance of the AT-GSC is lower and upper bounded by the SC and the MRC, respectively. We observed that the MS-GSC with a threshold set of δ = 0.5 shows almost the same BER performance as that of the AT-GSC. The BER performance of the NT-GSC with a threshold set of δ = 0.5 is shown in Figure 5-2 (c). As shown in the figure, the NT-GSC performs better than the AT-GSC and the MS-GSC using a threshold set such that the average number of rake fingers activated is the same. When the Vehicular B channel profile is applied, each generalized selection combining method (GSC, MS-GSC, AT-GSC, and NT-GSC) shows the same trend as for the case of the Vehicular A channel profile. The only difference lies in the combined SNR and the BER performance, since each channel profile has a different power profile.

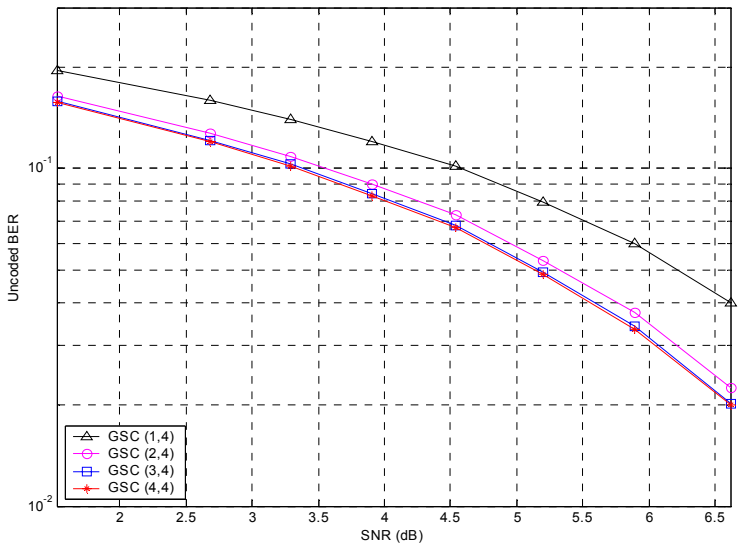

(a) Original GSC

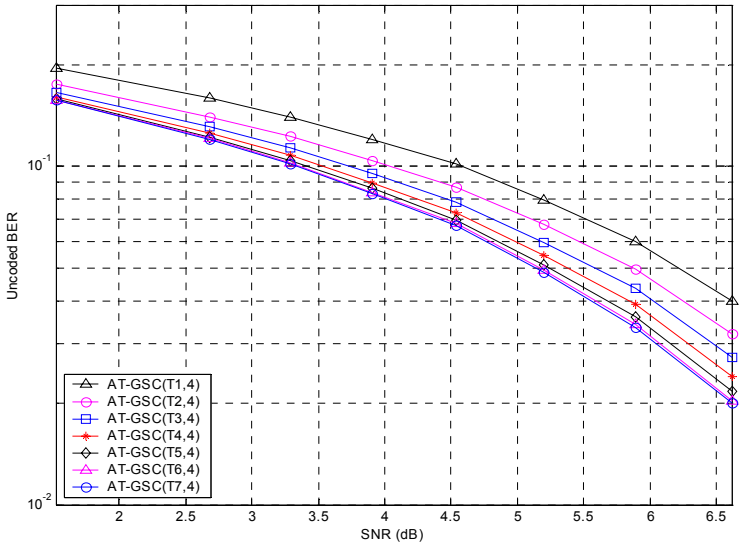

(b) AT-GSC

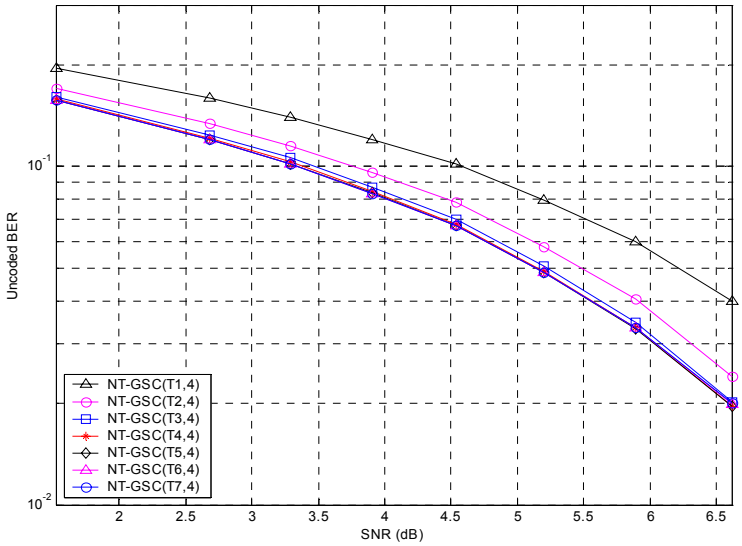

(c) NT-GSC

Figure 5-2. BER Performance with Vehicular A Channel

When the Pedestrian A channel profile is applied with two rake fingers, our simulation results indicate that the performance difference between GSC (1, 2) and GSC (2, 2) is negligible. Since the first multipath signal is strong, it results in a large amount of interference for the second multipath signal (for user data). This interference also results in an imperfect channel estimation when the second rake finger processes a multipath signal (for the CPICH). Thus, the

contribution of the second multipath signal is small or negligible. Therefore, in the following, only the Pedestrian B and the Vehicular A channel profiles are applied to evaluate the performance of the proposed adaptive rake combiners.

5.3 Performance of Adaptive Rake Combiners

The BER performance as well as the power reduction of the adaptive rake combining scheme proposed in Chapter 3 are presented in this section. To generate the feedback information for the outer loop of the proposed adaptive rake combiners, the current BER performance is estimated on every frame at the rate of 100 Hz. To adjust the number of rake fingers activated for the inner loop of the adaptive rake combiner, the combined signal quality is evaluated in order to check whether it meets the given threshold value provided from the outer loop at the pilot symbol rate of 15 kHz (= 3.84 MHz / 256). The control logic to evaluate the BER and the combined signal quality operates at a much lower frequency compared with the chipping rate (3.84 MHz), at which rake fingers operate. Hence, the power dissipation due to the control logic would be small when implemented in the CMOS technology. (Note that the power dissipation is roughly proportional to the operating frequency in the CMOS.) Thus, the power reduction of the adaptive rake combiner can be represented as the average number of rake fingers deactivated.

The performance of adaptive rake combiners under various conditions for the ITU Pedestrian B channel profile with a fixed amount of noise is summarized in Table 5-1. The first column under "Condition" represents operating conditions, in which the desired target BER and the average combined SNR with the MRC are presented. A fixed amount of noise is added to the received signal at the receiver, and we obtain an average combined SNR for five fingers with the MRC. The relative noise power to the signal power of the first multipath is –12.0 dB, –11.5 dB, -11.0 dB, and -10.5 dB, which yields 3.66 dB, 4.25 dB, 4.85 dB, and 5.47 dB of the combined SNR, respectively. The second column under "Performance" has three items such that an average BER, a normalized standard deviation of the BER (Normal STD), and an average number of rake fingers deactivated (Finger saving). The normalized standard deviation is computed as the ratio of standard deviation over the mean of erroneous bits. The column "MRC" represents the performance of the conventional MRC rake combiner. The last four columns (GSC, MS-GSC,

AT-GSC, and NT-GSC) represent the performance of the adaptive rake combiner employing GSC, MS-GSC, AT-GSC, and NT-GSC, respectively. For brevity, we call them as GSC, MS-GSC, AT-GSC, and NT-GSC, respectively, in the following.

As presented in Table 5-1, all four GSCs achieve the required BER performance for the most cases except the AT-GSC under the target BER of 8 %. However, the deviation is less than 1 % ($\frac{8.05 - 8.0}{8.0}$ = 0.625 %), which may be insignificant for a channel decoder. The GSC and the MS-GSC show comparable performance in terms of the average number of fingers deactivated, and their power reduction due to the deactivated fingers is as high as 52.2 % (= 2.61/4) for the target BER of 10 %. The AT-GSC and the NT-GSC also show the comparable performance, and their power reduction is up to 54.0 %. The MS-GSC shows the smallest normalized standard deviation, which results in the least burst errors. Meanwhile, the AT-GSC shows the largest normalized standard deviation.

Table 5-1. Performance of Adaptive Rake Combiners with Fixed Noise (Pedestrian B)

Condition		Performance	MRC	GSC	MS-GSC	AT-GSC	NT-GSC
Target BER	SNR						
10 %	3.66 dB	BER	8.14 %	9.39 %	9.62 %	9.92 %	9.67 %
		Normal STD	32.31 %	25.25 %	19.06 %	33.34 %	26.94 %
		Finger saving	0	1.76	1.67	1.93	1.93
	4.25 dB	BER	6.42 %	8.56 %	9.16 %	9.10 %	8.91 %
		Normal STD	35.05 %	24.46 %	17.10 %	34.50 %	26.13 %
		Finger saving	0	2.60	2.61	2.64	2.70
8 %	4.25 dB	BER	6.55 %	7.50 %	7.69 %	8.05 %	7.72 %
		Normal STD	36.21 %	29.90 %	22.42 %	38.96 %	31.39 %
		Finger saving	0	1.57	1.56	1.83	1.82
	4.85 dB	BER	5.05 %	6.80 %	7.29 %	7.35 %	7.11 %
		Normal STD	38.67 %	27.52 %	19.79 %	39.85 %	30.05 %
		Finger saving	0	2.42	2.46	2.52	2.56
6 %	4.85 dB	BER	5.06%	5.60 %	5.62 %	5.79 %	5.60 %
		Normal STD	39.34 %	33.11 %	28.58 %	39.61 %	34.53 %
		Finger saving	0	1.16	1.08	1.23	1.23
	5.47 dB	BER	3.73 %	4.87 %	5.01 %	5.30 %	5.00 %
		Normal STD	44.39 %	32.32 %	24.36 %	47.35 %	36.42 %
		Finger saving	0	2.08	1.99	2.15	2.20

The simulation results under the ITU Vehicular A channel profile with a fixed amount of noise are summarized in Table 5-2. The same amount of noise described above for Table 5-1 is added for the ITU Vehicular A channel profile, which results in 3.90 dB, 4.54 dB, 5.20 dB, and 5.89 dB of the average combined SNR for four fingers with the MRC, respectively. Each adaptive rake combiner achieves the required BER performance for the most cases except the AT-GSC under the target BER of 8 %. As in the above case, the deviation is only 0.25 %. The NT-GSC shows the best performance in terms of power reduction, while the GSC shows the worst performance. The power reduction with the NT-GSC ranges from 44.5 % (= 1.78/4) to

67.8 % (= 2.71/4). As in the case of the Pedestrian B channel profile, the MS-GSC and the AT-GSC also show the smallest and the largest normalized standard deviation, respectively.

Table 5-2. Performance of Adaptive Rake Combiners with Fixed Noise (Vehicular A)

Condition		Performance	MRC	GSC	MS-GSC	AT-GSC	NT-GSC
Target BER	SNR						
10 %	3.90 dB	BER	8.48 %	9.87 %	9.67 %	9.93 %	9.59 %
		Normal STD	22.19 %	26.45 %	21.86 %	27.25 %	25.21 %
		Finger saving	0	1.61	1.88	1.91	2.12
	4.54 dB	BER	6.63 %	9.58 %	8.98 %	8.96 %	8.76 %
		Normal STD	23.48 %	26.06 %	21.58 %	26.57 %	23.95 %
		Finger saving	0	2.27	2.62	2.54	2.67
8 %	4.54 dB	BER	6.66 %	7.92 %	7.65 %	8.02 %	7.68 %
		Normal STD	23.61 %	29.07 %	22.94 %	29.27 %	27.09 %
		Finger saving	0	1.56	1.84	1.90	2.13
	5.20 dB	BER	4.89 %	7.69 %	7.05 %	7.05 %	6.87 %
		Normal STD	28.27 %	30.73 %	25.93 %	31.87 %	28.95 %
		Finger saving	0	2.31	2.66	2.58	2.71
6 %	5.20 dB	BER	4.88 %	5.67 %	5.27 %	5.71 %	5.35 %
		Normal STD	27.44 %	36.00 %	26.91 %	35.86 %	31.59 %
		Finger saving	0	1.22	1.39	1.50	1.78
	5.89 dB	BER	3.41 %	5.67 %	4.97 %	5.15 %	4.94 %
		Normal STD	30.13 %	34.41 %	28.57 %	36.88 %	31.89 %
		Finger saving	0	2.20	2.55	2.48	2.68

To verify the ability of the proposed adaptive rake combiner to dynamically adapt to the environment, a variable amount of noise is considered for the simulation. A random amount of noise is added at each simulation run, and 100 runs are performed. The difference between the maximum and the minimum combined SNRs is about 1.2 dB for 100 runs with a random amount of noise. The result is almost the same as with a fixed amount of noise. The performance of adaptive rake combiners under the Pedestrian B and under the Vehicular A channel profiles is summarized in Table 5-3 and Table 5-4, respectively. As presented in the two tables, each

adaptive rake combiner achieves the required BER performance for most cases. With the exception of a few cases, the maximum deviation is less than 0.5 %. The NT-GSC shows the best performance in terms of power reduction, in which the maximum power reduction is 65.8 % (= 2.63/4). As in the case of a fixed amount of noise, the MS-GSC and the AT-GSC show the smallest and the largest normalized standard deviation, respectively.

Table 5-3. Performance of Adaptive Rake Combiners with Variable Noise (Pedestrian B)

Condition		Performance	MRC	GSC	MS-GSC	AT-GSC	NT-GSC
Target BER	SNR						
10 %	3.66 dB	BER	8.31 %	9.49 %	9.76 %	10.01 %	9.75 %
		Normal STD	36.35 %	27.86 %	22.60 %	35.28 %	29.69 %
		Finger saving	0	1.70	1.64	1.85	1.86
	4.25 dB	BER	6.40 %	8.55 %	9.07 %	9.09 %	8.92 %
		Normal STD	39.82 %	25.73 %	19.85 %	34.69 %	27.19 %
		Finger saving	0	2.56	2.51	2.57	2.61
8 %	4.25 dB	BER	6.43 %	7.51 %	7.81 %	8.02 %	7.77 %
		Normal STD	42.89 %	31.38 %	25.42 %	39.54 %	32.81 %
		Finger saving	0	1.69	1.72	1.88	1.88
	4.85 dB	BER	5.14 %	6.83 %	7.21 %	7.41 %	7.15 %
		Normal STD	46.37 %	30.11 %	24.01 %	40.75 %	31.67 %
		Finger saving	0	2.41	2.39	2.51	2.54
6 %	4.85 dB	BER	4.99 %	5.67 %	5.71 %	6.03 %	5.78 %
		Normal STD	45.48 %	35.97 %	31.64 %	44.67 %	38.11 %
		Finger saving	0	1.45	1.35	1.59	1.58
	5.47 dB	BER	3.71 %	4.91 %	5.05 %	5.33 %	5.02 %
		Normal STD	53.16 %	36.03 %	30.28 %	48.98 %	39.02 %
		Finger saving	0	2.16	2.10	2.24	2.26

Table 5-4. Performance of Adaptive Rake Combiners with Variable Noise (Vehicular A)

Condition		Performance	MRC	GSC	MS-GSC	AT-GSC	NT-GSC
Target BER	SNR						
10 %	3.90 dB	BER	8.46 %	9.88 %	9.63 %	9.80 %	9.54 %
		Normal STD	26.77 %	25.37 %	22.03 %	26.46 %	24.60 %
		Finger saving	0	1.52	1.72	1.79	1.95
	4.54 dB	BER	6.69 %	9.40 %	8.81 %	8.90 %	8.66 %
		Normal STD	31.20 %	26.41 %	24.14 %	28.66 %	26.19 %
		Finger saving	0	2.16	2.50	2.48	2.60
8 %	4.54 dB	BER	6.50 %	8.04 %	7.71 %	7.91 %	7.62 %
		Normal STD	33.17 %	29.64 %	24.93 %	31.79 %	28.31 %
		Finger saving	0	1.59	1.85	1.92	2.05
	5.20 dB	BER	4.91 %	7.46 %	6.78 %	6.86 %	6.66 %
		Normal STD	38.87 %	30.98 %	28.24 %	34.81 %	31.33 %
		Finger saving	0	2.18	2.52	2.49	2.63
6 %	5.20 dB	BER	4.92 %	5.98 %	5.58 %	5.80 %	5.57 %
		Normal STD	38.14 %	33.65 %	29.79 %	35.54 %	32.44 %
		Finger saving	0	1.27	1.42	1.50	1.66
	5.89 dB	BER	3.27 %	5.40 %	4.59 %	4.77 %	4.57 %
		Normal STD	45.16 %	35.24 %	30.94 %	39.92 %	34.93 %
		Finger saving	0	2.05	2.40	2.36	2.56

In summary, the simulation results indicate that the proposed adaptive rake combining scheme works well with all GSC methods to maintain the required BER performance. The adaptive scheme with the NT-GSC shows good performance in terms of finger saving, and the power reduction is as high as 67.8 %. The adaptive scheme with the MS-GSC shows the smallest normalized standard deviation of the BER for the all cases, which is somewhat expected.

5.4 Summary

In this chapter, we presented the simulation results to verify the proposed minimum selection GSC method and an adaptive rake combining scheme to reduce power dissipation by a mobile rake receiver. To verify the validity of the proposed adaptive scheme, four rake combining schemes were applied to a mobile rake receiver for the WCDMA system. Simulation environment considered in the simulations was briefly described in Section 5.1. The BER performances of the original GSC, the AT-GSC, the NT-GSC, and the proposed MS-GSC were presented in Section 5.2. Finally, the BER performance as well as the power reduction of the proposed adaptive rake combining scheme were presented in Section 5.3.

The simulation results indicate that the proposed adaptive rake combining scheme works well with all GSC methods to maintain the required BER performance. The adaptive scheme with the MS-GSC shows the smallest normalized standard deviation of the BER for the all cases.

Chapter 6 Conclusion

Smart antenna technology is a promising means to overcome signal impairments in wireless personal communications. When spatial signal processing achieved through smart antennas is combined with temporal signal processing, the space-time processing can mitigate interference and multipath to yield higher network capacity, coverage, and quality.

In this dissertation, we propose a dual smart antenna system incorporated into handsets for the third generation wireless personal communication systems in which the two antennas are separated by a quarter wavelength (3.5 cm). We examine the effectiveness of a dual smart antenna system with diversity and adaptive combining schemes and propose a new combining scheme called hybrid combining. The proposed hybrid combiner combines diversity combiner and adaptive combiner outputs using maximal ratio combining (MRC). Since these diversity combining and adaptive combining schemes exhibit somewhat opposite and complementary characteristics, the proposed hybrid combining scheme aims to exploit the advantages of the two schemes.

To model dual antenna signals, we consider three channel models: loosely correlated fading channel model (LCFCM), spatially correlated fading channel model (SCFCM), and envelope correlated fading channel model (ECFCM). Each antenna signal is assumed to have independent Rayleigh fading in the LCFCM. In the SCFCM, each antenna signal is subject to the same Rayleigh fading, but is different in the phase due to a non-zero angle of arrival (AOA). The LCFCM and the SCFCM are useful to evaluate the upper and the lower bounds of the system performance. To model the actual channel of dual antenna signals lying in between these two channel models, the ECFCM is considered. In this model, two Rayleigh fading antenna signals for each multipath are assumed to have an envelope correlation and a phase difference due to a non-zero AOA. To obtain the channel profile, we adopt not only the geometrically based single

bounce (GBSB) circular and elliptical models, but also the International Telecommunication Union (ITU) channel model.

The simulation results indicate that the performance of the proposed hybrid combining scheme is always better than or equal to those of the adaptive and the diversity combining schemes for all simulation environments considered. For example, the SINR gain of the hybrid combiner over a single antenna system is 4.28 dB at BER = 10^{-2} with the ITU Pedestrian A channel profile. Meanwhile, the SINR gains of the diversity combiner and the adaptive combiner are 3.83 dB and 3.58 dB at the same condition, respectively.

In this dissertation, we also propose a new generalized selection combining (GSC) method called minimum selection GSC (MS-GSC) and an adaptive rake combining scheme to reduce the power consumption of mobile rake receivers. The proposed MS-GSC selects a minimum number of branches as long as the combined SNR is maintained larger than a given threshold. The proposed adaptive rake combining scheme which dynamically determines the threshold values is applicable to the three GSC methods: the absolute threshold GSC, the normalized threshold GSC (NT-GSC), and the proposed MS-GSC. Through simulation, we estimated the effectiveness of the proposed scheme for a mobile rake receiver for a wideband CDMA system. We also suggest a new power control strategy to maximize the benefit of the proposed adaptive scheme. The simulation results indicate that the proposed adaptive rake combining scheme works well with all GSC methods to maintain the required BER performance. The adaptive scheme with the NT-GSC shows good performance in terms of finger saving, and the power reduction is as high as 67.8 %. The adaptive scheme with the MS-GSC shows the smallest normalized standard deviation for the all cases.

In summary, we investigated the effectiveness of smart antennas at handsets. We proposed a hybrid combining scheme, a new generalized selection combining scheme, and an adaptive rake combining scheme, all of which improve the performance of smart antennas at handsets.

References

[1] J. Litva and T. K. Lo, *Digital Beamforming in Wireless Communications*, Artech House, Massachusetts, 1996.

[2] A. J. Paulraj and B. C. Ng, "Space-Time Modems for Wireless Personal Communications," *IEEE Personal Communications*, pp. 36-48, February 1998.

[3] R. Kohno, "Spatial and Temporal Communication Theory Using Adaptive Antenna Array," *IEEE Personal Communications*, pp. 28-35, February 1998.

[4] J. H. Winters, "Smart Antennas for Wireless Systems," *IEEE Personal Communications*, pp. 23-27, February 1998.

[5] L. C. Godara, "Applications of Antenna Arrays to Mobile Communications, Part I: Performance Improvement, Feasibility, and System Considerations," *Proceedings of the IEEE*, Vol. 85, No. 7, pp. 1031-1060, July 1997.

[6] L. C. Godara, "Applications of Antenna Arrays to Mobile Communications, Part II: Beam-Forming and Direction-of-Arrival Considerations," *Proceedings of the IEEE*, Vol. 85, No. 8, pp. 1195-1245, August 1997.

[7] A. J. Paulraj and C. B. Papadias, "Space-Time Processing for Wireless Communications," *IEEE Signal Processing Magazine*, pp. 49-83, November 1997.

[8] J. Razavilar, F. Rashid-Farrokhi, and K. J. R. Liu, "Software Radio Architecture with Smart Antennas: A Tutorial on Algorithms and Complexity," *IEEE Journal of Selected Areas in Communications*, Vol. 17, No. 4, pp. 662-676, April 1999.

[9] J. C. Liberti, Jr. and T. S. Rappaport, *Smart Antennas for Wireless Communications: IS-95 and Third Generation CDMA Applications*, Prentice Hall, New Jersey, 1999.

[10] W. C. Jakes, *Microwave Mobile Communications*, John Wiley, New York, 1974.

[11] J. S. Thompson, P. M. Grant, and B. Mulgrew, "Smart Antenna Arrays for CDMA Systems," *IEEE Personal Communications*, pp. 16-25, October 1996.

[12] S. Affes and P. Mermelstein, "A New Receiver Structure for Asynchronous CDMA: STAR – The Spatio-Temporal Array-Receiver," *IEEE Journal on Selected Areas in Communications*, Vol. 16, No. 8, pp. 1411-1422, October 1998.

[13] H. J. Sing, J. R. Crux, and Y. Wang, "Fixed Multibeam Antennas Versus Adaptive Arrays for CDMA Systems," *IEEE Vehicular Technology Conference*, pp. 27-31, September 1999.

[14] M. Dell'Anna and A. H. Aghvami, "Performance of Optimum and Suboptimum Combining at the Antenna Array of a W-CDMA System," *IEEE Journal of Selected Areas in Communications*, Vol. 17, No. 12, pp. 2123-2137, December 1999.

[15] J. H. Winters, C. C. Martin, and T. Zhuang, "A Two-Element Adaptive Antenna Array for IS-136 Base Stations," *IEEE Communications Letters*, Vol. 3, No. 3, pp. 60-62, March 1999.

[16] C. H. Gowda, V. Annampedu, and R. Viswanathan, "Diversity Combining in Antenna Array Base Station Receiver for DS/DMA System," *IEEE Communications Letters*, Vol. 2, No. 7, pp. 180-182, July 1998.

[17] A. F. Naguib and A. Paulraj, "Performance of Wireless CDMA with M-ary Orthogonal Modulation and Cell Site Antenna Arrays," *IEEE Journal of Selected Areas in Communications*, Vol. 14, No. 9, pp. 1770-1783, December 1996.

[18] Y. S. Song and H. M. Kwon, "Analysis of a Simple Smart Antenna for CDMA Wireless Communications," *IEEE Vehicular Technology Conference*, pp. 254-258, May 1999.

[19] C. B. Dietrich, K. Dietze, J. R. Nealy, and W. L. Stutzman, "Spatial, Polarization, and Pattern Diversity for Wireless Handheld Terminals," *IEEE Transactions on Antennas and Propagation*, Vol. 49, No. 9, pp. 1271-1281, September 2001.

[20] http://www.qualcomm.com/hdr/pdfs/HDR_Tech_Airlink.pdf, "1x High Data Rate (1xHDR) Airlink Overview," April 2000.

[21] G. Dolmans and L. Leyten, "Performance Study of an Adaptive Dual Antenna Handset for Indoor Communications," *IEE Proceedings of Microwaves, Antennas and Propagation*, Vol. 146, No. 2, pp. 138-1444, April 1999.

[22] P. B. Wong and D. C. Cox, “Low-Complexity Cochannel Interference Cancellation and Macroscopic Diversity for High-Capacity,” *IEEE Transactions on Vehicular Technology*, Vol. 47, No. 1, pp. 124-132, February 1998.

[23] P. B. Wong and D. C. Cox, “Low-Complexity Diversity Combining Algorithm and Circuit Architectures for Co-Channel Interference Cancellation and Frequency-Selective Fading Mitigation,” *IEEE Transactions on Communications*, Vol. 44, No. 9, pp. 1107-1116, September 1996.

[24] http://www.3gpp.org/.

[25] H. Holma and A. Toskala, *WCDMA for UMTS: Radio Access for Third Generation Mobile Communications*, Wiley, New York, 2000

[26] http://www.3gpp.org/ftp/Specs/2000-12/R1999/25_series/25101-350.zip, “3GPP TS 25.101 UE Radio Transmission and Reception (FDD),” 3GPP, December 2000.

[27] B. O’Hara and A. Petrick, *The IEEE 802.11 Handbook: A Designer’s Companion*, IEEE Press, New Jersey, 1999.

[28] S. W. Kim, D. S. Ha, and J. H. Kim, “Performance Gain of Smart Dual Antennas at Handsets in 3G CDMA System,” *The 5th CDMA International Conference*, Vol. 2, pp. 223-227, November 2000.

[29] S. W. Kim, D. S. Ha, and J. H. Kim, “Performance of Smart Antennas with Adaptive Combining at Handsets for the cdma2000 System,” *International Conference on Third Generation Wireless and Beyond*, pp. 882-887, May/June 2001.

[30] S. W. Kim, D. S. Ha, and J. H. Kim, “Performance Gain of Smart Antennas with Diversity Combining at Handsets for the 3GPP WCDMA System,” *The 13th International Conference on Wireless Communications*, pp. 235-242, July 2001.

[31] S. W. Kim, D. S. Ha, J. H. Kim, and J. H. Kim, "Performance Gain of Smart Antennas with Hybrid Combining at Handsets for the 3GPP WCDMA System," *The Fourth International Symposium on Wireless Personal Multimedia Communication*s, pp. 289-294, September 2001.

[32] S. W. Kim, D. S. Ha, J. H. Kim, and J. H. Kim, "Performance of Smart Antennas with Adaptive Combining at Handsets for the 3GPP WCDMA System," *The IEEE Vehicular Technology Conference*, pp. 2048-2052, October 2001.

[33] R. B. Ertel and J. H. Reed, "Generation of Two Equal Power Correlated Rayleigh Fading Envelopes," *IEEE Communications Letters*, pp. 276-278, October 1998.

[34] R. B. Ertel, P. Cardieri, K. W. Sowerby, T. S. Rappaport, and J. H. Reed, "Overview of Spatial Channel Models for Antenna Array Communication Systems," *IEEE Personal Communications*, pp. 10-22, February 1998.

[35] R. B. Ertel and J. H. Reed, "Angle and Time of Arrival Statistics for Circular and Elliptical Scattering Models," *IEEE Journal of Selected Areas in Communications*, Vol. 17, No. 11, pp. 1829-1840, November 1999.

[36] R. B. Ertel, "Antenna Array Systems: Propagation and Performance," Ph. D. Dissertation, Department of Electrical and Computer Engineering, Virginia Polytechnic Institute and State University, July 1999.

[37] ITU ITU-R M.1225, "Guidelines for Evaluations of Radio Transmission Technologies for IMT-2000," 1997.

[38] N. Kong, T. Eng, and L. B. Milstein, "A Selection Combining Scheme for RAKE Receivers," *IEEE International Conference on Universal Personal Communications*, pp. 426-430, November 1995.

[39] T. Eng, N. Kong, and L. B. Milstein, "Comparison of Diversity Combining Techniques for Rayleigh-Fading Channels," *IEEE Transactions on Communications*, Vol. 44, No. 9, pp. 1117-1129, September 1996.

[40] N. Kong and L. B. Milstein, "Average SNR of a Generalized Diversity Selection Combining Scheme," *IEEE Communications Letters*, Vol. 3, No. 3, pp. 57-59, March 1999.

[41] N. Kong and L. B. Milstein, "SNR of Generalized Diversity Selection Combining with Nonidentical Rayleigh Fading Statistics," *IEEE Transactions on Communications*, Vol. 48, No. 8, pp. 1266-1271, August 2000.

[42] M. Z. Win and J. H. Winters, "Virtual Branch Analysis of Symbol Error Probability for Hybrid Selection/Maximal-Ratio Combining in Rayleigh Fading," *IEEE Transactions on Communications*, Vol. 49, No. 11, pp. 1926-1934, November 2001.

[43] M.-S. Alouini and M. K. Simon, "An MGF-based Performance Analysis of Generalized Selection Combining over Rayleigh Fading Channels," *IEEE Transactions on Communications*, Vol. 48, No. 3, pp. 401-415, March 2000.

[44] M.-S. Alouini and M. K. Simon, "Performance of Coherent Receivers with Hybrid SC/MRC over Nakagami-*m* Fading Channels," *IEEE Transactions on Vehicular Technology*, Vol. 48, No. 4, pp. 1155-1164, July 1999.

[45] A. Annamalai and C. Tellambura, "Error Rates for Hybrid SC/MRC Systems on Nakagami-m Channels," *IEEE Wireless Communications and Networking Conference*, pp. 227-231, September 2000.

[46] Y. Ma and C. C. Chai**,** "Unified Error Probability Analysis for Generalized Selection Combining in Nakagami Fading Channels," *IEEE Journal on Selected Areas in Communications*, Vol. 18, No. 11, pp. 2198-2210, November 2000.

[47] N. Kong, "Average Signal-to-Interference-plus-Noise Ratio of a Generalized Optimum Selection Combiner for Non-identical Independent Rayleigh Fading Channels in the Presence of Co-channel Interference," *IEEE International Conference on Communications*, pp. 990-994, June 2001.

[48] M. Z. Win and J. H. Winters, "Analysis of Hybrid Selection/Maximal-Ratio Combining in Rayleigh Fading," *IEEE Transactions on Communications*, Vol. 47, No. 12, pp. 1773-1776, December 1999.

[49] J. A. Ritcey and M. Azizoglu, "Performance Analysis of Generalized Selection Combining with Switching Constraints," *IEEE Communications Letters*, Vol. 4, No. 5, pp. 152-154, May 2000.

[50] C. M. Lo and W. H. Lam, "Approximate BER Performance of Generalized Selection Combining in Nakagami-*m* Fading," *IEEE Communications Letters*, Vol. 5, No. 6, pp. 254-256, June 2001.

[51] L. Yue, "Analysis of Generalized Selection Combining Techniques," *IEEE Vehicular Technology Conference*, pp. 1191-1195, May 2000.

[52] A. I. Sulyman and M. Kousa, "Bit Error Rate Performance of a Generalized Diversity Selection Combining Scheme in Nakagami Fading Channels**,"** *IEEE Wireless Communications and Networking Conference*, pp. 1080-1085, September 2000.

[53] M. K. Simon and M.-S. Alouini**,** "Performance Analysis of Generalized Selection Combining with Threshold Test per Branch (T-GSC)," *IEEE Global Telecommunications Conference*, pp. 1176-1181, November 2001.

[54] J. G. Proakis, *Digital Communications*, McGraw-Hill, New York, 1995.

[55] S. Haykin, *Adaptive Filter Theory*, Prentice Hall, New Jersey, 1996.

[56] J. H. Reed, *Software Radios: A Modern Approach to Radio Engineering*, Prentice Hall, New Jersey, 2002.

[57] J. H. Winters, "Optimum Combining in Digital Mobile Radio with Cochannel Interference," *IEEE Transactions on Vehicular Technology*, Vol. VT-33, No. 3, pp. 144-155, August 1984.

[58] J. Salz and J. H. Winters, "Effect of Fading Correlation of Adaptive Arrays in Digital Mobile Radio," *IEEE Transactions on Vehicular Technology*, pp. 1049-1057, November 1994.

[59] S. Tanaka, A. Harada, M. Sawahashi, and F. Adachi, "Experiments on Coherent Adaptive Antenna Array Diversity for Wideband DS-CDMA Mobile Radio," *IEEE Journal of Selected Areas in Communications*, Vol. 18, No. 8, pp. 1495-1504, August 2000.

[60] S. Tanaka, M. Sawahashi, and F. Adachi, "Pilot Symbol-Assisted Decision-Directed Coherent Adaptive Array Diversity for DS-CDMA Mobile Radio Reverse Link," *IEICE Transactions on Fundamentals*, Vol. E80-A, No. 12, pp. 2445-2454, December 1997.

[61] R. H. Clarke, "A Statistical Theory of Mobile-Radio Reception," The Bell System Technical Journal, Vol. 47, No. 6, pp. 957-1000, July-August 1968.

[62] J. S. Colburn, Y. Rahmat-Samii, M. A. Jensen, and G. J. Pottie, "Evaluation of Personal Communications Dual-Antenna Handset Diversity Performance," *IEEE Transactions on Vehicular Technology*, Vol. 47, No. 3, pp. 737-746, August 1998.

[63] R. Prasad and T. Ojanpera, "An Overview of CDMA Evolution Toward Wideband CDMA," *IEEE Communications Surveys*, Vol.1, No. 1, pp. 2-29, Fourth Quarter 1998.

[64] L. B. Milstein, "Wideband Code Division Multiple Access," *IEEE Journal of Selected Areas in Communications*, Vol. 18, No. 8, pp. 1344-1354, August 2000.

[65] http://www.cdg.org/frame_3giis.html, "Wideband cdmaOne (TIA cdma2000) Radio Transmission Technology Proposal," International Telecommunication Union, Radiocommunication Study Groups, June 1998.

[66] T. S. Rappaport, *Wireless Communications: Principles and Practice*, Prentice Hall, New Jersey, 1996.

[67] http://www.3gpp.org/ftp/tsg_ran/WG1_RL1/TSGR1_18/Docs/PDFs/R1-01-0030.pdf

[68] G. Yeap, *Practical Low Power Digital VLSI design*, Kluwer Academic Publishers, Massachusetts, 1998.

[69] N. H. Weste and K. Eshraghian, *Principles of CMOS VLSI Design: A System Perspective*, Addison Wesley, 1992.

[70] A. P. Chandrakasan, S. Sheng, and R. W. Brodersen, "Low-Power CMOS Digital Design," *IEEE Journal of Solid-State Circuits*, Vol. 27, No. 4, pp. 473-484, April 1992.

[71] A. P. Chandrakasan, M. Potkonjak, R. Mehra, J. Rabaey, and R. W. Brodersen, "Optimizing Power Using Transformation," *IEEE Transactions on Computer-Aided Design and Integrated Circuits and Systems*, Vol. 14, No. 1, pp. 12-31, January 1995.

[72] A. P. Chandrakasan and R. W. Brodersen, "Minimizing Power Consumption in Digital CMOS Circuits," *Proceedings of IEEE*, Vol. 83, No. 4, pp. 498-523, April 1995.

[73] B. Daneshrad, J. N. Duan, E. Grayver, C. T. Huang, S. W. Kim, and L. J. Ko, "Parametrizable VLSI Application Specific Datapaths for High Speed Data Communications," *International Journal of Wireless Information Networks*, Vol. 6, No. 4, pp. 285-301, October 1999.

[74] M. C. Jeruchim, P. Balaban, and K. S. Shanmugan, *Simulation of Communication Systems*, Plenum Press, New York, 1994.

[75] S. L. Miller, *EE 689: Wireless Communication Systems*, Lecture Note, Department of Electrical Engineering, Texas A&M University, January 2001.

Appendix A: Simulation Model for the 3GPP WCDMA System

This appendix describes Matlab codes used for simulating the 3GPP WCDMA system. The Matlab codes to evaluate the performance of the hybrid combiner and to verify the MS-GSC method and the adaptive rake combining scheme are presented.

A.1 Matlab Codes for the Hybrid Combiner

There are three parts in the main module for the hybrid combiner (HC). The first part defines the system and model parameters. A simulation core of the main module constitutes the second part, in which a number of simulations are run to evaluate the average system performance. The last part is a post processing, where the BERs are calculated and the simulation results are saved as a binary file.

A.1.1 System and Model Parameters

The first part of the main module to define the system and model parameters is presented in Figure A-1. These parameters include the channel model, the Monte Carlo simulation, downlink signaling, an OVSF code and a scramble code, the common pilot symbol, a pulse shaping FIR filter, the multiple access interference, receivers, receiving signal, the GBSB model, the ECFCM, and so forth.

```
% Channel Model Parameters
ITU_mode = 3; % ITU mode: 1) Pedestrian A, 2) Pedestrian B, 3) Vehicular A, and 4) Vehicular B
rho = 0.50;   % Envelope correlation
d = 0.25;     % element separation (normalized by wavelength) such as 0.125, 0.25, 0.375, and 0.5
if ITU_mode == 1 | ITU_mode == 2
```

```
   vhr = 3;   % velocity of the users (km/h)
else
   vhr = 50;
end
CHPF_model = 3;            % Channel profile: 1) GBSB Elliptical, 2) GBSB Circular, 3) ITU
channel_model = 4;         % channel model selection (1: SCFCM, 2: LCFCM, 3: rho-envelope
correlated, 4: rho-envelope correlated with constant phase difference)
if ITU_mode == 1
   L = 4;                  % # multipaths in the channel
   M = 2;                  % # RAKE fingers (M<=L)
else
   L = 6;
   if ITU_mode == 2
      M = 5;
   elseif ITU_mode == 3 | ITU_mode == 4
      M = 4;
   end
end

% Simulation (Monte Carlo) Parameters
no_iter = 5000;                   % Maximum number of Iteration
min_no_iter = 50;                 % Minimum number of iterations
max_error_count = 16745;          % Number of errors count for Monte Carlo Simulation
ebno = 10*log10(2);               % AWGN with 1/2 power of desired signal power (sum of each
multipath power)
SINR_min = -17;
SINR_max = -10;
SINR_step = 1;
SINR_start = SINR_min;
total_no_iter = no_iter*ones((SINR_max-SINR_min+1)/SINR_step,1);
no_pilot_sym_avg = 1;             % Number of pilot symbols to be used to obtain average power
valid_frame = 3;                  % skip (valid_frame - 1) frames to give the converging time for
adaptive combining (AC with N-LMS)
                                  % This number should be smaller than block_frame if frame is 1.

% Downlink WCDMA signal parameters
K = 8;                            % # users
des_usr_indx = floor(K/2)+1;      % Desired user index
sf_no = 13;                       % slot format number (0-16) for user's DPCH
s_format = slot_format(sf_no);    % returns slot format: s_format(1)=sf, s_format(2)= Ndata1,
s_format(3)= Ndata3, s_format(4)= Ntpc, s_format(5)= Ntfci, s_format(6)= Npilot
sf_index = s_format(1);           % spreading factor index
sf_user = sf_index.*ones(K,1);    % spreading factor for the users DP(D/C)CH (32 for I and Q)
sf_common = 256;                  % spreading factor for CCPCH
pri_pilot = 1+j;                  % P-CPICH (Primary Common Pilot Channel) signal
ovsf_code_numb = floor(linspace(3,sf_index,K))';
block_frame = 4;                  % # blocks of frames (Total # of frame = block_frame*frame)
frame = 1;                        % # frames in a block of frames
slot_frame = 15;                  % # slots per frame
pilot_slot = s_format(6);         % # pilot symbols per slot
chip_frame = 38400;               % # chips per frame
samp_chip = 4;                    % # samples per chip
```

```
% Downlink OVSF and long scrambling codes
load ovsf32all.mat ovsf32all;                   % Loading OVSF codes with SF 32
ovsf_cpich = ones(1,sf_common);
ovsf_user = ovsf32all(ovsf_code_numb,:);        % OVSF codes for each user
load sc_code_dl_32_all.mat sc_code_dl_32_all;   % Loading Scrambling codes of n=32
scramb_code = sc_code_dl_32_all(1,:);           % Scrambling code for the downlink
scramb_code_user = scramb_code.'*ones(1,frame); % repeating the scrambling code for the frames in
a block
scramb_code_user = scramb_code_user(:);
clear sc_code_dl_32_all ovsf32all;

% Pliot symbols and root-raised cosine pulse-shape filter coefficents
pilot = pilot_table_dl(pilot_slot);      % loading pilot bits for a frame from pilot symbol table
load p_shape_coeff.mat b;                % loading pulse-shaping filter coefficient
sym_slot = sum(s_format(2:6));           % symbols per slot
d_sym_slot = sum(s_format(2:3));         % user data symbols per slot
c_sym_slot = sum(s_format(4:5));         % control symbols per slot (TPC+TFCI not include Pilot)
sym_frame = slot_frame * sym_slot;       % symbols per frame
d_sym_frame = slot_frame * d_sym_slot;   % user data symbols per frame
cpich_slot = 20;                         % P-CPICH symbols per slot
cpich_frame = slot_frame * cpich_slot;   % P-CPICH symbols per frame
no_symbol_cpich = sym_slot/cpich_slot;   % ratio of the number of user symbols to the number of
P-CPICH symbols
no_symbol_slot = sym_slot/2;

% MAI from adjacent cells
NBS = 1;                                          % # adjacent cells
K1 = 8;                                           % # users
L1 = 2;                                           % # multipaths
load sc_code_dl_4128_all.mat sc_code_dl_4128_all;   % Loading Scrambling codes of n=32
scramb_code1 = sc_code_dl_4128_all(1,:);            % Scrambling code for the downlink
scramb_code_user1 = scramb_code1.'*ones(1,frame);   % repeating the scrambling code
scramb_code_user1 = scramb_code_user1(:);
clear sc_code_dl_4128_all;
ovsf_code_numb1 = (3:K1+2)';
load ovsf32all.mat ovsf32all;                     % Loading OVSF codes with SF 32
ovsf_user1 = ovsf32all(ovsf_code_numb1,:);        % OVSF codes for each user
clear ovsf32all;
theta_bs_LOS1 = (-1)*sign(randn(1))*rand(1)*pi/2;   % LOS AOA for uniformly distributed (-90, 90)
P_LOS1 = 1.0;                                     % Power of the LOS components (Relative power
of MAI)

% Receiver parameters
N = 2;                              % # antenna elements
mu = linspace (0.3, 0.3, M);        % multiple step sizes of each multipath for LMS
aQ = 3;                             % Number of pilot symbols to get the averaged power for LMS

% Channel parameters for the GBSB models
n_scat = 50;                    % # Scatters
tau_min = 10e-3/chip_frame;     % Minimum multipath delay (1 chip period in any frame)
if CHPF_model == 1
   tau_max = 20*tau_min;        % Maximum relative delay (20 chips for GBSB elliptical (D=800m))
   D = 800; % 0.5 mile          % Distance (m) of each user from the base station
```

```
elseif CHPF_model == 2
   tau_max = 61*tau_min;         % Maximum relative delay for GBSB circular (35, 48, 61, 74, 87,
99 chip for D = 2, 3, 4, 5, 6, 7 km)
   D = 4000; % 2.5 mile          % Distance (m) of each user from the base station
elseif CHPF_model == 3
   tau_max = 99*tau_min;         % Maximum relative delay when ITU Vehicular B is applied
   D = 7000;
end

% Wireless channel parameters
eta = 3.5;                        % path loss exponent
fc = 2.14e9;                      % Carrier frequency of Downlink (2.11 ~ 2.17 GHz)
P_LOS = 1;                        % Power of the LOS components from the users (normalized to 1W)
rayl_frame = block_frame*frame;   % # frames used to generate the rayleigh fading profile
theta_bs_LOS = (-1)*sign(randn(1))*rand(1)*pi/2;    % LOS AOA for uniformly distributed (-90, 90)
vsec = vhr*1e3*ones(1,1)/3600;    % velocity of the users (m/sec)
c = 3e8;                          % Speed of propagation (m/sec)
fm = vsec*fc/c;                   % Maximum Doppler spread (Hz)
theta_v = theta_bs_LOS;           % Direction of motion of the mobiles (wrt LOS)

% Received signal at Mobile Station
fs = chip_frame*samp_chip*100;    % Sampling rate of the transmitted baseband signal (10ms frame)
max_delay = floor(tau_max*fs);    % maximum multipath delay in samples
signal_block = frame*chip_frame*samp_chip;  % length of the signal observation window in samples

% Power budget for the common pilot (20%)
K_pilot = floor(K/4);
P_ratio = sqrt(K_pilot)/2;
Other_Power = K_pilot + K - 1;
K_pilot1 = floor(K1/4);
P_ratio1 = sqrt(K_pilot1)/2;
Other_Power1 = K_pilot1 + K1 -1;

% Model parameters for the ECFCM
if channel_model == 3 | channel_model == 4
   lamda = find_lamda_from_rho(rho);
   L_matrix = [ 1 0; 1/sqrt(2)*lamda*(1+j) sqrt(1-lamda^2)];
end
```

Figure A-1 System and Model Parameters for the HC

A.1.2 Simulation Core

The second part of the main module is a simulation core, in which simulation is iterated for a number of times to evaluate the average system performance. Figure A-2 presents the simulation core for the HC. There are several loops in the simulation core. The most outer loop specifies the number of iterations. The second outer loop is for different SINRs. The third outer loop repeats for a number of frames for each simulation run. There are several inner loops in this

third outer loop. The first and the second inner loops are to generate the transmitted user signal and to generate multipath signals for this user signal, respectively. The third and the fourth inner loops are to generate the transmitted signal from other base station and to generate multipath signals for this interference signal, respectively. Each multipath signal is despread in the last inner loop using a rake finger.

```
for iter = 1:no_iter %% loop 1
   theta_bs_LOS = (-1)*sign(randn(1))*rand(1)*pi/2;
   if CHPF_model == 1
      [tau,theta_bs,P,alpha] = … % GBSB elliptical model
      vec_ch_ellip_dl_1(n_scat,L,D,tau_max,tau_min,P_LOS,theta_bs_LOS,eta);
   elseif CHPF_model == 2
      [tau,theta_bs,P,alpha] = … % GBSB circular model
      vec_ch_circ_dl_1(n_scat,L,D,tau_max,tau_min,P_LOS,theta_bs_LOS,eta);
   elseif CHPF_model == 3
      [tau,theta_bs,P,alpha] = … % ITU channel model
      vec_ch_umts_dl_1(n_scat,L,D,tau_max,tau_min,P_LOS,theta_bs_LOS,eta,ITU_mode);
   end
   tau_samp = round(tau*fs);                    % multipath delays in chip samples
   fd = abs(fm*cos(theta_bs-theta_v));          % doppler spread for each multipath
   I = find(fd < 1);                            % If doppler spread < 1 map it to 1
   fd(I) = 1;
   P_all = sum(P(1:M));

   for SINR = SINR_start:SINR_step:SINR_max %% loop 2
      theta_bs_LOS1 = (-1)*sign(randn(1))*rand(1)*pi/2;
      P_all_1 = (P_all/(10^(SINR/10))-(Other_Power+10^((-1)*ebno/10))*P_all)/(Other_Power1+1);
      % Channel profile for MAI
      if CHPF_model == 1
         [tau1,theta_bs1,P1,alpha1] = …
         vec_ch_ellip_dl_2(n_scat,L1,D,tau_max,tau_min,P_all_1,theta_bs_LOS1,eta);
      else
         [tau1,theta_bs1,P1,alpha1] = …
         vec_ch_circ_dl_2(n_scat,L1,D,tau_max,tau_min,P_all_1,theta_bs_LOS1,eta);
      end
      tau_samp1 = round(tau1*fs);                   % multipath delays in chip samples
      fd1 = abs(fm*cos(theta_bs1-theta_v));         % doppler spread for each multipath
      I1 = find(fd1 < 1);                           % If doppler spread < 1 map it to 1
      fd1(I1) = 1;
      w_in_lms(1:N,1:M) = [ones(1,M);zeros(N-1,M)]; % Initialization of weight vectors for LMS
      e = zeros(block_frame*frame*slot_frame*cpich_slot/2,M); % Initialization of error for LMS

      for frame_count = 1:block_frame %% loop 3
         pcpi = (pri_pilot*P_ratio)*scramb_code_user;   % Primary Common Pilot Signal
         for i = 1:K %% loop 4-1
            s = wcdma_signal_sym_dl_1(frame,slot_frame,samp_chip,s_format,ovsf_user(i,:),…
                scramb_code,pilot_slot,pilot,b,i,des_usr_indx);
            pcpi = s + pcpi;
         end %% loop 4-1
```

```
clear s;
sh_s = p_shape_1(b,pcpi,samp_chip,'sqrtrc','xmittr');   % Pulse-shaping of DPDCH
x_i = zeros(N,max_delay + signal_block);   % Initialization of the received signal

for ii = 1:L %% loop 4-2
   % User's spatial signature vector, A
   if channel_model == 1       % SCFCM
      A = channel_vector_dl(theta_bs(ii,1),alpha(ii,1),tau_samp(ii,1),N,d,frame,…
          sym_frame/2,sf_user(i,1),samp_chip,fd(ii,1),rayl_frame,size(x_i,2),…
          max_delay,ii,L,des_usr_indx,des_usr_indx,frame_count);
   elseif channel_model == 2   % LCFCM
      A = channel_vector_dl_1(theta_bs(ii,1),alpha(ii,1),tau_samp(ii,1),N,d,frame,…
          sym_frame/2,sf_user(i,1),samp_chip,fd(ii,1),rayl_frame,size(x_i,2),…
          max_delay,ii,L,des_usr_indx,des_usr_indx,frame_count);
   elseif channel_model == 3   % original ECFCM
      A = channel_vector_dl_2(theta_bs(ii,1),alpha(ii,1),tau_samp(ii,1),N,d,frame,…
          sym_frame/2,sf_user(i,1),samp_chip,fd(ii,1),rayl_frame,size(x_i,2),…
          max_delay,ii,L,des_usr_indx,des_usr_indx,frame_count);
   elseif channel_model == 4   % ECFCM
      A = channel_vector_dl_3(theta_bs(ii,1),alpha(ii,1),tau_samp(ii,1),N,d,frame,…
          sym_frame/2,sf_user(i,1),samp_chip,fd(ii,1),rayl_frame,size(x_i,2),…
          max_delay,ii,L,des_usr_indx,des_usr_indx,frame_count);
   end
   S = sig_matrix_1(tau_samp(ii,1),sh_s,size(x_i,2),max_delay); % User's signal vector
   for iii = 1:N %% loop 5-1
       rcx(iii,:) = A(iii,:).*S;
   end %% loop 5-1
   x_i = x_i + rcx;                     % Receiver signal from each multipath
end %% loop 4-2
clear rcx S sh_s;

% MAI gereration
pcpi1 = (pri_pilot*P_ratio1)*scramb_code_user1;   % Primary Common Pilot Signal
for i = 1:K1 %% loop 4-3
   s1 = wcdma_signal_sym_dl_1(frame,slot_frame,samp_chip,s_format,ovsf_user(i,:),…
       scramb_code,pilot_slot,pilot,b,i,des_usr_indx);
   pcpi1 = s1 + pcpi1;
end %% loop 4-3
clear s1;

sh_s1 = p_shape_1(b,pcpi1,samp_chip,'sqrtrc','xmittr');      % Pulse-shaping of DPDCH
x_i1 = zeros(N,max_delay + signal_block); % Initialization of the received signal
for ii = 1:L1 %% loop 4-4
   % User's spatial signature vector, A
   if channel_model == 1       % SCFCM
      A1 = channel_vector_dl(theta_bs1(ii,1),alpha1(ii,1),tau_samp1(ii,1),N,d,frame,…
          sym_frame/2,sf_user(i,1),samp_chip,fd1(ii,1),rayl_frame,size(x_i,2),…
          max_delay,ii,L1,des_usr_indx,des_usr_indx,frame_count);
   elseif channel_model == 2   % LCFCM
      A1 = channel_vector_dl_1(theta_bs1(ii,1),alpha1(ii,1),tau_samp1(ii,1),N,d,frame,…
          sym_frame/2,sf_user(i,1),samp_chip,fd1(ii,1),rayl_frame,size(x_i,2),…
          max_delay,ii,L1,des_usr_indx,des_usr_indx,frame_count);
   elseif channel_model == 3   % original ECFCM
```

```
            A1 = channel_vector_dl_2(theta_bs1(ii,1),alpha1(ii,1),tau_samp1(ii,1),N,d,frame,…
                sym_frame/2,sf_user(i,1),samp_chip,fd1(ii,1),rayl_frame,size(x_i,2),…
                max_delay,ii,L1,des_usr_indx,des_usr_indx,frame_count);
        elseif channel_model == 4   % ECFCM
            A1 = channel_vector_dl_3(theta_bs1(ii,1),alpha1(ii,1),tau_samp1(ii,1),N,d,frame,…
                sym_frame/2,sf_user(i,1),samp_chip,fd1(ii,1),rayl_frame,size(x_i,2),…
                max_delay,ii,L1,des_usr_indx,des_usr_indx,frame_count);
        end
        S1 = sig_matrix_1(tau_samp1(ii,1),sh_s1,size(x_i1,2),max_delay);
        for iii = 1:N %% loop 5-2
            rcx1(iii,:) = A1(iii,:).*S;
        end %% loop 5-2
        x_i1 = x_i1 + rcx1;                          % Receiver signal from each multipath
    end %% loop 4-4
    clear rcx1 S1 sh_s1;

    shuffle = floor((size(x_i1,2)-1)*rand(1));       % Make two cells asynchronous
    x_i1 = [x_i1(:,shuffle+1:end) x_i1(:,1:shuffle)]; % Shuffle the MAIs
    x = x_i + x_i1 + noise_4(sf_user(des_usr_indx),ebno,size(x_i),P,M,Other_Power); % AWGN
    clear x_i x_i1;
    load user_data.mat user_data;                    % desired user's DPDCH data symbols
    x = p_shape_1(b,x.',samp_chip,'sqrtrc','rcvr');  % SQRT-RC filtering at the receiver
    x = x.';

    for i = 1:M %% loop 4-5
        % Frame Synchronization and Decimation
        x_chip = x(:,tau_samp(i,1)+1:samp_chip:end);
        x_chip = x_chip(:,1:chip_frame*frame);       % proper sizing of the chip samples
        % De-scrambling and de-spreading
        for ii = 1:N %% loop 5-3
            x_chip(ii,:) = x_chip(ii,:).*scramb_code_user'; % De-scrambling
            y_I(ii,:) = (reshape(x_chip(ii,:),…
                        length(ovsf_user(des_usr_indx,:)),…
             sym_frame/2*frame).'*ovsf_user(des_usr_indx,:)').'/size(ovsf_user(des_usr_indx,:),…
                        2);      % De-spreading for DPCH
            y_P(ii,:) = (reshape(x_chip(ii,:),length(ovsf_cpich), …
                        cpich_frame/2*frame).'*ovsf_cpich').'/size(ovsf_cpich,2);
        end %% loop 5-3
        z_finger_1(i,:) = y_I(1,:);
        z_pilot_1(i,:) = y_P(1,:);
        z_finger_2(i,:) = y_I(2,:);
        z_pilot_2(i,:) = y_P(2,:);

        % N-LMS weight adaptation
        [w_lms, w_end_lms, e] = lms_weight1(mu(i), aQ, alpha(i), N, w_in_lms(:,i), y_P, …
                              e, pri_pilot, cpich_slot/2, frame_count, frame, slot_frame, i);
        w_in_lms(:,i) = w_end_lms;

        w1_lms = ones(1, sym_frame/cpich_frame)'*w_lms(1,:);
        w2_lms = ones(1, sym_frame/cpich_frame)'*w_lms(2,:);
        w1_lms = reshape(w1_lms, 1, size(w1_lms,1)*size(w1_lms,2));
        w2_lms = reshape(w2_lms, 1, size(w2_lms,1)*size(w2_lms,2));
        z_pilot_lms(i,:) = y_P(1,:).*conj(w_lms(1,:)) + y_P(2,:).*conj(w_lms(2,:));
```

```
            z_finger_lms(i,:) = y_I(1,:).*conj(w1_lms) + y_I(2,:).*conj(w2_lms);
        end %% loop 4-5

        % Phase rotaion using the known pilot signal
        [new_z_fin_1] = phase_rotate_1 (frame, slot_frame, z_finger_1, z_pilot_1, …
                        s_format, sf_common, pri_pilot); % (Antenna 1)
        [new_z_fin_2] = phase_rotate_1 (frame, slot_frame, z_finger_2, z_pilot_2, …
                        s_format, sf_common, pri_pilot); % (Antenna 2)
        [new_z_fin_lms] = phase_rotate (frame, slot_frame, z_finger_lms, z_pilot_lms, …
                        s_format, sf_common, pri_pilot);

        z_all_1 = sum (new_z_fin_1,1);     % Combining each multipath signal for antenna 1
        z_all_2 = sum (new_z_fin_2,1);     % Combining each multipath signal for antenna 2
        % Maximal ratio combining (MRC) based on data signal (S+N) after rake combining
        z_all_3 = (2./(abs(z_all_1)+(abs(z_all_2)))).*(abs(z_all_1).*z_all_1 + …
                  abs(z_all_2).*z_all_2);
        z_all_4 = sum (new_z_fin_lms,1);   % Adaptive combining based on N-LMS
        % Hybrid combining of DC and AC outputs using MRC
        z_all_5 = (abs(z_all_3).*z_all_3 + abs(z_all_4).*z_all_4);

        % Hard decision for data detection of I/Q channel
        z_I_1 = sign(real(z_all_1));
        z_Q_1 = sign(imag(z_all_1));
        z_I_2 = sign(real(z_all_2));
        z_Q_2 = sign(imag(z_all_2));
        z_I_3 = sign(real(z_all_3));
        z_Q_3 = sign(imag(z_all_3));
        z_I_4 = sign(real(z_all_4));
        z_Q_4 = sign(imag(z_all_4));
        z_I_5 = sign(real(z_all_5));
        z_Q_5 = sign(imag(z_all_5));
        z_I_1 = z_I_1(:);   z_Q_1 = z_Q_1(:);
        z_I_2 = z_I_2(:);   z_Q_2 = z_Q_2(:);
        z_I_3 = z_I_3(:);   z_Q_3 = z_Q_3(:);
        z_I_4 = z_I_4(:);   z_Q_4 = z_Q_4(:);
        z_I_5 = z_I_5(:);   z_Q_5 = z_Q_5(:);
        data_out_1 = extract_data (frame, slot_frame, z_I_1, z_Q_1, s_format);     % Antenna 1
        data_out_2 = extract_data (frame, slot_frame, z_I_2, z_Q_2, s_format);     % Antenna 2
        data_out_3 = extract_data (frame, slot_frame, z_I_3, z_Q_3, s_format);     % DC
        data_out_4 = extract_data (frame, slot_frame, z_I_4, z_Q_4, s_format);     % AC
        data_out_5 = extract_data (frame, slot_frame, z_I_5, z_Q_5, s_format);     % HC
        % Number of error symbols
        %------------------------
        Nerror_1(frame_count,1) = length(find(data_out_1 ~= user_data));
        Nerror_2(frame_count,1) = length(find(data_out_2 ~= user_data));
        Nerror_3(frame_count,1) = length(find(data_out_3 ~= user_data));
        Nerror_4(frame_count,1) = length(find(data_out_4 ~= user_data));
        Nerror_5(frame_count,1) = length(find(data_out_5 ~= user_data));
    end %% loop 3

    % Symbol error rate
    % Error count before valid frame
    sinr_index = (SINR-SINR_min)/SINR_step+1;
```

```
      Ne_I_1(sinr_index,iter) = sum(Nerror_1(1:valid_frame-1),1);
      Ne_I_2(sinr_index,iter) = sum(Nerror_2(1:valid_frame-1),1);
      Ne_I_3(sinr_index,iter) = sum(Nerror_3(1:valid_frame-1),1);
      Ne_I_4(sinr_index,iter) = sum(Nerror_4(1:valid_frame-1),1);
      Ne_I_5(sinr_index,iter) = sum(Nerror_5(1:valid_frame-1),1);
      % Error count from valid frame
      Ne_V_1(sinr_index,iter) = sum(Nerror_1(valid_frame:end),1);
      Ne_V_2(sinr_index,iter) = sum(Nerror_2(valid_frame:end),1);
      Ne_V_3(sinr_index,iter) = sum(Nerror_3(valid_frame:end),1);
      Ne_V_4(sinr_index,iter) = sum(Nerror_4(valid_frame:end),1);
      Ne_V_5(sinr_index,iter) = sum(Nerror_5(valid_frame:end),1);
      Ne_V_6(sinr_index,iter) = sum(Nerror_6(valid_frame:end),1);
   end %% loop 2

   % Iterating simulations are stopped when the predefined number of errors is occurred
   % It can save the simulation time for lower SINR cases.
   if iter >= min_no_iter & SINR_start <= SINR_max
      if ( sum(Ne_I_5((SINR_start-SINR_min)/SINR_step+1,:)) + …
           sum(Ne_V_5((SINR_start-SINR_min)/SINR_step+1,:)) ) > max_error_count
         total_no_iter((SINR_start-SINR_min)/SINR_step+1) = iter; % # iterations for each SINR
         SINR_start = SINR_start + SINR_step;          % Change the starting value
         save total_no_iter_file -ascii total_no_iter;
      end
   end
end %% loop 1
```

Figure A-2 Simulation Core for the HC

The simulation core also contains several functions. They include a channel profile generator, a downlink signal generator, a multipath signal vector generator, a noise generator, a phase rotator for the coherent combining, and an N-LMS antenna weight generator.

A.1.3 Post Processing

The last part of the main module is presented in Figure A-3, in which the BERs are calculated and the simulation results are saved as a binary file. It consists of three sub-parts. The first sub-part is to calculate BERs for each antenna and each combining scheme. The second one is to define a file name to save the simulation results, while the last one is to save the simulation results into this file.

```
% BERs for each antenna and each combining scheme
no_sym_iter = d_sym_frame*frame*block_frame;   % Number of frames to be simulated
Ps_av_1 = ((sum(Ne_I_1,2)+sum(Ne_V_1,2))./total_no_iter)/no_sym_iter; % Antenna 1
Ps_av_2 = ((sum(Ne_I_2,2)+sum(Ne_V_2,2))./total_no_iter)/no_sym_iter; % Antenna 2
```

```
Ps_av_3 = ((sum(Ne_I_3,2)+sum(Ne_V_3,2))./total_no_iter)/no_sym_iter; % DC
Ps_av_4 = ((sum(Ne_I_4,2)+sum(Ne_V_4,2))./total_no_iter)/no_sym_iter; % AC
Ps_av_5 = ((sum(Ne_I_5,2)+sum(Ne_V_5,2))./total_no_iter)/no_sym_iter; % HC
SINR = SINR_min:SINR_step:SINR_max;

% Defene a file name to save the simulation results
sim_mode = 'HC';
if CHPF_model == 1
   file_head = 'ell';
elseif CHPF_model == 2
   file_head = 'cir';
elseif CHPF_model == 3
   if ITU_mode == 1
      file_head = 'itu_pa';
   elseif ITU_mode == 2
      file_head = 'itu_pb';
   elseif ITU_mode == 3
      file_head = 'itu_va';
   elseif ITU_mode == 4
      file_head = 'itu_vb';
   end
end
if d == 0.125
   ant_dis = 'd18';
elseif d == 0.25
   ant_dis = 'd14';
elseif d == 0.375
   ant_dis = 'd38';
elseif d == 0.5
   ant_dis = 'd12';
end
if rho == 0.1
   rho_d = 'r01';
elseif rho == 0.3
   rho_d = 'r03';
elseif rho == 0.5
   rho_d = 'r05';
elseif rho == 0.7
   rho_d = 'r07';
elseif rho == 0.9
   rho_d = 'r09';
end

% Save the simulation results into the file
[outfilename, errormessage] = sprintf('BER_%s_%s_v%d_%s_%s_M%d_c%d', sim_mode, …
                              file_head, vhr, ant_dis, rho_d, M, channel_model);
if channel_model == 1 | channel_model == 2
   save(outfilename,'M','max_error_count','*_iter','Ps_*','Ne_*','SINR','ebno' );
elseif channel_model == 3 | channel_model == 4
   save(outfilename,'M','max_error_count','*_iter','Ps_*','Ne_*','SINR','ebno', …
        'rho','lamda', 'L_matrix' );
end
```

Figure A-3 Post Processing for the HC

A.2 Matlab Codes for the MS-GSC and the Adaptive Combining Scheme

The main module for the MS-GSC and the adaptive rake combining scheme consists of three parts as that for the hybrid combiner. They include the system and model parameters, a simulation core, and a post processing part.

A.2.1 System and Model Parameters

The first part of the main module to define the system and model parameters is presented in Figure A-4. Most parameters are the same as those for the HC described in the previous section. The only differences are an operating SNR environment and threshold sets for each GSC (MS-GSC, AT-GSC, and NT-GSC).

```
% Basic parameters for the simulation
snr_mode = 1;                   % SNR mode: 1) same 2) one more 3) two more
target_BER = 0.10;              % Target BER 0.10, 0.08, 0.06
noise_mode = 1;                 % Noise mode: 1) fixed 2) variable
CHPF_model = 3;                 % Channel profile: 1) GBSB Elliptical, 2) GBSB Circular, 3) ITU
ITU_mode = 3;        % UMTS mode: 1) Pedestrian A 2) Pedestrian B, 3) Vehicular A, 4) Vehicular B
threshold_set = 1;              % Threshold set: 1) coarse 2) medium 3) fine
no_iter = 100;                  % Monte-Carlo Iteration number
count_frame = 4;                % The first frame to count erroneous bits
block_frame = 6;                % # blocks of frames (Total # of frame = block_frame*frame)

% Operating SNR environment
if snr_mode == 1
   delta_BER1 = 0.22*0.10;      % Delta BER for GSC
   delta_BER2 = 0.12*0.10;      % Delat BER for MS-GSC, AT-GSC, and NT-GSC
   if target_BER == 0.10
      snr_0 = -12.0;
   elseif target_BER == 0.08
      snr_0 = -11.5;
   elseif target_BER == 0.06
      snr_0 = -11.0;
      delta_BER1 = 0.25*0.10;
      delta_BER2 = 0.20*0.10;
   end
elseif snr_mode == 2
   delta_BER1 = 0.20*0.10;
   delta_BER2 = 0.10*0.10;
   if target_BER == 0.10
      snr_0 = -11.5;
   elseif target_BER == 0.08
      snr_0 = -11.0;
   elseif target_BER == 0.06
```

```
      snr_0 = -10.5;
      delta_BER1 = 0.25*0.10;
      delta_BER2 = 0.20*0.10
   end
elseif snr_mode == 3
   if target_BER == 0.10
      snr_0 = -11.0;
   end
end
if noise_mode == 1
   ebno_power = [snr_0];
else
   ebno_power = [snr_0-0.5 snr_0 snr_0+0.5];
end
ebno_index = size(ebno_power,2);
no_pilot_sym_avg = 1;

% Channel parameters
if ITU_mode == 1 | ITU_mode == 2
   vhr = 3;                                        % velocity of the users (km/h)
elseif ITU_mode == 3 | ITU_mode == 4
   vhr = 50;
end
if ITU_mode == 1
   L = 4;                                          % # multipaths in the channel
   M = 2;                                          % # RAKE fingers (M<=L)
else
   L = 6;
   if ITU_mode == 2
      M = 5;
   elseif ITU_mode == 3 | ITU_mode == 4
      M = 4;
   end
end
OLoop = 5; ILoop = 15;
c_index_init = ceil(M/2);

% Define a threshold set for each GSC
if CHPF_model == 1
   msgsc_power = [1.0 2.0 3.0 4.0 5.0 6.0 7.0];
   atgsc_power = [5.0 3.0 1.5 1.0 0.6 0.3 0.1];
   ntgsc_power = [0.8 0.5 0.3 0.2 0.1 0.05 0.01];
elseif CHPF_model == 2
   msgsc_power = [1.0 2.0 3.0 4.0 5.0 6.0 7.0];
   atgsc_power = [5.0 3.0 1.5 1.0 0.6 0.3 0.1];
   ntgsc_power = [0.8 0.5 0.3 0.2 0.1 0.05 0.01];
elseif CHPF_model == 3
   if threshold_set == 1
      if ITU_mode == 2
         % Threshold set for Pedestrian B with 5 fingers
         % Finger saving  4     3.5  3    2.5  2.0   1.5  1.0   0.5   0
         msgsc_power = [0.01    1.95 2.68 3.3  4.0   4.8  5.8   7.2   30.0];
         atgsc_power = [30.0    1.68 1.1  0.81 0.61  0.44 0.3   0.17  0.000001];
```

```
         ntgsc_power = [0.99999 0.74 0.54 0.38 0.275 0.19 0.125 0.065 0.000001];
      else
         % Threshold set for Vehicular A with 4 fingers
         % Finger saving  3     2.5   2.0  1.5   1.0  0.5   0
         msgsc_power = [0.01    1.55  2.3  3.15  4.2  5.8   30.0];
         atgsc_power = [30.0    1.1   0.62 0.38  0.22 0.1   0.000001];
         ntgsc_power = [0.99999 0.54  0.3  0.175 0.1  0.042 0.000001];
      end
   elseif threshold_set == 2
      if ITU_mode == 2
         % Threshold set for Pedestrian B with 5 fingers
         %msgsc_power = [0.1  1.67 2.23 2.75 3.2  3.8  4.5  5.3  6.5  30.0];
         %atgsc_power = [30.0 2.25 1.45 1.1  0.87 0.67 0.5  0.35 0.20 0.001];
         %ntgsc_power = [0.99 0.84 0.67 0.53 0.42 0.31 0.22 0.15 0.09 0.001];
         % Finger saving  4   3.7   3.3  3    2.7   2.3  2.0  1.7  1.3  1.0   0.7  0.3  0
         msgsc_power = [0.01  1.7   2.35 2.68 3.05  3.45 4.05 4.5  5.5  5.8   6.5  8.0  30.0];
         atgsc_power = [30.0  2.45  1.5  1.07 0.925 0.75 0.61 0.53 0.4  0.31  0.25 0.1  0.0001];
         ntgsc_power = [0.999 0.83  0.69 0.54 0.45  0.35 0.28 0.22 0.18 0.12  0.09 0.03 0.0001];
      else
         % Threshold set for Vehicular A with 4 fingers
         % Finger saving  3   2.7  2.3  2.0  1.7  1.3  1.0  0.7  0.3  0
         msgsc_power = [0.01  1.2  1.75 2.3  2.83 3.47 4.2  5.4  7.5  30.0];
         atgsc_power = [30.0  1.7  0.95 0.65 0.48 0.35 0.22 0.14 0.07 0.0001];
         ntgsc_power = [0.999 0.68 0.47 0.3  0.22 0.15 0.1  0.06 0.03 0.0001];
      end
   end
end
msgsc_index = size (msgsc_power, 2);
ms_index_init = ceil(msgsc_index/2);
atgsc_index = size (atgsc_power, 2);
at_index_init = ceil(atgsc_index/2);
ntgsc_index = size (ntgsc_power, 2);
nt_index_init = ceil(ntgsc_index/2);

% Downlink WCDMA signal parameters
K = 8;                          % # users
des_usr_indx = floor(K/2)+1;    % Desired user index
sf_no = 13;                     % slot format number (0-16) for user's DPCH
s_format = slot_format(sf_no);  % returns slot format: s_format(1)=sf, s_format(2)= Ndata1,
s_format(3)= Ndata3, s_format(4)= Ntpc, s_format(5)= Ntfci, s_format(6)= Npilot
sf_index = s_format(1);         % spreading factor index
sf_user = sf_index.*ones(K,1);  % spreading factor for the users DP(D/C)CH (32 for I and Q)
sf_common = 256;                % spreading factor for CCPCH
pri_pilot = 1+j;                % P-CPICH (Primary Common Pilot Channel) signal
ovsf_code_numb = floor(linspace(3,sf_index,K))';
block_frame = 4;                % # blocks of frames (Total # of frame = block_frame*frame)
frame = 1;                      % # frames in a block of frames
slot_frame = 15;                % # slots per frame
pilot_slot = s_format(6);       % # pilot symbols per slot
chip_frame = 38400;             % # chips per frame
samp_chip = 4;                  % # samples per chip

% Downlink OVSF and long scrambling codes
```

```
load ovsf32all.mat ovsf32all;                    % Loading OVSF codes with SF 32
ovsf_cpich = ones(1,sf_common);
ovsf_user = ovsf32all(ovsf_code_numb,:);         % OVSF codes for each user
load sc_code_dl_32_all.mat sc_code_dl_32_all;    % Loading Scrambling codes of n=32
scramb_code = sc_code_dl_32_all(1,:);            % Scrambling code for the downlink
scramb_code_user = scramb_code.'*ones(1,frame); % repeating the scrambling code for the frames in
a block
scramb_code_user = scramb_code_user(:);
clear sc_code_dl_32_all ovsf32all;

% Pliot symbols and root-raised cosine pulse-shape filter coefficents
pilot = pilot_table_dl(pilot_slot);      % loading pilot bits for a frame from pilot symbol table
load p_shape_coeff.mat b;                % loading pulse-shaping filter coefficient
sym_slot = sum(s_format(2:6));           % symbols per slot
d_sym_slot = sum(s_format(2:3));         % user data symbols per slot
c_sym_slot = sum(s_format(4:5));         % control symbols per slot (TPC+TFCI not include Pilot)
sym_frame = slot_frame * sym_slot;       % symbols per frame
d_sym_frame = slot_frame * d_sym_slot;   % user data symbols per frame
cpich_slot = 20;                         % P-CPICH symbols per slot
cpich_frame = slot_frame * cpich_slot;   % P-CPICH symbols per frame
no_symbol_cpich = sym_slot/cpich_slot;   % ratio of the number of user symbols to the number of
P-CPICH symbols
no_symbol_slot = sym_slot/2;

% Receiver parameters
N = 2;                                   % # antenna elements
d = 0.25;                                % element separation (normalized by wavelength)

% Channel parameters for the GBSB models
n_scat = 50;                      % # Scatters
tau_min = 10e-3/chip_frame;       % Minimum multipath delay (1 chip period in any frame)
if CHPF_model == 1
   tau_max = 20*tau_min;          % Maximum relative delay (20 chips for GBSB elliptical (D=800m))
   D = 800; % 0.5 mile            % Distance (m) of each user from the base station
elseif CHPF_model == 2
   tau_max = 61*tau_min;          % Maximum relative delay for GBSB circular (35, 48, 61, 74, 87,
99 chip for D = 2, 3, 4, 5, 6, 7 km)
   D = 4000; % 2.5 mile           % Distance (m) of each user from the base station
elseif CHPF_model == 3
   tau_max = 99*tau_min;          % Maximum relative delay when ITU Vehicular B is applied
   D = 7000;
end

% Wireless channel parameters
eta = 3.5;                         % path loss exponent
fc = 2.14e9;                       % Carrier frequency of Downlink (2.11 ~ 2.17 GHz)
P_LOS = 1;                         % Power of the LOS components from the users (normalized to 1W)
rayl_frame = block_frame*frame;    % # frames used to generate the rayleigh fading profile
theta_bs_LOS = (-1)*sign(randn(1))*rand(1)*pi/2;    % LOS AOA for uniformly distributed (-90, 90)
vsec = vhr*1e3*ones(1,1)/3600;     % velocity of the users (m/sec)
c = 3e8;                           % Speed of propagation (m/sec)
fm = vsec*fc/c;                    % Maximum Doppler spread (Hz)
theta_v = theta_bs_LOS;            % Direction of motion of the mobiles (wrt LOS)
```

```
% Received signal at Mobile Station
fs = chip_frame*samp_chip*100;    % Sampling rate of the transmitted baseband signal (10ms frame)
max_delay = floor(tau_max*fs);    % maximum multipath delay in samples
signal_block = frame*chip_frame*samp_chip;  % length of the signal observation window in samples

% Power budget for the common pilot (20%)
K_pilot = floor(K/4);
P_ratio = sqrt(K_pilot)/2;
Other_Power = K_pilot + K - 1;
```

Figure A-4 System and Model Parameters for the GSCs

A.2.2 Simulation Core

The second part of the main module is a simulation core, which is presented in Figure A-5. This simulation core consists of several loops. The most outer loop specifies the number of iterations. The second outer loop is for different SNRs. The third outer loop repeats for a number of frames for each simulation run. There are several inner loops in this third outer loop. The first and the second inner loops are to generate the transmitted user signal and to generate multipath signals for this user signal, respectively. The third inner loop is to despread each multipath signal using a rake finger, while the last inner loop is to find a moving average of signal power for each pilot symbol.

```
for iter = 1:no_iter %% loop 1
   c_index1  = c_index_init;  c_index2  = c_index_init;
   ms_index1 = ms_index_init; ms_index2 = ms_index_init;
   at_index1 = at_index_init; at_index2 = at_index_init;
   nt_index1 = nt_index_init; nt_index2 = nt_index_init;
   theta_bs_LOS = (-1)*sign(randn(1))*rand(1)*pi/2;
   if CHPF_model == 1
      [tau,theta_bs,P,alpha] = …
         vec_ch_ellip_dl_1(n_scat,L,D,tau_max,tau_min,P_LOS,theta_bs_LOS,eta);
   elseif CHPF_model == 2
      [tau,theta_bs,P,alpha] = …
         vec_ch_circ_dl_1(n_scat,L,D,tau_max,tau_min,P_LOS,theta_bs_LOS,eta);
   elseif CHPF_model == 3
      [tau,theta_bs,P,alpha] = …
         vec_ch_umts_dl_1(n_scat,L,D,tau_max,tau_min,P_LOS,theta_bs_LOS,eta,ITU_mode);
   end
   tau_samp = round(tau*fs);                % multipath delays in chip samples
   fd = abs(fm*cos(theta_bs-theta_v));      % doppler spread for each multipath
   I = find(fd < 1);                        % If doppler spread < 1 map it to 1
   fd(I) = 1;
```

```
for ol = 1:OLoop %% loop 2
   if mod (ol, 5) == 1
      no_index = ceil(rand(1)*ebno_index);
      if ol == 1
         sort_i_gsc_1 = M:-1:1;
         sort_i_gsc_2 = M:-1:1;
      end
   else
      no_index = no_index + sign(randn(1));
      if no_index == 0
         no_index = 1;
      elseif no_index == (ebno_index+1)
         no_index = ebno_index;
      end
   end

   for frame_count = 1:block_frame %% loop 3
      pcpi = (pri_pilot*P_ratio)*scramb_code_user;   % Primary Common Pilot Signal
      for i = 1:K %% loop 4-1
         s= wcdma_signal_sym_dl_1(frame,slot_frame,samp_chip,s_format,…
            ovsf_user(i,:),scramb_code,pilot_slot,pilot,b,i,des_usr_indx); %WCDMA signal
         pcpi = s + pcpi;
      end %% loop 4-1
      clear s;
      sh_s = p_shape_1(b,pcpi,samp_chip,'sqrtrc','xmittr');  % Pulse-shaping of DPDCH
      x_i = zeros(N,max_delay + signal_block);
      for ii = 1:L %% loop 4-2
         % User's spatial signature vector
         A = channel_vector_dl_1(theta_bs(ii,1),alpha(ii,1),tau_samp(ii,1),N,d,…
             frame,sym_frame/2,sf_user(i,1),samp_chip,fd(ii,1),rayl_frame,size(x_i,2),…
             max_delay,ii,L,des_usr_indx,des_usr_indx,frame_count);
         S = sig_matrix_1(tau_samp(ii,1),sh_s,size(x_i,2),max_delay); %User's signal
         for iii = 1:N %% loop 5-1
             %rcx(iii,:) = S; %code for verification
             rcx(iii,:) = A(iii,:).*S;
         end %% loop 5-1
         x_i = x_i + rcx;     % Receiver signal from each multipath
      end %% loop 4-2
      clear rcx S sh_s;

      x = x_i + noise_3(sf_user(des_usr_indx),ebno_power(no_index),…
          size(x_i),P,L,Other_Power);% AWGB
      clear x_i;
      load user_data.mat user_data;

      x = p_shape_1(b,x.',samp_chip,'sqrtrc','rcvr');% SQRT-RC filtering at the receiver
      x = x.';

      for i = 1:M %% loop 4-3
         % Frame Synchronization and Decimation
         x_chip = x(:,tau_samp(i,1)+1:samp_chip:end);
         x_chip = x_chip(:,1:chip_frame*frame);
         for ii = 1:N %% loop 5-2
```

```
            x_chip(ii,:) = x_chip(ii,:).*scramb_code_user';
            y_I(ii,:) = (reshape(x_chip(ii,:),length(ovsf_user(des_usr_indx,:)),…
sym_frame/2*frame).'*ovsf_user(des_usr_indx,:)').'/size(ovsf_user(des_usr_indx,:),2);
            y_P(ii,:) = (reshape(x_chip(ii,:),length(ovsf_cpich),…
                        cpich_frame/2*frame).'*ovsf_cpich').'/size(ovsf_cpich,2);
         end %% loop 5-2
         z_finger_1(i,:) = y_I(1,:);
         z_pilot_1(i,:) = y_P(1,:);
         z_finger_2(i,:) = y_I(2,:);
         z_pilot_2(i,:) = y_P(2,:);
      end %% loop 4-3

      % Phase rotation using the known pilot signal
      [new_z_fin_1] = phase_rotate_1 (frame, slot_frame, z_finger_1, z_pilot_1, …
                     s_format, sf_common, pri_pilot); % (Antenna 1)
      [new_z_fin_2] = phase_rotate_1 (frame, slot_frame, z_finger_2, z_pilot_2, …
                     s_format, sf_common, pri_pilot); % (Antenna 2)
      z_all_11 = sum (new_z_fin_1,1);                  % MRC for antenna 1
      z_all_12 = sum (new_z_fin_2,1);                  % MRC for antenna 2

      % Finding moving average of the power of pilot signal
      for ii = 1:M % loop 4-4
         for iii = 2:no_pilot_sym_avg % loop 5-3
            prev_1(iii) = (abs(z_pilot_1(ii,1))^2)/2;
            prev_2(iii) = (abs(z_pilot_2(ii,1))^2)/2;
         end % loop 5-3
         for iiii = 1:size(z_pilot_1,2) % loop 5-4
            prev_1(1) = (abs(z_pilot_1(ii,iiii))^2)/2;
            prev_2(1) = (abs(z_pilot_2(ii,iiii))^2)/2;
            mov_avg_1(ii, iiii) = sum(prev_1)/no_pilot_sym_avg;
            mov_avg_2(ii, iiii) = sum(prev_2)/no_pilot_sym_avg;
            for iii = 2:no_pilot_sym_avg % loop 6-1
               prev_1(no_pilot_sym_avg+2-iii) = prev_1(no_pilot_sym_avg+1-iii);
               prev_2(no_pilot_sym_avg+2-iii) = prev_2(no_pilot_sym_avg+1-iii);
            end % loop 6-1
         end % loop 5-4
      end % loop 4-4
      [sort_v_gsc_1 sort_i_gsc_1] = sort(mean(mov_avg_1,2));
      [sort_v_gsc_2 sort_i_gsc_2] = sort(mean(mov_avg_2,2));
      % Adaptive GSC
      [z_all_21] = gsc_op1(sort_i_gsc_1, new_z_fin_1, z_all_11, M, c_index1);
      [z_all_22] = gsc_op1(sort_i_gsc_2, new_z_fin_2, z_all_12, M, c_index2);
      % Sort the power of each multipath signal
      [sort_val_1 sort_ind_1] = sort(mov_avg_1);
      [sort_val_2 sort_ind_2] = sort(mov_avg_2);

      % Minimum Selection GSC (MS-GSC)
      [z_all_71 save_power_71] = msgsc_op1(mov_avg_1, sort_ind_1, new_z_fin_1, …
                                 z_all_11, no_symbol_cpich, M, msgsc_power, ms_index1);
      [z_all_72 save_power_72] = msgsc_op1(mov_avg_2, sort_ind_2, new_z_fin_2, …
                                 z_all_12, no_symbol_cpich, M, msgsc_power, ms_index2);
      % Absolue Theshold GSC (AT-GSC)
      [z_all_81 save_power_81] = atgsc_op1(mov_avg_1, sort_ind_1, new_z_fin_1, …
```

```
                              z_all_11, no_symbol_cpich, M, atgsc_power, at_index1);
[z_all_82 save_power_82] = atgsc_op1(mov_avg_2, sort_ind_2, new_z_fin_2, …
                              z_all_12, no_symbol_cpich, M, atgsc_power, at_index2);
% Normalzied Theshold GSC (NT-GSC)
[z_all_91 save_power_91] = ntgsc_op1(mov_avg_1, sort_ind_1, new_z_fin_1, …
                              z_all_11, no_symbol_cpich, M, ntgsc_power, nt_index1);
[z_all_92 save_power_92] = ntgsc_op1(mov_avg_2, sort_ind_2, new_z_fin_2, …
                              z_all_12, no_symbol_cpich, M, ntgsc_power, nt_index2);

% Hard decision for data detection of I/Q channel
z_I_11 = sign(real(z_all_11)); z_Q_11 = sign(imag(z_all_11));
z_I_12 = sign(real(z_all_12)); z_Q_12 = sign(imag(z_all_12));
z_I_21 = sign(real(z_all_21)); z_Q_21 = sign(imag(z_all_21));
z_I_22 = sign(real(z_all_22)); z_Q_22 = sign(imag(z_all_22));
z_I_71 = sign(real(z_all_71)); z_Q_71 = sign(imag(z_all_71));
z_I_72 = sign(real(z_all_72)); z_Q_72 = sign(imag(z_all_72));
z_I_81 = sign(real(z_all_81)); z_Q_81 = sign(imag(z_all_81));
z_I_82 = sign(real(z_all_82)); z_Q_82 = sign(imag(z_all_82));
z_I_91 = sign(real(z_all_91)); z_Q_91 = sign(imag(z_all_91));
z_I_92 = sign(real(z_all_92)); z_Q_92 = sign(imag(z_all_92));
z_I_11 = z_I_11(:);  z_Q_11 = z_Q_11(:);
z_I_12 = z_I_12(:);  z_Q_12 = z_Q_12(:);
z_I_21 = z_I_21(:);  z_Q_21 = z_Q_21(:);
z_I_22 = z_I_22(:);  z_Q_22 = z_Q_22(:);
z_I_71 = z_I_71(:);  z_Q_71 = z_Q_71(:);
z_I_72 = z_I_72(:);  z_Q_72 = z_Q_72(:);
z_I_81 = z_I_81(:);  z_Q_81 = z_Q_81(:);
z_I_82 = z_I_82(:);  z_Q_82 = z_Q_82(:);
z_I_91 = z_I_91(:);  z_Q_91 = z_Q_91(:);
z_I_92 = z_I_92(:);  z_Q_92 = z_Q_92(:);
% Data extraction
data_out_11=extract_data (frame,slot_frame,z_I_11,z_Q_11,s_format); % MRC-Ant 1
data_out_12=extract_data (frame,slot_frame,z_I_12,z_Q_12,s_format); % MRC-Ant 2
data_out_21=extract_data (frame,slot_frame,z_I_21,z_Q_21,s_format); % GSC-Ant 1
data_out_22=extract_data (frame,slot_frame,z_I_22,z_Q_22,s_format); % GSC-Ant 2
data_out_71=extract_data (frame,slot_frame,z_I_71,z_Q_71,s_format); % MS_GSC-Ant 1
data_out_72=extract_data (frame,slot_frame,z_I_72,z_Q_72,s_format); % MS_GSC-Ant 2
data_out_81=extract_data (frame,slot_frame,z_I_81,z_Q_81,s_format); % AT-GSC-Ant 1
data_out_82=extract_data (frame,slot_frame,z_I_82,z_Q_82,s_format); % AT-GSC-Ant 2
data_out_91=extract_data (frame,slot_frame,z_I_91,z_Q_91,s_format); % NT-GSC-Ant 1
data_out_92=extract_data (frame,slot_frame,z_I_92,z_Q_92,s_format); % NT-GSC-Ant 2

% Number of error symbols
Nerror_11(frame_count,1) = length(find(data_out_11 ~= user_data));
Nerror_12(frame_count,1) = length(find(data_out_12 ~= user_data));
Nerror_21(frame_count,1) = length(find(data_out_21 ~= user_data));
Nerror_22(frame_count,1) = length(find(data_out_22 ~= user_data));
Nerror_71(frame_count,1) = length(find(data_out_71 ~= user_data));
Nerror_72(frame_count,1) = length(find(data_out_72 ~= user_data));
Nerror_81(frame_count,1) = length(find(data_out_81 ~= user_data));
Nerror_82(frame_count,1) = length(find(data_out_82 ~= user_data));
Nerror_91(frame_count,1) = length(find(data_out_91 ~= user_data));
Nerror_92(frame_count,1) = length(find(data_out_92 ~= user_data));
```

```
fm_save_power_21(frame_count,1) = c_index1;
fm_save_power_22(frame_count,1) = c_index2;
fm_save_power_71(frame_count,1) = mean(save_power_71);
fm_save_power_72(frame_count,1) = mean(save_power_72);
fm_save_power_81(frame_count,1) = mean(save_power_81);
fm_save_power_82(frame_count,1) = mean(save_power_82);
fm_save_power_91(frame_count,1) = mean(save_power_91);
fm_save_power_92(frame_count,1) = mean(save_power_92);

% Update the index for next frame evaluation
if frame_count ~= block_frame
   Nerror_total = size (user_data, 1);
   targetN = target_BER * Nerror_total;
   deltaN1 = delta_BER1 * Nerror_total;
   deltaN2 = delta_BER2 * Nerror_total;
   % Update for GSC
   if Nerror_21(frame_count,1) < targetN - deltaN1 & c_index1 ~= 1
      c_index1 = c_index1 - 1;
   elseif Nerror_21(frame_count,1) > targetN & c_index1 ~= M
      c_index1 = c_index1 + 1;
   end
   if Nerror_22(frame_count,1) < targetN - deltaN1 & c_index2 ~= 1
      c_index2 = c_index2 - 1;
   elseif Nerror_22(frame_count,1) > targetN & c_index2 ~= M
      c_index2 = c_index2 + 1;
   end
   % Update for MS-GSC
   if Nerror_71(frame_count,1) < targetN - deltaN2 & ms_index1 ~= 1
      ms_index1 = ms_index1 - 1;
   elseif Nerror_71(frame_count,1) > targetN & ms_index1 ~= msgsc_index
      ms_index1 = ms_index1 + 1;
   end
   if Nerror_72(frame_count,1) < targetN - deltaN2 & ms_index2 ~= 1
      ms_index2 = ms_index2 - 1;
   elseif Nerror_72(frame_count,1) > targetN & ms_index2 ~= msgsc_index
      ms_index2 = ms_index2 + 1;
   end
   % Update for AT-GSC
   if Nerror_81(frame_count,1) < targetN - deltaN2 & at_index1 ~= 1
      at_index1 = at_index1 - 1;
   elseif Nerror_81(frame_count,1) > targetN & at_index1 ~= atgsc_index
      at_index1 = at_index1 + 1;
   end
   if Nerror_82(frame_count,1) < targetN - deltaN2 & at_index2 ~= 1
      at_index2 = at_index2 - 1;
   elseif Nerror_82(frame_count,1) > targetN & at_index2 ~= atgsc_index
      at_index2 = at_index2 + 1;
   end
   % Update for NT-GSC
   if Nerror_91(frame_count,1) < targetN - deltaN2 & nt_index1 ~= 1
      nt_index1 = nt_index1 - 1;
   elseif Nerror_91(frame_count,1) > targetN & nt_index1 ~= ntgsc_index
      nt_index1 = nt_index1 + 1;
```

```
            end
            if Nerror_92(frame_count,1) < targetN - deltaN2 & nt_index2 ~= 1
               nt_index2 = nt_index2 - 1;
            elseif Nerror_92(frame_count,1) > targetN & nt_index2 ~= ntgsc_index
               nt_index2 = nt_index2 + 1;
            end
         end
      end %% loop 3

      % Symbol error rate
      Ne_I_11(ol,iter) = sum(Nerror_11(count_frame:end),1);
      Ne_I_12(ol,iter) = sum(Nerror_12(count_frame:end),1);
      Ne_I_21(ol,iter) = sum(Nerror_21(count_frame:end),1);
      Ne_I_22(ol,iter) = sum(Nerror_22(count_frame:end),1);
      Ne_I_71(ol,iter) = sum(Nerror_71(count_frame:end),1);
      Ne_I_72(ol,iter) = sum(Nerror_72(count_frame:end),1);
      Ne_I_81(ol,iter) = sum(Nerror_81(count_frame:end),1);
      Ne_I_82(ol,iter) = sum(Nerror_82(count_frame:end),1);
      Ne_I_91(ol,iter) = sum(Nerror_91(count_frame:end),1);
      Ne_I_92(ol,iter) = sum(Nerror_92(count_frame:end),1);
      % Finger saving
      DF_S_21(ol,iter) = mean(fm_save_power_21(count_frame:end),1);
      DF_S_22(ol,iter) = mean(fm_save_power_22(count_frame:end),1);
      DF_S_71(ol,iter) = mean(fm_save_power_71(count_frame:end),1);
      DF_S_72(ol,iter) = mean(fm_save_power_72(count_frame:end),1);
      DF_S_81(ol,iter) = mean(fm_save_power_81(count_frame:end),1);
      DF_S_82(ol,iter) = mean(fm_save_power_82(count_frame:end),1);
      DF_S_91(ol,iter) = mean(fm_save_power_91(count_frame:end),1);
      DF_S_92(ol,iter) = mean(fm_save_power_92(count_frame:end),1);
   end %% loop 2
end %% loop 1
```

Figure A-5 Simulation Core for the GSCs

The simulation core contains almost the same functions as those for the HC. The only difference is that there are several GSC functions to combine each finger signal depending on the combining scheme of each GSC method. Functions to evaluate the current BER after each frame and to dynamically adjust the threshold values for each GSC method are included in this simulation core.

A.2.3 Post Processing

The last part of the main module is presented in Figure A-6. It consists of three sub-parts. They are almost the same as those for the HC. The only difference is that the first sub-part also includes the calculation of finger saving for each GSC method.

```
% BERs and finger savings for each GSC method
total_no_iter = no_iter*OLoop;
no_sym_iter = d_sym_frame*frame*(block_frame-count_frame+1)*total_no_iter;
Ps_av_11 = sum(sum(Ne_I_11,2))/no_sym_iter;
Ps_av_12 = sum(sum(Ne_I_12,2))/no_sym_iter;
Ps_av_21 = sum(sum(Ne_I_21,2))/no_sym_iter;
Ps_av_22 = sum(sum(Ne_I_22,2))/no_sym_iter;
Ps_av_71 = sum(sum(Ne_I_71,2))/no_sym_iter;
Ps_av_72 = sum(sum(Ne_I_72,2))/no_sym_iter;
Ps_av_81 = sum(sum(Ne_I_81,2))/no_sym_iter;
Ps_av_82 = sum(sum(Ne_I_82,2))/no_sym_iter;
Ps_av_91 = sum(sum(Ne_I_91,2))/no_sym_iter;
Ps_av_92 = sum(sum(Ne_I_92,2))/no_sym_iter;
Pp_av_21 = M - sum(sum(DF_S_21,2))/total_no_iter;
Pp_av_22 = M - sum(sum(DF_S_22,2))/total_no_iter;
Pp_av_71 = M - sum(sum(DF_S_71,2))/total_no_iter;
Pp_av_72 = M - sum(sum(DF_S_72,2))/total_no_iter;
Pp_av_81 = M - sum(sum(DF_S_81,2))/total_no_iter;
Pp_av_82 = M - sum(sum(DF_S_82,2))/total_no_iter;
Pp_av_91 = M - sum(sum(DF_S_91,2))/total_no_iter;
Pp_av_92 = M - sum(sum(DF_S_92,2))/total_no_iter;

% Defene a file name to save the simulation results
if noise_mode == 1
   sim_mode = 'CLGSC_fn';
else
   sim_mode = 'CLGSC_vn';
end
if CHPF_model == 1
   file_head = 'ell';
elseif CHPF_model == 2
   file_head = 'cir';
elseif CHPF_model == 3
   if snr_mode == 1
      if ITU_mode == 1
         file_head = 'umts_pa';
      elseif ITU_mode == 2
         file_head = 'umts_pb';
      elseif ITU_mode == 3
         file_head = 'umts_va';
      elseif ITU_mode == 4
         file_head = 'umts_vb';
      end
   elseif snr_mode == 2
      if ITU_mode == 1
         file_head = 'umts_pa_s1';
      elseif ITU_mode == 2
         file_head = 'umts_pb_s1';
      elseif ITU_mode == 3
         file_head = 'umts_va_s1';
      elseif ITU_mode == 4
         file_head = 'umts_vb_s1';
```

```
      end
   elseif snr_mode == 3
      if ITU_mode == 1
         file_head = 'umts_pa_s2';
      elseif ITU_mode == 2
         file_head = 'umts_pb_s2';
      elseif ITU_mode == 3
         file_head = 'umts_va_s2';
      elseif ITU_mode == 4
         file_head = 'umts_vb_s2';
      end
   end
end
if target_BER == 0.1
   t_ber = 't10';
elseif target_BER == 0.09
   t_ber = 't09';
elseif target_BER == 0.08
   t_ber = 't08';
elseif target_BER == 0.07
   t_ber = 't07';
elseif target_BER == 0.06
   t_ber = 't06';
elseif target_BER == 0.05
   t_ber = 't05';
elseif target_BER == 0.04
   t_ber = 't04';
elseif target_BER == 0.11
   t_ber = 't11';
elseif target_BER == 0.12
   t_ber = 't12';
end

% Save the simulation results into the file
[outfilename,errormessage] = sprintf('BER_%s_%s_%s_v%d_M%d',sim_mode,file_head,t_ber,vhr,M);
save(outfilename,'M','no_iter','total_no_iter','*_power','Ps_av_*','Pp_av_*','Ne_I_*', 'DF_S_*');
```

Figure A-6 Post Processing for the GSCs

Vita

SUK WON KIM

Suk Won Kim was born in Yongin, Korea on May 4, 1964. He received the Bachelor of Science and Master of Science degrees in Mathematics from Seoul National University, Seoul, Korea in 1987 and 1991, respectively. He received another Master of Science degree in Electrical Engineering from the University of California at Los Angles (UCLA), Los Angeles, CA in 1999. From 1991 to 1995, he worked at the Semiconductor Division of Samsung Electronic Co., Ltd., Kiheung, Korea, where he was involved in the development of ASIC CAD tools and cell libraries. In 1999, he started his Ph.D. program at Virginia Polytechnic Institute and State University, Blacksburg, VA. He was awarded a scholarship from Samsung Electronic Co., Ltd. for pursuing his Ph.D. degree. His research interests include ASIC design for wireless communication systems, low-power VLSI design, and smart antennas for the third generation wideband CDMA systems.